Water Imbibition and Salt Diffusion in Gas Shales: A Field and Laboratory Study

by

Ebrahim Ghanbari

A thesis submitted in partial fulfillment of the requirements for the degree of

Master of Science

in

Petroleum Engineering

Department of Civil and Environmental Engineering

University of Alberta

Abstract

Hydraulic fracturing treatment has been increasingly applied to stimulate shale gas reservoirs. During hydraulic fracturing, a large amount of fracturing water is injected into the target formation. However, only a small fraction of injected fluid, typically 10 to 20 %, can be recovered during clean-up phase. The fate of non-recovered fracturing water is still poorly understood. Further, the injected water interacts with reservoir system and therefore, the produced water contains valuable information about the nature of the stimulated reservoir.

In this thesis, we analyze flowback field data, conduct simulation studies and perform a series of imbibition/diffusion experiments to (1) investigate the reasons behind low water recovery, (2) characterize the created fracture network and (3) identify dominant parameters and mechanisms that control ion diffusion and liquid imbibition rates.

The volumetric and chemical analysis of flowback data suggests that the geometry of the created fracture network has a significant effect on early time fluid production and salinity profile of flowback water. Wells with simple fracture network have a high water recovery and low gas production. The salinity profile of these wells gradually increases and then reaches a plateau. On the other hand, wells with complex fracture network have a low water recovery and high gas production. The salinity profile of these wells keeps increasing even at the end of flowback process.

The imbibition experiments show that, fracturing water imbibition into shale matrix can partially explain low water recovery after fracturing treatment. It is also found that, in addition to capillary pressure, intrinsic rock properties such as depositional lamination, organic material distribution and clay content, control the liquid imbibition rates in gas shale. The diffusion experiments indicate that shale sample properties such as porosity, permeability, clay content and depositional lamination have a significant effect on salt diffusion rate.

Simulation studies show that the counter current imbibition of fracturing water

during the shut-in time can result in a significant gas build-up in the fractures and therefore increases early time gas production rate. Furthermore, increasing the complexity of fracture network increases the gas production and decreases the water recovery.

Dedicated to my beloved parents, brothers and sisters for their love, endless support and encouragment.

Acknowledgements

I would like to express my sincerest love and gratitude to my family back home, my parents, my brothers Mohammad, Ali and Hassan and my sisters Maryam and Amineh, for their unflagging support and endless love, throughout my studies.

I am very thankful to my supervisor, Dr. Hassan Dehghanpour, for having faith in me, for giving me an opportunity to work on this project, for all of his encouragement and support, and for granting me freedom to explore my ideas.

I would like to thank Dr. Juliana Leung and Dr. David Potter, my examining committee members.

I gratefully acknowledge the financial support from Natural Sciences and Engineering Council of Canada (NSERC), FMC Technologies, Trican Well Services and Nexen Energy ULC for this research. I thank BC Oil and Gas Commissions and Nexen Energy ULC for providing samples and flowback data. My thanks are also extended to Computer Modelling Group Ltd. (CMG) for providing the CMG software package for the simulation study.

I am grateful to Mr. Doug Bearinger and Mr. Claudio Virues for the informative discussions and valuable suggestions. I would also like to express my gratitude to our technician, Mr. Todd Kinnee, for providing technical assistance in lab and helping me out with my experiments.

I want to thank my group fellows Ali, Mahdie, Ashkan, Obinna, Qing, Mingxiang and Oluwatobi for exchanging ideas and concepts. I would like to extend my thanks to my dearest friends Siavash, Ehsan, Sajjad, Ali, Seyyed, Alireza, Behrooz and Mohsen for their friendly encouragements.

Finally, I would like to thank all those who helped and inspired with me throughout my research.

Table of Contents

List of Tables

List of Figures

Chapter 1

Introduction

In this chapter, an introduction to unconventional gas resources and shale gas is presented. Then objective and scope of this work and the thesis structure are described.

1.1 Overview of Unconventional Gas Resources

Unconventional gas resources often requires special completion, stimulation and/or production techniques to produce economically. Furthermore, it can be described as natural gas reservoirs that are not trapped in structural/stratigraphic accumulations in a porous, permeable and buoyancy driven systems (Hamblin, 2006). Such resources are often referred to as continuous gas as they often cover a significant portion of a sedimentary basin. The exploitation of unconventional reservoirs are usually challenging due to the relatively unknown nature of these reservoirs. Generally, these reservoirs are known to have low and variable permeability, low flow rates, long production life and unusual pressure regimes (Dawson, 2005, Russum, 2005). The main streams of unconventional gas are currently being explored include 1) coalbed methane (CMB), 2) tight gas, 3) gas shale and 4) gas hydrate. Table 1.1 summarize the four streams of unconventional gas resources.

During recent years, unconventional resources have emerged as a significant source of energy supply in the United State and Canada. This is a response to ever increasing global demands on oil and gas and decreasing supply of conventional resources. Unconventional resources with ultra low matrix permeability are capable of producing oil and gas at economic rates when completed by hydraulically fractured horizontal wells (Ning et al., 1993). The development of Canada's unconventional gas resources continues to grow and is expected to play a major role

Table 1.1. Overview of unconventional gas reservoirs (Bustin and Clarkson, 1998, CSUG, 2010, Rice, 1993, Williams-kovacs, 2012, Williams-kovacs and Clarkson, 2011)

Resources	Overview
Coalbed Methane	• Natural gas formed in organic-rich coal seams • Often found at shallow depths • Often produce with large quantity of water • Contain significant adsorbed gas • Produce pure gas consisting over 90 % of methane
Tight Gas	• Natural gas reservoir with low porosity and permeability • Dense reservoir rock • Require massive stimulation and fracturing treatment • Variable matrix mineralogical composition
Shale Gas	• Natural gas contanined within organic shale sequence • Extremely low matrix permeability (from 0.01 to 0.0001 md) • Low matrix porosity (generally 3 to 9%) • Gas stored as a combination of adsorbed gas and free gas • Often highly hetrogeneous and laminated • Variable TOC and matrix mineralogical properties
Gas Hydrate	• Ice-like subtances and composed of water and natural gas • Form at low temperature and high pressure

in shaping Canada's long term natural gas supply. In 2010, unconventional gas resources provided more than 30% of the Canada's natural gas production (Heffernan and Dawson, 2010). Table 1.2 summarizes the Canada's gas in place and marketable gas resources.

Table 1.2. Canada's estimated gas in place and marketable gas resources (Heffernan and Dawson, 2010)

Gas Resources	Gas in Place (TCF)	Marketable Gas (TCF)
Conventional	692	357
Coalbed Methane	801	34-129
Tight Gas	1311	215-476
Shale Gas	1111	128-343
Total	3915	733-1304

1.2 Introduction to Shale Gas

Shale gas can be defined as natural gas resources stored in organic rich fined grained reservoirs in which gas is stored as a combination of adsorbed and free gas. The free

gas is stored within the matrix and fracture porosity and adsorbed gas is stored on the surface of the organic fraction and some clay (Bustin et al., 2009, Faraj et al., 2004, Hamblin, 2006, Rokosh et al., 2009). The fraction of adsorbed gas depends on geological and geochemical properties and ranges from about 20% in Barnett Shale to 85% in Lewis and Antrim Shale (Drake, 2007). Adsorbed gas tends to desorb off the rock surface as pressure is reduced in the reservoir, which is commonly associated with free gas production from fracture network (Bustin et al., 2009, Drake, 2007). Shale gas plays dominated by free gas production are commonly quartz-rich while those dominated by adsorbed gas production are rich in organic materials and clay minerals (Drake, 2007).

Shale gas is typically dry gas and it is primarily composed of methane (more than 90 %) with small portions of carbon dioxide, nitrogen, ethane, propane and water. However, similar to coalbed methane, some gas shale plays simultaneously produce both biogenic gas and water (Frantz et al., 2005). Furthermore, some gas shale reservoirs (i.e. Eagle Ford Shale) also produce wet gas and gas condensate (Energy Minerals Division, 2010).

In contrast to conventional gas reservoirs, gas shale reservoirs commonly have a very large areal extent and significant thickness (up to 1500 ft) and therefore can cover significant portions of sedimentary basins (Faraj et al., 2004, Jenkins and Boyer II, 2008). Although it is possible for the entire rock volume to contain some gas, it is desirable to find economic spot which contain high volume of gas-in-place. Conventional gas reservoirs, are commonly much smaller as they are composed of permeable rock sealed by impermeable cap rock (Williams-kovacs, 2012).

1.3 Field Observations

Field observations point to two common and interesting production behavior in shale formations.

1.3.1 Effect of Well Shut-in on Water and Gas Production

Some shale gas and oil wells undergo month-long shut-in times after multi-stage hydraulic fracturing stimulation. Field data indicate that in some wells extended shut-in period surprisingly increases the early time gas flow rate (Fakcharoenphol et al., 2014). As an example, Figures 1.1a and 1.1b respectively show the effects of extended well shut-in on early time water and gas production of a hydraulically

fractured well in Marcellus shale (Cheng, 2012). After fracturing treatment, the well was placed on production for a short period of time before it underwent a six-month long shut-in period. When the well was reopened, gas production rate increases and the water production rate decreases, significantly. The dominant mechanisms that improve gas rate and decrease water recovery are still poorly understood.

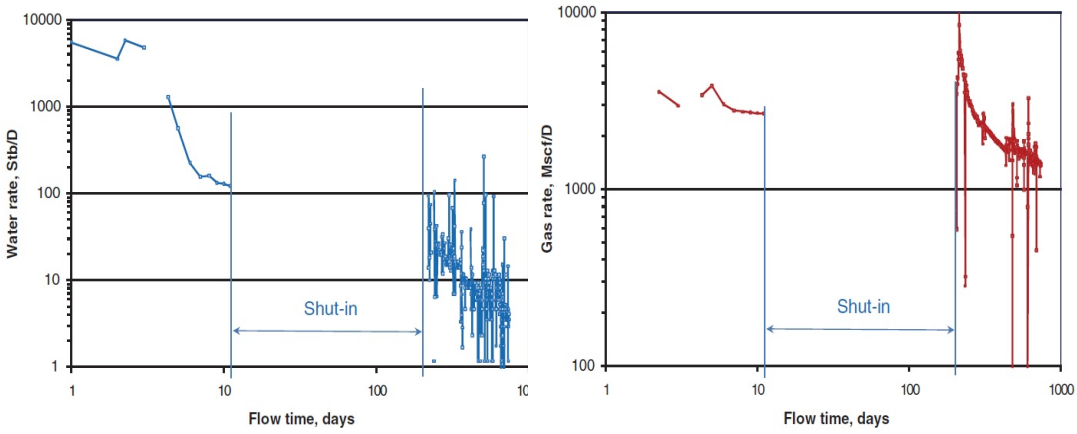

(a) (b)

Figure 1.1. Field production data of a Marcellus shale gas well (A) water production, (B) gas production. After six months of shut-in period, water rate decreases and gas rate increases (Cheng, 2012)

1.3.2 Salinity Profile of Flowback Water

Field data indicate that after hydraulic fracturing in the Horn River Basin and other gas producing shales, the concentration of dissolved salt in produced water significantly increases with time (Blaunch et al., 2009, Haluszczak et al., 2013). As an example, Figure 1.2 shows the chloride concentration in produced water after hydraulic fracturing treatment for several wells completed in the Marcellus shale. The questions are (1) whether the increase in salt concentration of flowback water is due to the dissolution of shale constituents or diffusion of the in situ brine in the injected water and, (2) what parameters and mechanisms control the salinity profile of flowback water.

1.4 Objective and Scope of Work

The overall objectives of this research is to investigate the dominant mechanisms that could explain (1) the observed behavior of early time water and gas production and (2) the increase in salt concentration of flowback water. Understanding the un-

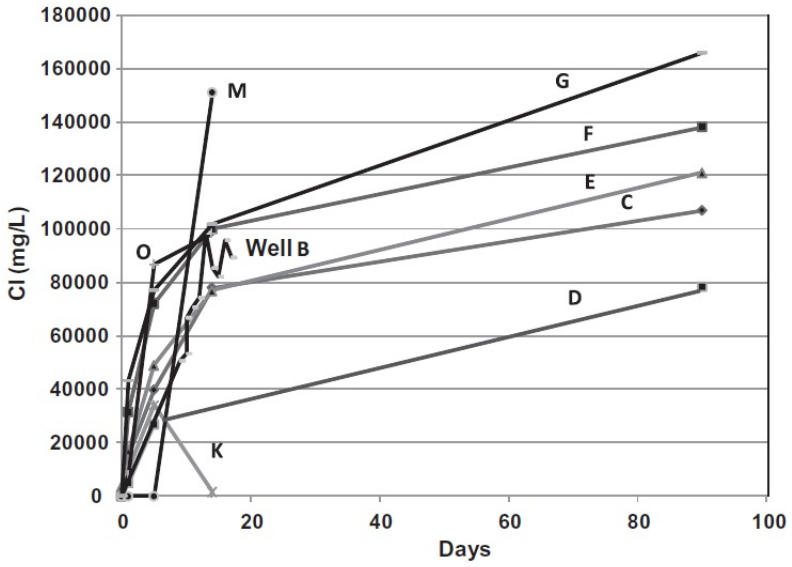

Figure 1.2. Chloride concentration in produced water vs. day after hydraulic fracturing treatment. Figure from Haluszczak et al. (2013) and data from Blaunch et al. (2009) and Hayes (2009)

derlying physics should lead to new insights that would explain the flow mechanisms and ultimately lead to the development of techniques to (1) optimize the fracturing and flowback operations and (2) characterize the created fracture network.

1.5 Thesis Organization

This study is divided into seven chapters. The outline and organization of these chapters are as follows:

Chapter 1 presents an introduction to unconventional gas resources and gas shales. In this chapter, we also describe the research objectives and scope of this work.

Chapter 2 presents the relevant literature including hydraulic fracturing stimulation, fracturing operation, flowback data analysis and fluid flow in low permeability reservoirs.

Chapter 3 presents a qualitative analysis of early time water and gas production and chemical data obtained from a pad of hydraulically fractured horizontal wells completed in the Horn River Basin.

Chapter 4 presents an experimental study to investigate the interactions between fracturing fluid and reservoir system during shut-in period.

Chapter 5 presents an experimental study to investigate the effects of initial

water saturation, sample expansion and depositional lamination on ion diffusion and liquid imbibition.

Chapter 6 presents numerical simulation study of flowback process to investigate the effects of extended shut-in time, the complexity of fracture network and capillary pressure on early time water and gas production.

Chapter 7 presents the conclusions and recommendations.

Chapter 2

Literature Review

In this chapter, we firstly reviewed the properties of the shale members related to this study. Then, the relevant literature including hydraulic fracturing stimulation, fluid flow in low permeability reservoirs, fracturing fluid flowback and effects of flowback efficiency on short term and long term production are reviewed.

2.1 Introduction to the Horn River Basin

The Horn River Basin is located in northeastern B.C., and is extended northward into the Northwest Territories (Figure 2.1). The areal extent of this basin is about 1.28 million hectares (Beaudoin and Shaw, 2009). Clays, fine siliceous (silica-rich) muds, and organic matter from dead plankton were deposited in the deeper and poorly oxygenated section of the Horn River Basin and were converted into shale deposits, over time. The shales have been sub-divided into, from the bottom up, the Evie, Otter Park and, Muskwa shales (Figure 2.2) and contain enough organic material to produce natural gas, economically (BC Minstry of Energy and Mines, 2011). Total thickness of the these shale members is approximately 160 to 180 meters (Novlesky et al., 2010). Some of the gas migrated into the Presquile barrier and was locally trapped in conventional oil and gas pools (National Energy Board, 2006). The substantial gas resources in the Horn River Basin made it the third largest North American natural gas accumulation discovered before 2010 (Graham, 2009). Table 2.1 shows the gas in place (GIP) and marketable gas for the shale formations of the Horn River Basin.

Figure 2.1. Location of the Horn River Basin and other unconventional resources recognized in British Columbia (BC Minstry of Energy and Mines, 2011)

Table 2.1. Gas in Place (GIP) and marketable gas for the shales of the HRB (BC Minstry of Energy and Mines, 2011)

Shale Formations	Gas in Place (GIP) (TCF)	Marketable Gas (TCF)
Muskwa	132	25
Otter Park	159	24
Evie	143	20
Total	434	69

2.1.1 Muskwa Shale

Muskwa is comprised of gray to black, radioactive, organic-rich, pyritic, siliceous shales, and is characterized on well logs by high gamma ray and high resistivity (BC Minstry of Energy and Mines, 2011). This shale member is overlain by silt-rich Fort Simpson formation. In the Horn River Basin, Muskwa is 30 m thick adjacent to the Presqu'ile barrier reef and thickens to over 60 m in the vicinity of the Bovie Lake Structure on the western side of the basin (BC Minstry of Energy and Mines, 2011). However, Muskwa thins considerably where Otter Park thickness reaches its maximum in the southeast corner of the Horn River Basin. Unlike Otter Park and

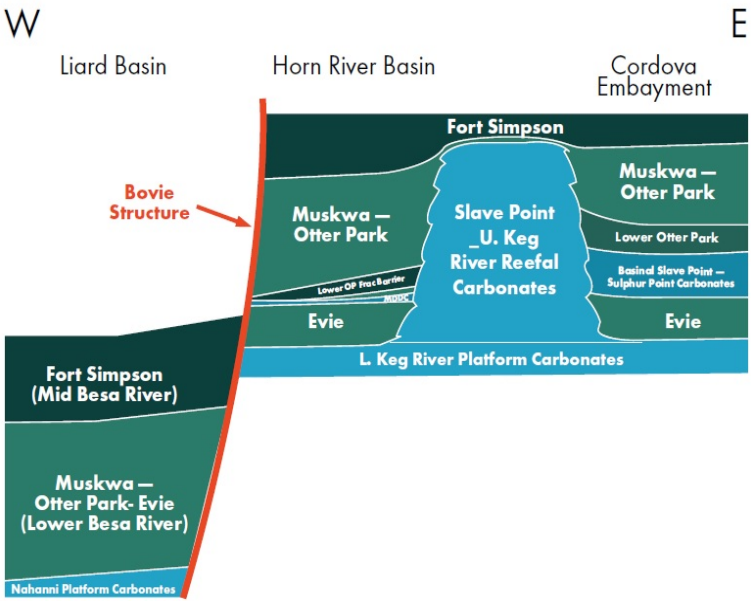

Figure 2.2. Cross section showing the Horn River Basin (Ross and Bustin, 2008).

Evie, Muskwa is not restricted to the Horn River Basin, and is present through the rest of northeastern British Columbia (Ross and Bustin, 2008).

2.1.2 Otter Park Shale

Otter Park is comprised of siliceous and organic-rich shales deposited at the depth of 2200 to 2700 m (Rogers et al., 2010). Otter Park Shale reaches a maximum thickness of over 270 m in the southeast corner of the Horn River Basin, where it consists of medium to dark grey calcareous shale with lower radioactivity and resistivity on well logs than Evie and Muskwa Shales. Otter Park thins to the north and west, and begins to include radioactive siliceous black shale beds (BC Minstry of Energy and Mines, 2011). Otter Park and Muskwa are generally connected with hydraulic fractures and wells completed in these formations are in production communication (Novlesky et al., 2010).

2.1.3 Evie Shale

Evie Shale consists of dark gray to black, radioactive, organic-rich, pyritic and siliceous shale. This unit can be recognized on well logs by relatively high gamma ray and high resistivity (BC Minstry of Energy and Mines, 2011). The uppermost part of the unit includes more silt and generally has low radioactivity and resistivity. In the Horn River Basin, Evie is over 75 m thick and thins westward to less

than 40 m thick in the vicinity of the Bovie Lake Structure (western margin of the basin). The Evie Shale overlies limestones and dolostones of the Lower Keg River Formation.

In this study we analyze flowback field data obtained from a well pad completed in the shale members of the Horn River Basin. We also conduct a series of imbibition and diffusion experiments on actual core samples collected from the same shale members.

2.2 Hydraulic Fracturing

Hydraulic fracturing is one of the most promising completion technologies for unlocking the potential of unconventional gas resources such as coalbed methane, tight gas and gas shale reservoirs (Figure 2.3). The first commercial fracturing treatment was performed in 1947 using gasoline-based napalm gel frac fluid (Howard and Fast, 1970). Approximately 20 years later, guar-based crosslinked fluids were introduced and became the basis of the fracturing fluid (Veatch et al., 1989). By the the 1980s, it was common for operators to inject a great amount of proppant (more than 2 million lbm) using 60 ppgt guar crosslink gel (Pearson et al., 1988). In 1997, Mayerhofer et al. (1997) claimed that proppants are not required to have a successful and efficient hydraulic fracturing treatment. This study laid the foundation of slick water treatment which is sometimes referred to as a waterfrac or riverfrac (Palisch et al., 2010, Schein, 2005). Nowadays, slick water is commonly used as the primary fracturing fluid with low proppant concentrations to stimulate low permeability reservoirs (Cheng, 2012). Slick water treatments are successful because of (1) the necessity of cost cutting (2) efficient cleanup and less formation damage after hydraulic fracturing particularly in the low permeability reservoirs and (3) the creation of more complex fractures. (Cipolla et al., 2009, Fredd et al., 2001, Mayerhofer et al., 1997, Palisch et al., 2010, 2005, Schein, 2005, Warpinski et al., 2005).

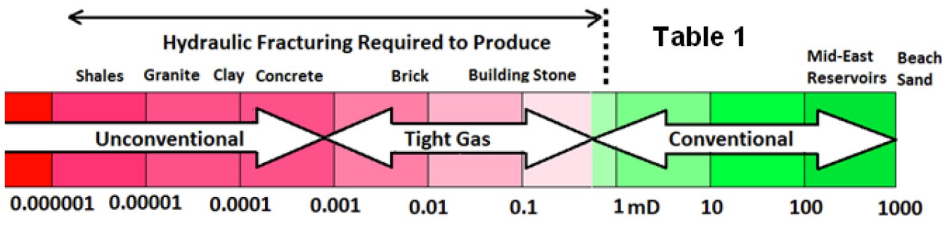

Figure 2.3. Permeability range of producing formations and where fracturing is required (King, 2012)

A hydraulic fracture is created by pumping a great amount of fracturing fluid into the wellbore to increase downhole pressure at the target shale formation to exceed the fracture gradient of the rock (Harper, 2008). The rock cracks and the fracture fluid continues further into the rock, extending the crack. Fracture vertical growth may extend up to a few hundred feet or more above the pay zone, where there are no natural upper rock frac barriers immediately over the pay zone. The fracture growth is also limited by increasing fracturing fluid loss into the surrounding permeable rock (King, 2012). Fracturing fluid leakoff may result in formation matrix damage, adverse formation fluid interactions, or alter fracture geometry and thereby decrease production efficiency (Penny et al., 1985). Furthermore, natural fractures are present in nearly all gas productive shales (King, 2010). Hydraulic fractures can intercept and reactivate pre-existing natural fractures and create a complex fracture network. Some researchers observed that increasing the fracturing fluid injection rate in small steps would often preferentially open the natural fracture system, while higher rates would form more planar hydraulic fractures (Gale et al., 2007, Overbey et al., 1988, Yost and Overbey, 1989). Micro-seismic data (Figure 2.4) also indicates that the intersection of natural fractures with hydraulic fractures can create a larger stimulated area.

2.3 Shut-in Phase

Some shale gas and oil wells undergo month-long shut-in times after multi-stage hydraulic fracturing stimulation. Extended shut-in time can result in extensive fracturing fluid imbibition into rock matrix which can severely damage absolute permeability of the reservoir through clay swelling and clay fines dispersion (Scott et al., 2007). Furthermore, in low-permeability reservoirs, capillary pressure can be several hundreds psi (as high as 2000 psi) (Holditch, 1979, Penny et al., 2006) and therefore, fracturing fluid imbibition results in fluid retention (Bazin et al., 2010, Dutta et al., 2014, Economides and Martin, 2007). This process, called water blocking, causes the relative permeability of gas to be reduced and thus decreases the gas production, dramatically (Shaoul et al., 2011). On the other hand, Wang et al. (2012) investigated the impact of each damage mechanism and concluded that a higher fracturing water recovery does not always result in a higher gas production. Furthermore, previous simulation studies (Agrawal and Sharma, 2013, Cheng, 2012, Settari et al., 2002) and field observations (Adefidipe et al., 2014, Ghanbari et al.,

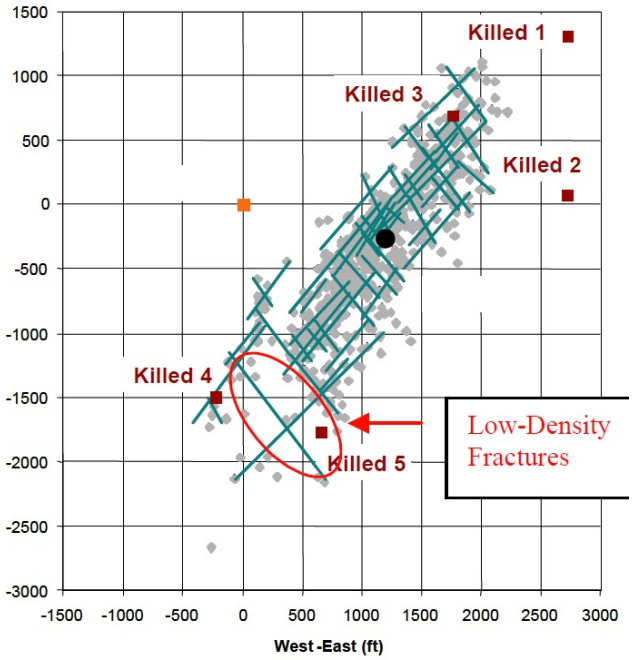

Figure 2.4. Plan view of fracture structure plot from one fracturing treatment in Barnett shale, showing the size and complexity of created fracture systems in the hydraulic (NE SW) and natural fractures (NW SE) orientations (Fisher et al., 2002)

2013) show that effective imbibition and extended shut-in can improve early time gas production.

2.4 Fracturing Fluid Flowback Phase

After hydraulic fracturing operation, the clean-up process of fracturing fluid takes place by opening the well for flowback. In other words, fracturing fluid flowback is referred to the first few hours to weeks of the well's productive life immediately following the cessation of the hydraulic fracturing operations and soaking period (Crafton, 2010). Many operators reported unpredictable production performance during flowback phase. However, there is clear evidence that shows initial and ultimate performance of the fractured wells are related to flowback operation (Crafton et al., 2009). Careful management of flowback process is critical to (1) decrease damage to the stimulated reservoir volume (SRV) (Crafton, 2008, 2010) (2) improve well clean-up (Crafton, 1998) and (3) obtain accurate physical and chemical data measurement. The measured flowback data can be used to characterize the reservoir and created fracture network due to hydraulic fracturing operation.

2.4.1 Volumetric Analysis of Flowback

During hydraulic fracturing, a great amount of water-based hydraulic fracturing fluid with low proppant concentration is injected into the target formation to create multiple fractures and increase the contact surface between the wellbore and reservoir (Holditch and Tschirhart, 2005, Palisch et al., 2010). However, only a small fraction of injected fluid, typically 10 to 20%, can be recovered during the flowback phase (Cheng, 2012, King, 2012). The amount of fracturing fluid recovery in gas shales depends on the reservoir properties, the type of fracturing fluid and the frac design (King, 2010). Cheng (2012) investigated the effects of capillary pressure, shut-in time and relative permeability on water saturation in fractures and matrices. The author concluded that imbibition of fracturing fluid is the primary mechanism for fracturing fluid loss and inefficient water recovery. This conclusion is also supported by several imbibition experiments conducted on samples from gas shale reservoirs (Dehghanpour et al., 2013, 2012, Lan et al., 2014b, Makhanov et al., 2014, Roychaudhuri et al., 2011). Fan et al. (2010) stated that wells with less water recovery have better early gas production rates. The authors explained this behavior by the complexity of created fracture network. The more complex fracture network, the lower water recovery and higher early time gas production. Parmar et al. (2014, 2012, 2013) investigated the effects of gravity segregation on load recovery and concluded that a significant portion of fracturing fluid could be retained in the vertical fracture below the horizontal wells due to gas fingers and poor sweep efficiency.

2.4.2 Rate and Pressure Transient Analysis of Flowback

Production data analysis of hydraulically stimulated tight reservoirs has been a promising method for characterizing fracture network in the past decade. Fisher et al. (2005) characterized the created fracture network using fracture-mapping technologies and presented correlations between production response and various fracture parameters. Several researchers (Behmanesh et al., 2013, Cheng et al., 2009, Clarkson et al., 2013, Medeiros et al., 2008, Samandarli et al., 2012, Song and Ehlig-Economides, 2011) employed rate transient analysis (RTA) and pressure transient analysis (PTA) methods for describing reservoir and/or hydraulic fracture properties for stimulated wells. Many authors have also proposed simplified analysis equations that can be used to estimate various fracture parameters such as hydraulic fracture half-length and fracture-matrix contact area (Ali et al., 2013, Bello, 2009,

Siddiqui et al., 2012).

Flowback rate and pressure transient analysis has been recently used to complement the production data analysis for characterizing the induced fracture network. Several investigators (Abbasi et al., 2012, 2014, Crafton, 2010, Crafton and Gunderson, 2006) have proposed analytical models for analyzing high frequency rate and pressure data measured during early-time (single phase water flow) of flowback operations. Clarkson et al. (2013) developed two-phase flowback and determined fracture parameters such as effective fracture half-length and fracture permeability. More recently, Ezulike and Dehghanpour (2014d) and Ezulike and Dehghanpour (2014b) extended the existing linear dual-porosity model and developed an interpretation workflow for analyzing flowback data to (1) estimate effective fracture half-length and volume of interconnected secondary fracture (2) evaluate flowback performance and (3) forecast hydrocarbon recovery.

2.4.3 Chemical Analysis of Flowback

An interesting observation in the Horn River Basin and some other gas producing shales is that the concentration of dissolved salt in flowback water significantly increases with time (Blaunch et al., 2009, Pritz and Kirby, 2010, Rowan et al., 2011). Some researchers concluded that the increase in salts concentration of flowback water is due to the dissolution of shale constituents in injected water and/or diffusion of in situ brine in the injected water (Blaunch et al., 2009, Gdanski et al., 2010, Haluszczak et al., 2013). Similar to imbibition rate, the ion diffusion rate from the shale sample into water depends on porosity, permeability, contact surface and clay content (Ballard et al., 1994, Zolfaghari et al., 2014b).

Flowback chemical analysis has been used for differentiating formation water from fracturing water and evaluating the true load recovery. Woodroof et al. (2003), and Asadi et al. (2008) presented chemical analysis models for monitoring and optimizing fracturing fluid cleanup. Gdanski et al. (2007) incorporated a chemistry layer to a 2-D numerical simulator. This simulator was used to history-match the composition of flowback fluid. More recently, Bearinger (2013) analyzed flowback salt concentration data from hydraulically fractured horizontal wells completed in the Horn River Basin. This comparative field study infers that the architecture of induced fracture network can affect the load recovery and the shape of salt concentration-cumulative produced water profile. Bearinger (2013) explained the observed trends

in flowback salt concentration profiles by hypothesizing that the water recovered from induced hydraulic fractures has a different chemical signature than the water recovered from reactivated secondary fractures.

2.5 Modeling of Fluid Flow in Fractured Low Permeability Reservoirs

Modeling fractured reservoirs requires a special treatment because there is significant thermodynamic disequilibrium between low permeability matrix and high permeability fracture network. When fractured rocks are subjected to pressure change, the thermodynamic disequilibrium propagates rapidly through fracture network but only slowly into tight matrix. Therefore, there is a considerable pressure difference in the fractures and matrix. To handle this problem, Barenblatt et al. (1960) developed the double-porosity conceptual model for fluid flow in fractured rocks. Later, Warren and Root (1963) introduced this concept to the petroleum literature to describe the behavior of naturally fractured reservoir. In this model, the fractured rocks are divided into 1) primary porosity or matrix continuum, which represents highly interconnected small pores and 2) secondary porosity or fracture continuum, which represents the fracture network, see Figure 2.5.(a). Matrix and fracture interactions are controlled through transfer functions. Kazemi et al. (1976) was the first researcher to merge the dual porosity model with a numerical simulation model. The simulating grid blocks consist of number of matrix blocks separated by inter-connected fractures. In this model, it was assumed that each continuum is in thermodynamics equilibrium.

Although, the variation of thermodynamic state in the fracture continuum can be typically neglected, it can be significant in the matrix continuum. In the double-porosity model, the rate of fluid mass transfer from porous matrix block to fractures is approximated by the quasi-steady-state equation (Bai and Elsworth, 1993) which can handle problems involving single-phase (Moench, 1983) and high permeable matrix rock such as conventional sandstone reservoirs. However, in low permeability formations such as shale reservoirs, the period of transient flow between matrix and fractures can be very long. Furthermore, the thermodynamic conditions may vary strongly over the small distances in the vicinity of fractures (Pruess, 1985). To solve this problem, Pruess (1985) extended the double-porosity method and introduce multiple interacting continua (MINC) model, see Figure 2.5.(b). The MINC model

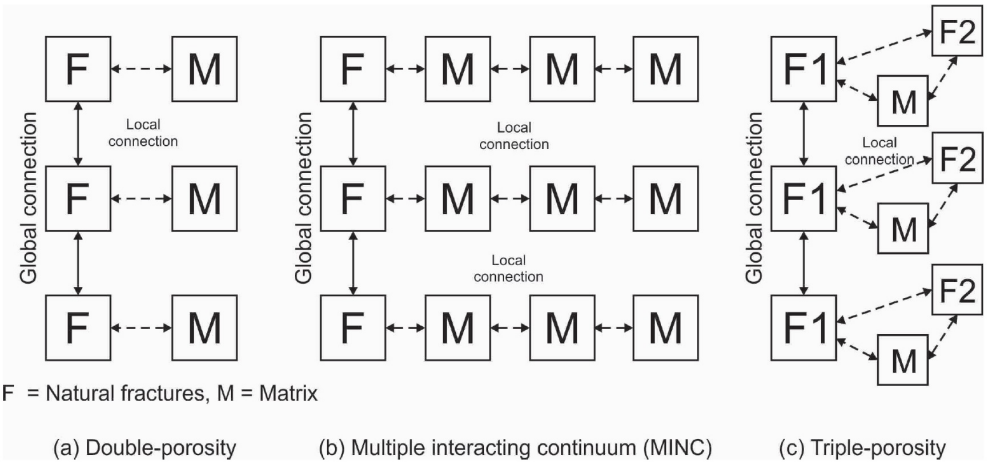

Figure 2.5. Schematic of different concepts for handling fracture-matrix interaction (Fakcharoenphol, 2013)

assumes that the change in the thermodynamic conditions of fluid flowing is mainly controlled by the distance from the closest fracture. Therefore, this model discretizes the fractured rocks into a sequence of nested volume elements. The outer matrix element is connected to both fractures and other inner matrix elements. In the MINC model, each volume element has a definite thermodynamic state (Pruess, 1985).

Hydraulic fracturing in gas shale reservoirs has often resulted in complex fracture network, as evidenced in microseismic monitoring (Fisher et al., 2002). Furthermore, fracture distribution studies of outcrop shows a wide range fracture width and length (Kazemi et al., 2005) and fracture length can be varied from centimeters to hundreds of meters. Therefore, the hydraulic fractures model used in industry today for simulating bi-wing planar fractures in a conventional reservoir are not appropriate for simulating fracturing treatment in the gas shale reservoirs with complex fracture network. To overcome this problem, Wu et al. (2004), Ezulike and Dehghanpour (2014a), Ezulike and Dehghanpour (2014c) and Kazemi et al. (2005) introduced a triple-porosity model including large-scale fractures (F1), small-scale fractures (F2), and tight rock matrix (M), see Figure 2.5(c).

Chapter 3

Volumetric and Chemical Analysis

This chapter presents a qualitative analysis of early time water and gas production and chemical data obtained from a pad of hydraulically fractured horizontal wells completed in the Horn River Basin. First, we present the well pad description and the summary of completion design used for different wells. Second, we categorize the wells based on the load recovery and early time gas production and present the possible fracture systems for each group. Then, we present the diagnostic gas and water ratio plots of three different wells. Finally, we present the salinity profiles of flowback water and discuss the relation between the created fracture network and the change in salinity of flowback water.

3.1 Well Pad Description

Flowback water and gas production data, are collected from a pad of 18 hydraulically fractured horizontal wells completed in Muskwa (MU), Otter Park (OP) and Evie (EV) formations. Three wells are placed at the right side of the pad and three wells at the left side in each formation. Figure 3.1 shows the layout of these wells. In each formation, three wells are completed on the right side and another three wells are completed on the left side of the well pad. This results in the total of six wells in each formation, and the total of 18 wells for the pad. Table 3.1 presents the summary of completion design for these wells.

The horizontal sections of all of the wells are drilled parallel to the minimum horizontal stress direction. There is a major natural fracture set that strikes close to the maximum horizontal stress direction. Other mostly healed fracture sets are at

intermediate angles to the principal horizontal stresses. The fracturing fluid used for the treatment is the same for all wells and mainly consists of fresh water. However, the total injected volume is different for each well. During the flowback operation, the cumulative water and gas production were measured and the salinity and Barium concentration of produced water was measured frequently.

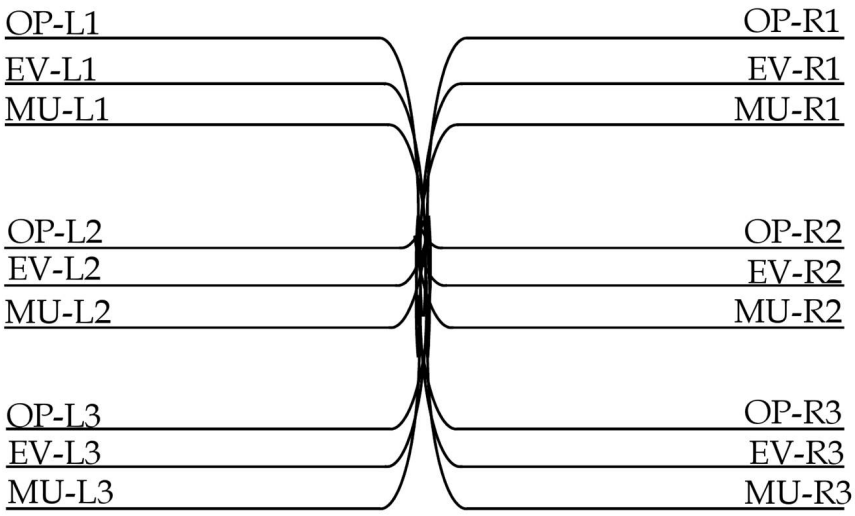

Figure 3.1. Layout of the well pad drilled and completed in the Horn River Basin. Total of eighteen wells were drilled, nine wells on the right side of the pad and nine wells on the left side of the pad

3.2 Volumetric Analysis of Early Time Production Data

The volumetric analysis of early time production data is presented in two sections. In the first section, we compare the early time flowback efficiency and cumulative gas recovery after 72 hours and classify the wells into different groups. In the second section, we compare the cumulative water and gas production versus time to identify different flow regimes.

3.2.1 Final Water Recovery During the Flowback Period

Figure 3.2 shows a comparative graphical presentation of cumulative gas production and flowback efficiency of different wells completed in Muskwa, Otter Park and Evie formations. Cumulative water recovery after 72 hours is considered here because the majority of fluid flowback occurs during the first 72 hours of production (Asadi et al., 2008). Based on cumulative gas production and flowback efficiency (Figure 3.2), the wells can be classified into two groups:

Table 3.1. Completion design summary of a well pad of eighteen wells completed in the Horn River Basin

	Well Name	Stage Spacing (m)	Horizontal Well Length (m)	Fracture Stages	Total Injected Volume (m^3)
Muskwa	MU-R1	40	2317	18	51523.0
	MU-R2	25	2300	18	54231.6
	MU-R3	25	2296	18	51153.1
	MU-L1	25	2315	16	45392.1
	MU-L2	25	2314	17	49543.0
	MU-L3	25	2310	16	45533.0
Otter Park	OP-R1	40	2319	18	51753.5
	OP-R2	40	2314	19	55338.9
	OP-R3	25	2297	19	32619.5
	OP-L1	25	2315	17	47516.0
	OP-L2	25	2312	17	48361.0
	OP-L3	25	2312	19	42360.0
Evie	EV-R1	40	2312	18	60326.1
	EV-R2	40	2313	19	100000.0
	EV-R3	40	2305	20	63677.9
	EV-L1	25	2314	21	53349.5
	EV-L2	25	2311	20	51417.8
	EV-L3	25	2307	20	51561.8

- Low water and high gas production. Wells OP-R2, OP-R3, OP-L3, EV-L1, EV-L3 and EV-R3 belong to this group.
- High water and low gas production. Wells MU-R2, MU-R3, MU-L2, MU-L3 and OP-L1 belong to this group.

This classification is more pronounced when we plot cumulative gas production and flowback efficiency for each well, as shown in Figure 3.3.

Proposed Fracture Systems

Low water and high gas production To explain the low water and high gas production of these wells, we consider a complex fracture system similar to what was assumed by Fan et al. (2010). Hydraulic fracturing can create a complex fracture system that consists of hydraulic fractures (primary fractures) and induced and/or reactivated/active natural fractures (secondary fractures (Figure 3.4a). The existence of secondary fractures in the Horn River Basin is also noted by Rogers et al. (2010). At the end of treatment, the primary fractures are filled with the injected proppants and water however; the secondary fractures are mainly filled with wa-

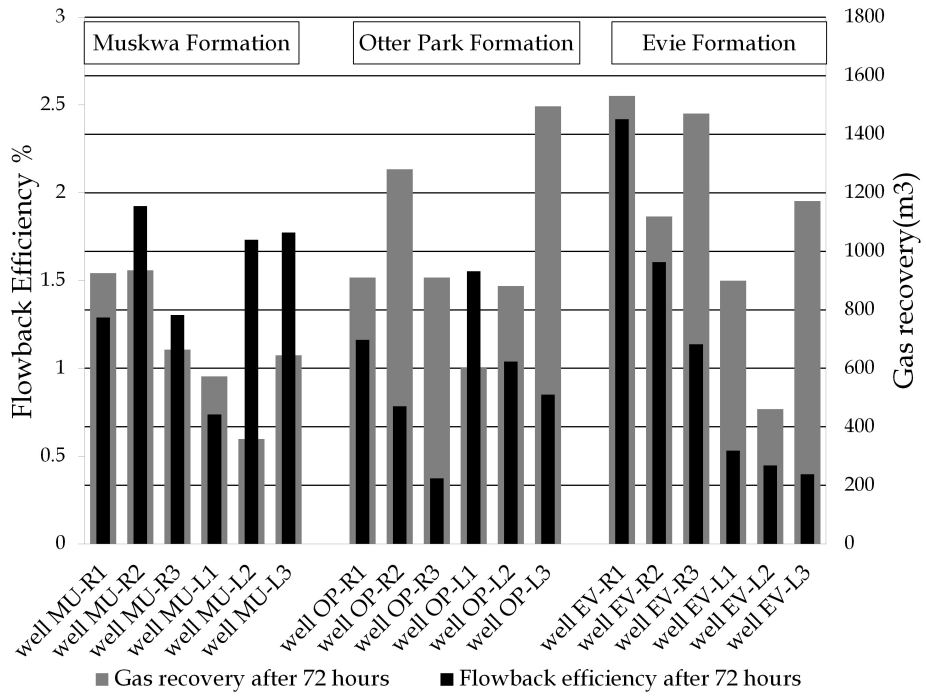

Figure 3.2. Comparison of flowback efficiency and cumulative gas recovery 72 hours after placing the wells on flowback

ter. Therefore, aperture size of primary fractures is higher than that of secondary fractures. After putting the fractured well on flowback, the majority of water remaining in the primary fractures flows back toward the well due to high fracture conductivity and pressure draw down. However, lower fracture conductivity and pressure draw down of the secondary fractures result in water trapping in these fractures. Furthermore, the tortuous nature of the secondary fractures can also increase the possibility of water trapping. The water retained in fractures can imbibe into the matrix and spread away from fracture face deep into the reservoir due to capillary pressure, water adsorption by clay minerals and chemical osmosis (Chenevert, 1970a, Cheng, 2012, Dehghanpour et al., 2013, Hale et al., 1993, Yeung and Mitchell, 1993). The water imbibition can also result in counter-current expelling of gas from matrix into the fractures during shut-in period (Dehghanpour et al., 2012). The expelled gas from matrix (free gas) accumulates in the primary and secondary fractures and flows back with water during first hours of flowback. Logically, as the complexity of fracture network increases, the water trapping and counter current imbibition rate increase that can potentially result in low flowback efficiency and high early gas production. Furthermore, pre-existing natural fractures can host gas

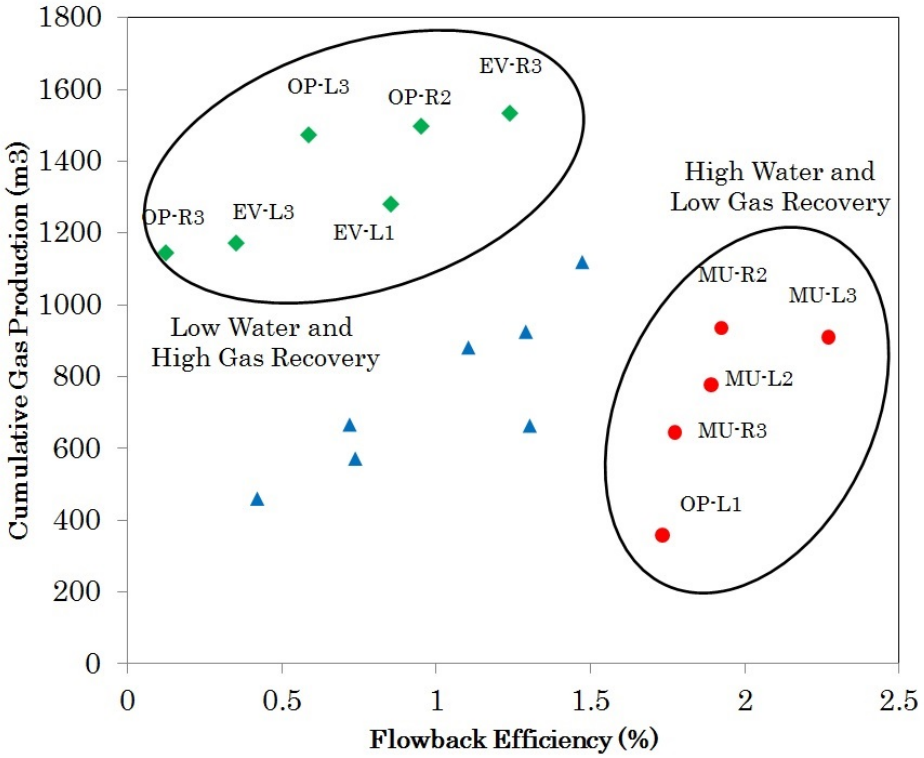

Figure 3.3. The plot of cumulative gas production versus flowback efficiency for wells with (1) high water and low gas recovery and (2) low water and high gas recovery

before fracturing. After hydraulic fracturing and during the shut-in period, this gas can move to the primary fractures mainly due to pressure draw down and gravity segregation. It is also anticipated that the portion of vertical fractures below the horizontal well hosts more water compared with the portion above the well, due to the gravity segregation (Parmar et al., 2014, 2012, 2013).

High water and low gas production One explanation for high water recovery and low gas production can be that the induced fracture network in this case is less complex than that in the previous case. Figure 3.4b schematically illustrates the assumed simple fracture scenario. Hydraulic fracturing in these wells may generate longer primary fractures with less amount of secondary fractures. Therefore, the injected water mainly accumulates in the primary fractures and can be produced more easily. Furthermore, when the complexity of fracture system decreases, the created contact surface decreases, accordingly. As a result, the extent of counter-current water imbibition decreases. In other words, compared with the previous case, here before opening the well there is less free gas inside the fractures and

wellbore, due to a reduced interface available for counter-current imbibition.

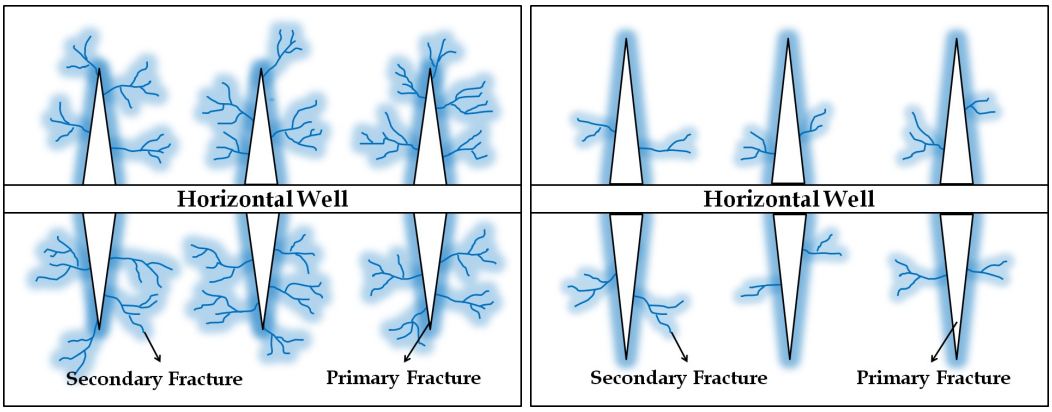

(a) (b)

Figure 3.4. Schematic illustration of the proposed complex fracture system (a) and simple fracture system (b). Complex fracture system has more secondary fractures which increase the water loss and gas production.

3.2.2 Water and Gas Recovery During Flowback Period

Water and Gas Rate Profiles Figures 3.5a, 3.5c and 3.5e show water and gas flow rate of wells MU-L2, OP-L3 and EV-L1 completed in Muskwa, Otter Park and Evie formations. The production profiles of these wells can be divided into two regions. In the first region, the water flow rate ramps up. In the second region, water and gas production gradually winds down as a result of fracture depletion. Furthermore, gas rate profiles of theses wells show an immediate gas breakthrough. This immediate breakthrough usually does not occur in tight oil and gas wells, where there is an initial period of single-phase water flow (Abbasi et al., 2012, 2014). The immediate breakthrough is mainly due to 1) an extended shut-in period (around 2 months) for this particular well pad, 2) the possibility of strong counter-current water imbibition into the Horn River shales (Dehghanpour et al., 2013, 2012, Makhanov, 2013), and 3) the initial gas in the existing active natural fractures as discussed above.

Diagnostic Plots of Gas and Water Ratio Figure 3.5b, 3.5d and 3.5f show gas water ratio (GWR) versus cumulative gas production plots of the same wells. A similar diagnostic plot was also used by Ilk et al. (2010) for flowback analysis. The shape of gas water ratio profiles of this well and other wells completed in this pad show two general signatures:

Signature 1. This signature can be identified by a negative slope ($\frac{dGWR}{dGp} < 0$) of gas water ratio versus cumulative gas production plot. This signature is dominant during the early time flowback and is followed by signature 2.

Signature 2. This signature can be identified by a positive slope ($\frac{dGWR}{dGp} > 0$) of gas water ratio versus cumulative gas production plot. Signature 2 mostly occurs at the late time scale of flowback operation.

Signature 1 shows the initial drop of gas and water flow rate ratio with time. This signature is correlated to region 1 of gas and water flow rate plots and can be an indication of water and free gas depletion from fractures. After placing the well on flowback, the fractures which are mainly filled with water and free gas deplete with the help of pressure draw down and gas expansion. However, it is also anticipated that gravity can also accelerate water production during the first hours of flowback operation. Gravity forces accelerate water transport from the portion of vertical fractures located above the horizontal well to the primary fractures. As a result, the water saturation and relative permeability of water in the primary fractures and water flow rate at the surface increase with time. The increase in water flow rate can be explained mathematically using darcy equations for gas and water ratio: 3.1

$$GWR = \frac{q_g}{q_w} = \frac{\mu_w}{\mu_g} \frac{k_{rg}}{k_{rw}} \frac{dp_g}{dp_w} \tag{3.1}$$

Where GWR is the gas and water flow rates ratio, q is the flow rate, μ is the viscosity, k_r is the relative permeability and dp is the pressure difference. Assuming equal pressure differences for both water and gas and constant ratio between water and gas viscosity, the GWR mainly depends on relative permeabilities. Therefore, the increase in relative permeability of water results in negative slope in GWR plots. It should be noted that we did not observe this negative slope in the flowback data of the fractured horizontal wells completed in the tight oil and tight gas reservoirs. The most probable explanation can be that the fractures in tight oil wells are dominantly filled with water as we do not see immediate oil breakthrough in these reservoirs and there is a short period of single phase water flow (Abbasi et al., 2012, 2014).

Signature 2 which is immediately observed after the signature 1 shows the increase in the gas and water ratio with time. This signature is correlated to Region 2 of water and gas rate plots and indicates water displacement by the gas introduced from the matrix (Ilk et al., 2010). The depletion of water from fractures decreases

the water saturation in the fractures and water production at the surface. The produced water from fractures is consequently replaced by the gas introduced from matrix into the fractures and stabilizes the gas flow rate. Accordingly, the decreasing water flow rate and stable gas flow rate result in signature 2 observed in GWR plots (Figure 3.5b, 3.5d and 3.5f).

In this Chapter 6, we present numerical simulation study of flowback process to investigate the effects of fracturing fluid imbibition into rock matrix on early time water and gas production. We also conduct a comprehensive sensitivity analysis to investigate the effects of reservoir and operational parameters such as shut-in time, capillary pressure and the complexity of created fracture network on early time water and gas production.

3.3 Chemical Analysis of Production Data

Change in Salt Content of Flowback Water Figure 3.6 shows the variations in the total dissolved solid (total salinity) of flowback water versus time for wells MU-R1, OP-R1 and EV-L1 completed in Muskwa, Otter Park and Evie formations, respectively. The salinity profiles for the other wells completed in the well pad are presented in Appendix A (Figures A.1, A.2 and A.3). The salinity profiles of MU-R1 and OP-R1 initially show a gradual increase and then reach a plateau at around 40000 ppm. However, the salinity profile of EV-L1 keeps increasing even after 70000 ppm.

The mineralogy of the reservoir rock and the composition of formation water are the dominant parameters controlling the chemistry and the salinity of flowback water. Interaction of injected water with highly saline formation water and minerals can significantly increase the flowback water salinity (Blaunch et al., 2009). Moreover, it is also believed that the change in salinity profiles of flowback water may reflect the change in aperture size and nature of the fractures hosting the produced water (Bearinger, 2013). The gradual increase in salinity profile of EV-L1 as opposed to those of MU-R1 and OP-R1 may indicate that the stimulated fracture network for EV-L1 is more dendritic than that for MU-R1 and OP-R1. In simple, the early water is recovered from the newly formed hydraulic fractures (primary fractures) that have an aperture size higher than that of reactivated natural fractures (secondary fractures). Therefore, salt concentration in the primary fractures with a low surface to volume ratio is expected to be lower than that in the sec-

ondary fractures with a relatively higher surface to volume ratio (Zolfaghari et al., 2014a). When the flowback process proceeds, the water from secondary fractures with a relatively higher salt concentration will be produced. This hypothesis is also in agreement with the proposed fracture systems in section 3.2.1. Well EV-L1 with a more complex fracture system shows a higher increase in salinity profile compared with wells MU-R1 and OP-R1.

Changes of Barium Concentration Figure 3.7 shows the change in concentration of barium versus time for wells MU-R1, OP-R1 and EV-R1 completed in Muskwa, Otter Park and Evie formations, respectively. The barium concentration profiles for the other wells completed in the well pad a re presented in Appendix B (Figures B.1, B.2 and B.3). The rise in the barium concentration of the flowback water was also observed in Marcellus shales (Blaunch et al., 2009). Interestingly, barium profiles of these wells are relatively parallel to their salinity profiles.

There is still debate over the sources of barium identified in flowback water. Barium can originate from the alteration of sediment-bearing rocks as this can release abundant amount of Ba^{2+} (Aloisi et al., 2004). Furthermore, precipitated salt crystals on the surfaces of natural fractures can be an additional source of barium. Zolfaghari et al. (2014b) analyzed the surfaces of the natural fractures for samples obtained from lower Keg River formation (located beside the Evie formation) and observed a notable concentration of barium on the surfaces of the natural fractures (Figure 3.8).

Barium can also mix with sulfate and generate barium sulfate scale deposition which reduces barium concentration in flowback water (Mackay et al., 2003). However, the chances of scale deposition is low in the studied wells because of 1) high reservoir temperature, 2) low sulfate concentration and 3) high connate water salinity (Dresel and Rose, 2010, Mackay et al., 2003, Todd and Yuan, 1992).

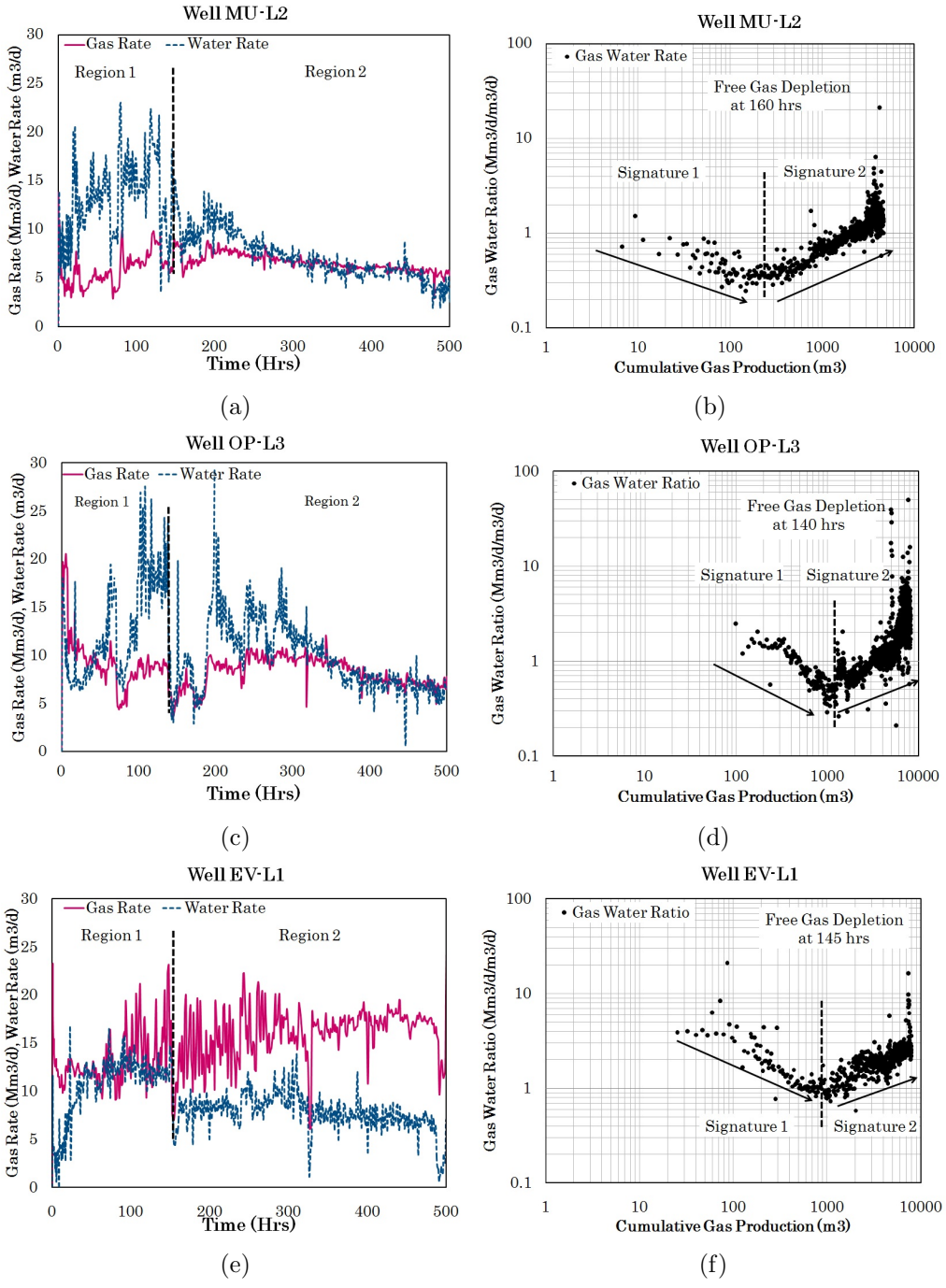

Figure 3.5. Water and gas flow rate vs. time (a, c and e) and GWR vs. cumulative gas production (b, d and f) of wells MU-L2, OP-L3 and EV-L1 completed in Muskwa, Otter Park and Evie formations.

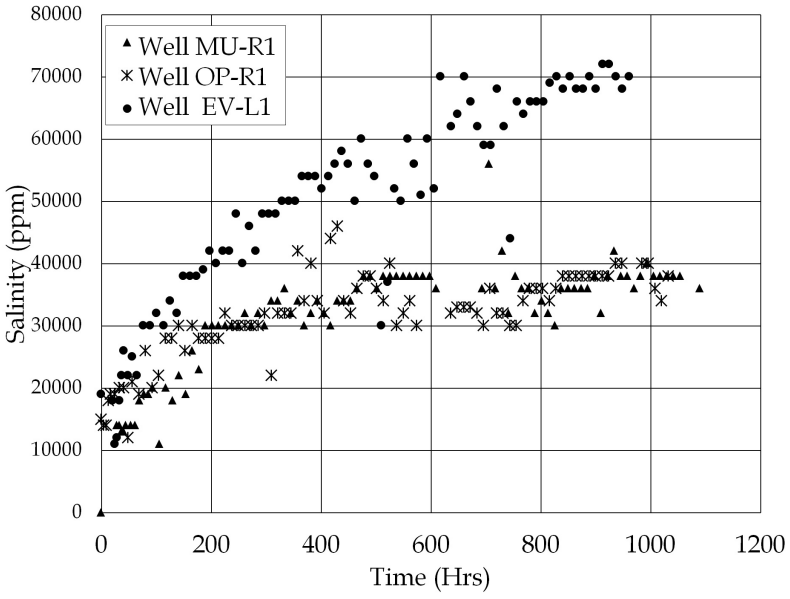

Figure 3.6. Comparison of flowback salt concentration for wells M-R1, OP-R1 and E-R1.

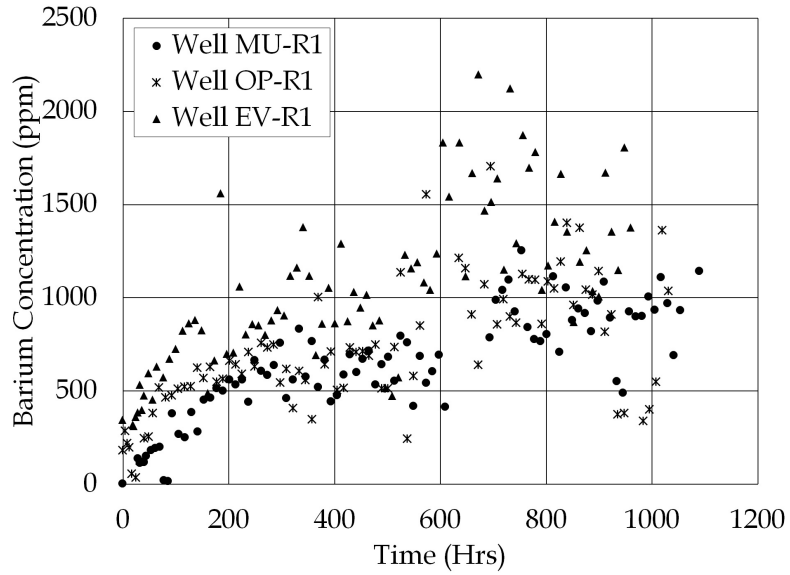

Figure 3.7. Comparison of Barium concentration in flowback water for wells M-R1, OP-R1 and E-R1.

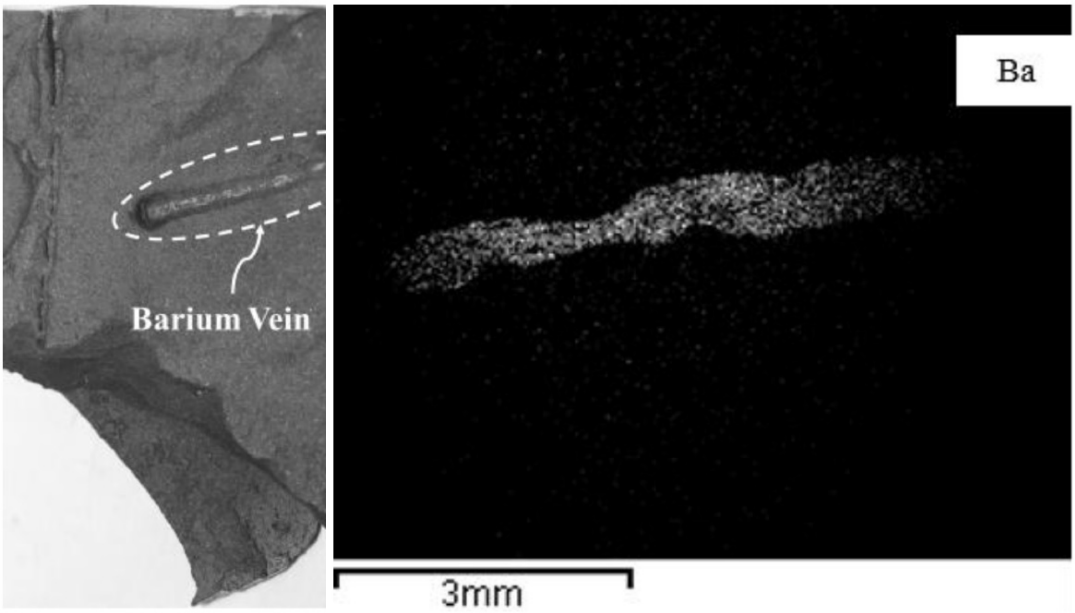

(a) (b)

Figure 3.8. (A) Pictures of barium vein found on the surface of a natural fracture for a sample obtained from Lower Keg River formation (B) the corresponding barium map from SEM-EDX analysis of the barium vein (Zolfaghari et al., 2014b)

Chapter 4

Salt Diffusion and Water Imbibition

To this end, we analyzed the early time water and gas production and chemical data obtained from wells completed in the Horn River Basin. This chapter complements our field data analysis and investigates the interactions between fracturing fluid and reservoir system during shut-in period. The objectives of this chapter are to 1) understand the parameters that control ion diffusion rate from rock into fracturing fluid, 2) understand whether the fracturing fluid imbibition is a possible reason for low water recovery or not? 3) investigate the possible correlation between ion diffusion and water imbibition rates, and 4) understand the origin of highly saline water produces during flowback phase.

4.1 Experiments

A set of diffusion/imbibition experiments are conducted on shale samples from Fort Simpson, Muskwa and Otter Park formations. We measure and compare the spontaneous water imbibition rate into shale samples. We also monitor the ion diffusion rate from shale samples to water using an electrical conductivity meter, during imbibition process. At the end, we did an elemental analysis using Inductively Coupled Plasma (ICP) and Automated Ferricyanide methods to quantify different types of ions in the water.

4.1.1 Materials

The experimental materials used for the imbibition/diffusion tests include fluid and shale samples .

Fluid Deionized water was used for imbibition/diffusion tests. The density and viscosity of deionized water are 1.0 (g / cm3) and 0.9 (cp), respectively.

Shale Samples A total of three shale samples were selected from the cores of two wells completed in the Horn River shales. The samples are classified into three sections of Fort Simpson (FS), Muskwa (M) and Otter Park (OP). These samples are not preserved and the formation water was vaporized after coring. However, the dissolved solutes in the formation water still remain in the pore space after vaporization. Before the experiments, the samples were intact and we did not observe any microfractures. The physical properties of these samples are listed in Table 4.1. The average concentration of different minerals determined by x-ray diffraction (XRD) analysis is given in Table 4.2. It should be noted that the XRD analysis is performed on the limited number of shale samples. However, due to heterogeneity, mineralogy can significantly change within each shale member. Therefore, average mineral concentration presented in Table 4.2 is just used for a qualitative explanation.

Table 4.1. Mass, average depth ,cross sectional area, and thickness of cores used in experiments

Formation	Depth(m)	Mass(g)	Area(cm^2)	Thickness(cm)
Fort Simpson	1757	256.247	78.5	1.6
Muskwa	1786	209.945	78.5	1.8
Otter Park	2629	202.776	78.5	1.4

Table 4.2. Average mineral concentration (wt %) of the three shale sections determined by x-ray diffraction

	Fort Simpson	Muskwa	Otter Park
Calcite	0.5 ± 0.4	0.9 ± 0.5	4.4 ± 0.2
Quartz	29 ± 1.3	45 ± 1.7	60.8 ± 1.2
Dolomite	2.7 ± 0.3	1.9 ± 0.3	2,6 ±0.2
Chlorite IIb2	6.5 ± 0.8	0	0
Illite 1Mt	55.4 ± 1.7	43.0 ± 1.7	25.7 ± 1.3
Plagioclase albite	4.1 ± 0.5	5.2 ± 0.5	3.7 ± 0.4
Pyrite	1.7 ± 0.2	4.0 ± 0.2	2.8 ± 0.1
Matrix density	2.747	2.79	2.78

4.1.2 Test Procedure

Large samples with core-size diameter are immersed in the deionized water and the electrical conductivity of the water and the weight gain of the samples are measured

at selected time intervals. All faces of samples are open for imbibition and diffusion. Figure 4.1 shows the schematic diagram of this experiment. At the final stage of experiments, an elemental analysis was performed, using Inductively Coupled Plasma (ICP) and Automated Ferricyanide methods (Lenar, 2000), to detect and quantify dissolved ions in water.

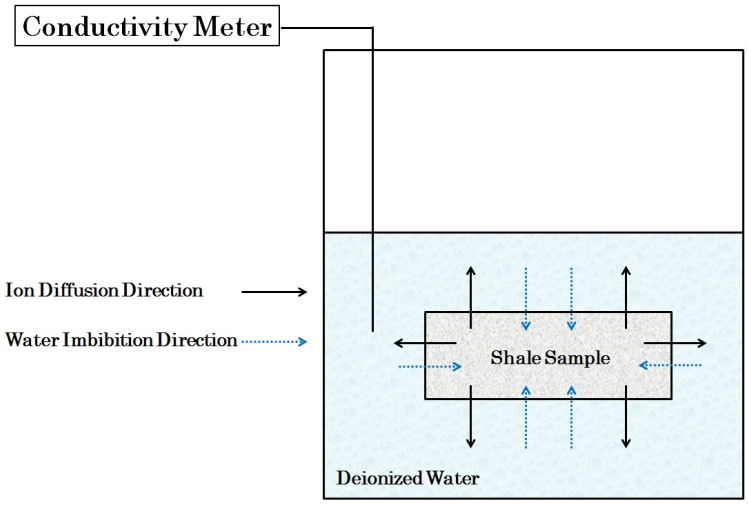

Figure 4.1. Schematic diagram of the diffusion test

4.2 Results and Discussion

Water Uptake and Expelling of Air Bubbles Figure 4.2 shows the samples before and after exposure to the deionized water at different times. Air bubbles expelled from samples indicate the counter-current air release as a result of the spontaneous water uptake. Furthermore, the pictures demonstrate generation of microfractures during the imbibition process. Based on this observation, we conclude that induced microfractures in Fort Simpson and Muskwa samples enhance the permeability and in turn imbibition rate.

Microfracture Induction and Sample Disintegration The water uptake of Fort Simpson and Muskwa samples results in microfracture induction and sample disintegration. However, water uptake does not significantly change the Otter Park samples, although some microfractures are induced (Fig. 4.2-4.3). This observation is in agreement with previous imbibition studies on gas shale samples (Kuila et al., 2014). Physical alteration degree greatly depends on clay content. Fort Simpson

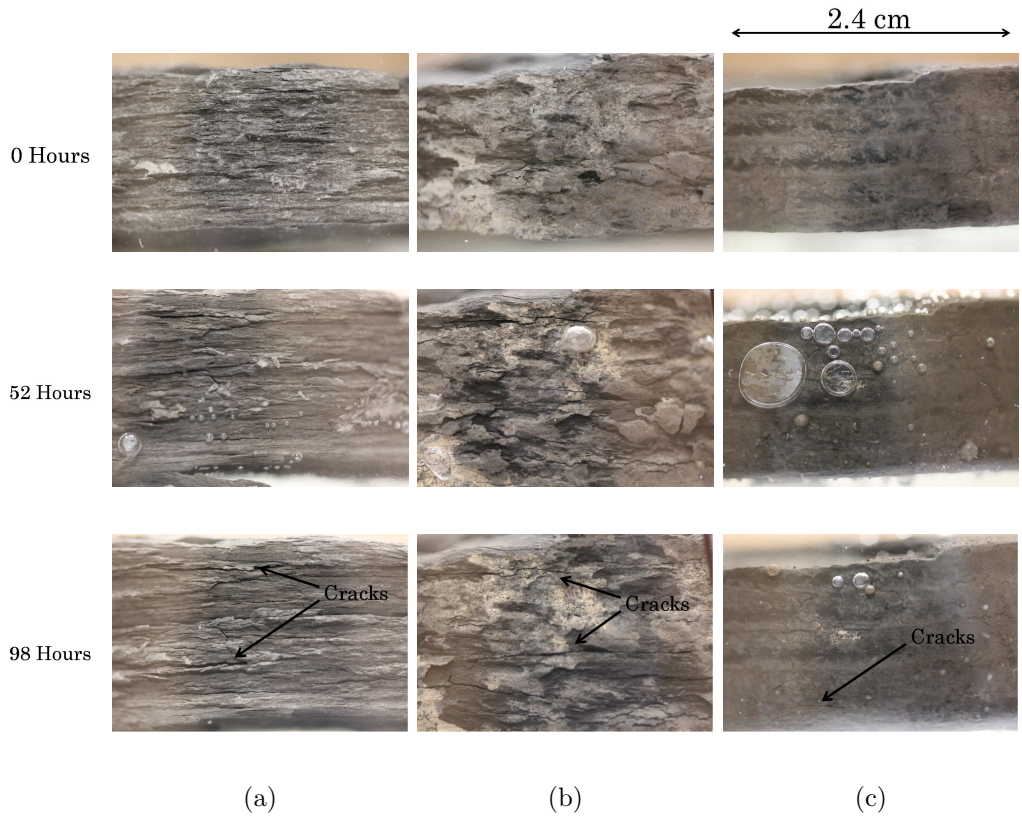

Figure 4.2. Pictures of Fort Simpson (a), Muskwa (b) and Otter Park (c) shale samples before and after exposure to the deionized water, show expelled bubbles and induced micro cracks.

has the highest clay concentration followed by Muskwa and Otter Park. Water adsorption on electrically charged clay surfaces generates internal stresses that can lead to expansion and spalling (Chenevert, 1970a, Olphen, 1953). XRD results show that illite is the dominant clay mineral in all of the samples and the swelling clays such as montmorillonite are negligible. However, previous studies (Chenevert, 1970a) show that an illitic shale can also be altered by water adsorption. Moreover, illite can contain small amounts of mixed layer clay which has a higher hydration tendency compared to illite (Steiger, 1982). Further, capillary effect is also known as an additional cause of shale swelling (Schmitt et al., 1994). The entrance of water into the pore network of a shale sample leads to pressurization of the air, which remains trapped inside the rock. The pore walls have to equilibrate these capillary forces which lead to the expansion of the unconfined shale samples.

One may argue that the observed microfractures are created as we used deionized water for the experiments. However previous experiments (Dehghanpour et al.,

2013) show that salinity does not have a strong effect on aqueous phase imbibition and a similar behavior was also observed when using a 6 wt. % KCl solution. However, our recent imbibition experiments show that using NaCl solution with 10, 15 and 20 wt. % as aqueous phase, reduces the microfracture induction and sample expansion.

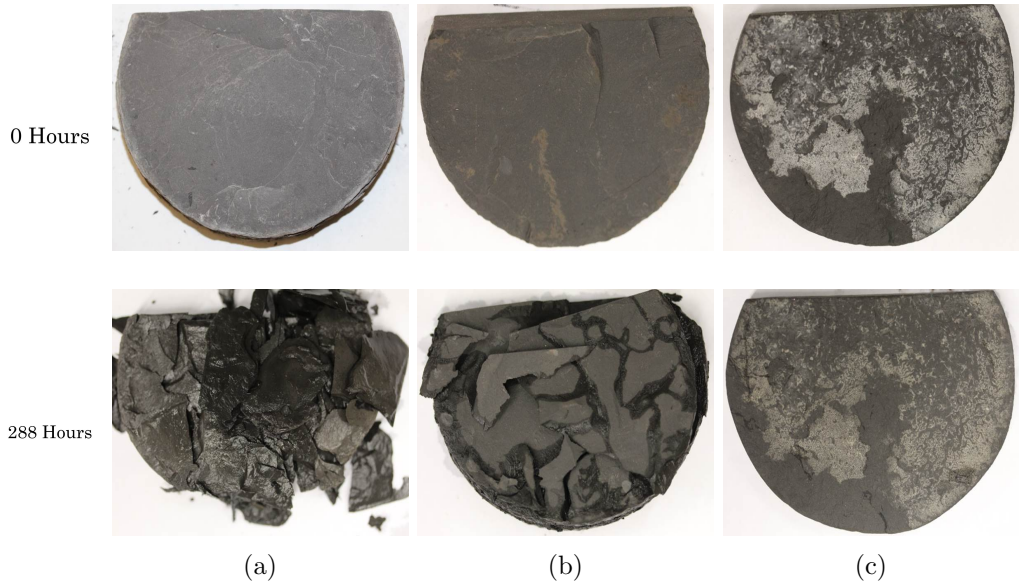

Figure 4.3. Pictures of Fort Simpson (a), Muskwa (b) and Otter Park (c) samples before and 288 hours after exposure to the water

Spontaneous Imbibition Rate in Different Rock Samples Figure 4.4 shows the normalized imbibed volume of deionized water into the shale samples versus time. Water imbibition rate is much higher in Fort Simpson sample than that in Muskwa and Otter Park samples. This result can be explained by the adsorption of water on the negatively charged clay layers. As shown in Figure 4.3, Fort Simpson sample, with a higher clay content and higher water adsorption compared to Muskwa and Otter Park samples, should have a higher water imbibition rate (Dehghanpour et al., 2013, 2012, Makhanov, 2013).

Ions Diffusion from Rock into Water Figure 4.5 shows the increase in conductivity of deionized water for Fort Simpson, Muskwa and Otter Park samples. The change in conductivity indicates ion transport from rock into the water. Advection and diffusion are the two main transport mechanisms for ion transport in and out of a porous medium. Advection occurs when a sufficient pressure drop is applied to

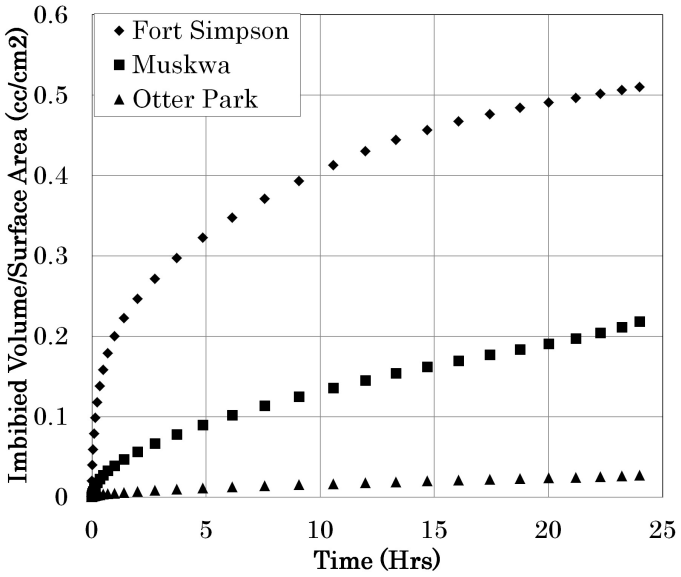

Figure 4.4. Normalized volume data for spontaneous imbibition of deionized water into different shale samples versus time (Makhanov, 2013).

cause fluid flow. However, diffusion is independent of pressure gradient and results from concentration gradient (Ballard et al., 1994). In our experiments, the bulk motion of water is slow and is in the opposite direction of ion transport. Therefore, ion transport is mainly controlled by diffusion and effect of advection is negligible. Figure 4.5 also illustrates the difference in conductivity profile of different samples. Fort Simpson has the highest electrical conductivity change with time followed by Muskwa and Otter Park. This observation can be explained by the difference in the lithology of the shale samples. The diffusion rate of ions from rock into the water depends on sample's aqueous solubility (Keller and Liovando, 1989). As water imbibes into samples, it dissolves/extracts ions from existing clay in the shale samples. Therefore, Fort Simpson with higher clay content than Muskwa and Otter Park is more soluble in water which results in higher diffusion rate. This explanation is also backed by the the visual results that Fort Simpson sample was completely disintegrated at the end of experiment (Figure 4.3). Furthermore, diffusion rate strongly depends on porosity. Water uptake of Fort Simpson results in significant physical alteration and porosity enhancement. The increase in porosity results in a lower tortuosity value, and in turn, in a higher effective diffusion coefficient. Furthermore, when the porosity is very low, surface interaction between the ions and shale minerals dominates. As porosity increases, surface interaction becomes less important and diffusion rate increases (Ballard et al., 1994).

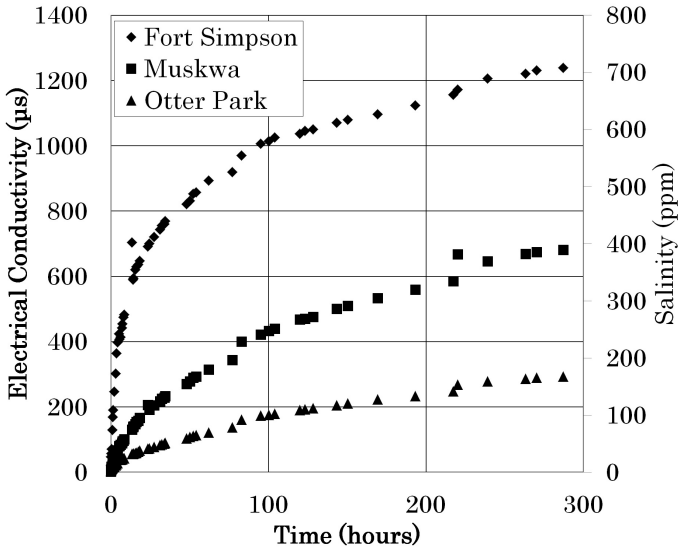

Figure 4.5. Change of electrical conductivity versus time for Fort Simpson, Muskwa, and Otter Park shale samples. The conversion factor from μS (micro Siemens) to ppm is 0.55.

Interestingly, Figure 4.6a that plots normalized imbibed volume versus square root of time (SQRT) is well correlated to Figure 4.6b that plots electrical conductivity versus square root of time. In both figures, Muskwa and Otter Park data points show a good linear relationship, while Fort Simpson data points can be divided into two relatively linear periods. The linear relationship in a SQRT plot indicates that the transport process can be described by a one-dimensional linear diffusion equation. Therefore, the transport of pressure during the imbibition process and that of ion during the diffusion process follow the linear diffusivity equation. The absence of one unique linear relationship for the imbibition profile of the Fort Simpson sample, observed in Figure 4.6a, can be explained by the generation of micorfractures in this sample. The higher slope (Region 1) of the Fort Simpson sample shows a higher imbibition rate and indicates that water imbibes through micro fractures which have a higher permeability. This region continues until water fills all the microfractures (Roychaudhuri et al., 2011). The lower slope (Region 2) shows a lower water imbibition rate and indicates that water imbibes into the matrix with ultra-low permeability. Less microfractures in the Muskwa and Otter Park samples explain the absence of Region 1 in Figure 4.6a (Makhanov, 2013). The shape of conductivity profile of the Fort Simpson sample can be also explained in a similar way. In simple, the effective diffusion coefficient for ion transport in microfractures is higher than that in the tight rock matrix.

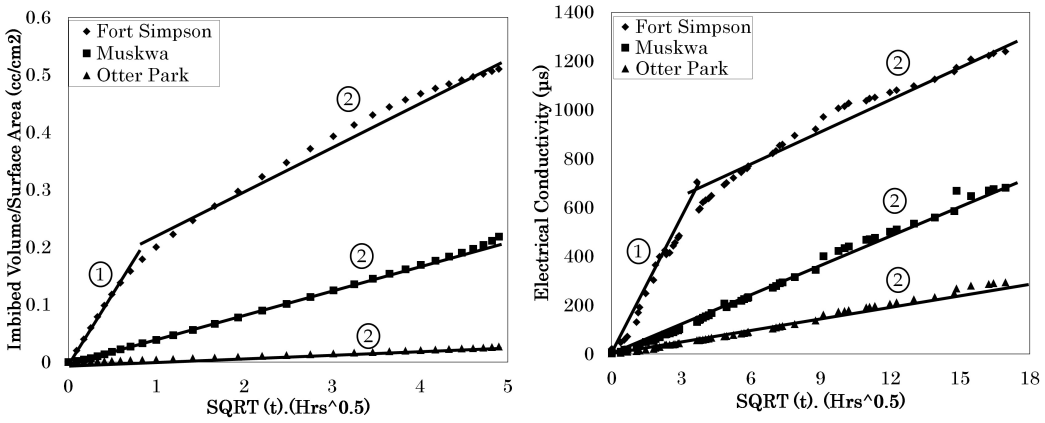

Figure 4.6. Normalized volume data for deionized water imbibition versus square root of time (a) and change of conductivity versus square root of time (b) for Fort Simpson, Muskwa, and Otter Park shale samples

Identifying the Type of Ions At the end of experiments, we did an elemental analysis to detect and quantify the dissolved ions in the water. Figure 4.7 shows the gram mole of ions in the water. Expectedly, sodium and chloride are the dominant ions in the water. The salt precipitated from the pore-water can be one possible source of sodium and chloride. The water which is imbibed into the shale samples, dissolves the salt remained in the pore from formation water dehydration. Afterwards, the ions diffuse from rock into the water. Furthermore, illites existing in the shale samples can be another possible source of sodium and chloride. Leaching of illitic shales yields relatively high concentrations of sodium and chloride (Keller and Liovando, 1989). Logically, the concentration of dissolved sodium and chloride for Fort Simpson sample is higher than that of Muskwa and Otter Park as its illite content is higher.

There are also considerable amounts of sulfate in the water. Some researchers reported the existence of sulfate in pore-water of some shale samples (Ballard et al., 1994). These sulfates are possibly originated from oxidation of the pyrite when shale samples were in exposure to the atmosphere and/or water (Woo et al., 2007). Observation of Reaction 4.1 shows that, in addition to the release of sulfates, oxidation of pyrite will release hydrogen ions, producing acidic conditions (Hutcheon, 1998).

$$FeS_2 + 8H_2O \Leftrightarrow Fe^{2+} + 2SO_4^{2-} + 16H^+ + 14e^- \tag{4.1}$$

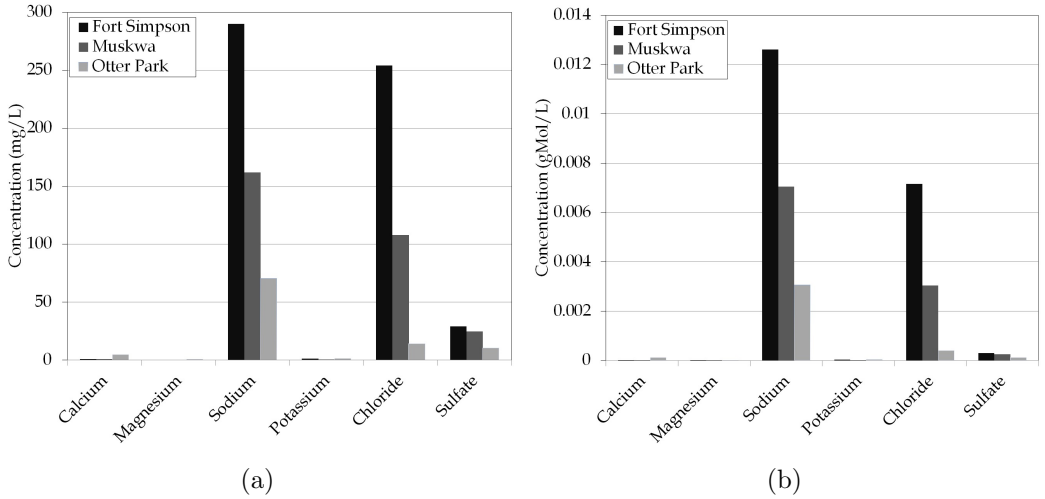

Figure 4.7. Elemental analysis of water at the end of experiment. The results are reported based on milligram per liter (a) and gram mole per liter (b).

Impact of Clay Surface Charge on Ion Diffusion Although sodium and chloride are the dominant ions in the water, the concentration of sodium in all samples is higher than that of chloride. One possible interpretation can be that leaching of illite results in sodium mobilization and generate a solution in which the concentration of sodium is higher than chloride. However, this reason can not justify the increase in the ratio of Na^+ to Cl^-. Since Fort Simpson sample has higher clay content, we expected higher ratio of Na^+ to Cl^- for this sample compared to that of Muskwa and Otter Park samples. The increasing trend in Na^+ to Cl^- ratio from Fort Simpson to Otter Park can be explained by the electric double layer properties of the clay particles existing in the shale samples. Clay particles will exhibit a net negative charge which is compensated by the accumulation of a layer of cations (diffuse layer) near the surfaces (Bassiouni, 1994). As a result, the passage of Cl^- anions is greatly restricted. However, Na^+ cations can freely move out from pore network of the shale to the deionized water. In the case that shales are fractured, there is less attraction between diffuse layer and Cl^- anions and they can leak and pass readily. Therefore, the lower Na^+/Cl^- ratio for the Fort Simpson sample can be explained by the presence of more fractures generated during spontaneous water imbibition since Fort Simpson has much higher illite content. One may argue that the excess sodium compared to chloride, comes from Plagioclase mineral which has sodium in its structure. However, the Plagioclase content of all samples is approximately the same while their Na^+/Cl^- ratios are significantly different. Therefore,

the existence of Plagioclase cannot justify the excess sodium in the water.

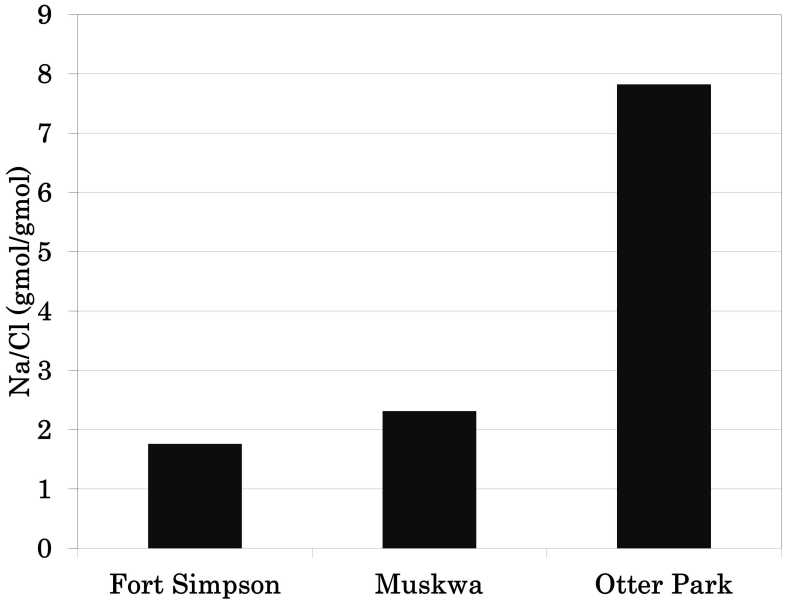

Figure 4.8. The ratio of Sodium to Chloride for different samples

Chapter 5

Impact of Lamination and Confining Stress on Imbibition/Diffusion

In previous works, Roychaudhuri et al. (2011) and Dehghanpour et al. (2013) showed that water adsorption by clay minerals produces water-induced microfractures and enhances the permeability of the shale samples. Dehghanpour et al. (2012) observed that fresh water uptake of dry shale samples obtained from the Horn River Basin is much higher than their oil uptake. On the other hand, Xu and Dehghanpour (2014) observed that the oil imbibition rate into crushed-shale packs is higher than water imbibition rates. Makhanov et al. (2014) and Makhanov (2013) investigated the effects of anisotropy on water imbibition rates and showed that water uptake for samples tested parallel to the lamination is higher than that for samples tested perpendicular to the lamination. Furthermore, in Chapter 4 we showed that the diffusion rate is correlated to water imbibition rates. Despite the recent studies, the following questions still remain unanswered: 1) Is the excess of water uptake of organic shales compared to that of oil is due to sample expansion and water induced microfracture? 2) Is imbibition anisotropy an intrinsic property of gas shales or it is caused by expansion of clay platelets? 3) What is the reason of higher liquid imbibition rates parallel to the lamination than that perpendicular to the lamination? 4) Does sample expansion affect the ion diffusion rates? 5) Is ion diffusion rate also an anisotropic phenomenon? and 6) How initial water saturation affects the water and oil imbibition and ion diffusion rates? In this chapter we aim at answering these questions.

5.1 Experiments

The imbibition/diffusion experiments conducted for this study can be categorized into three sets. In Set 1, we measure and compare spontaneous water and oil imbibition rates into dry and wet shale samples. We also monitor the ion diffusion rate from shale samples to water using an electrical conductivity meter, during imbibition process. The objective of this set is to investigate the effects of initial water saturation on ion diffusion and water imbibition rates. In Set 2, we measure and compare the ion diffusion and imbibition rates into confined and unconfined Otter Park and Evie shale samples. The objective of this set is to investigate the effects of sample expansion on ion diffusion and water imbibition rates. In Set 3, we measure and compare the ion diffusion and imbibition rates parallel and perpendicular to the lamination of the shale samples. The objective of this set is to understand the effects of anisotropy on liquid imbibition and ion diffusion rates.

5.1.1 Materials

The experimental materials include fluids used for imbibition tests and shale samples.

Fluids Kerosene and deionized (DI) water are used for the imbibition/diffusion tests. Density, viscosity and surface tension of fluids are listed in Table 5.1.

Table 5.1. Properties of different fluids used for imbibition experiments at 25 °C

Fluids	Density(g/cm^3)	Viscosity (cp)	Surface Tension (N/m)
DI Water	1.00	0.9	72
Kerosene	0.80	1.32	28

Shale Samples A total of 22 shale samples is used for this study. The core samples are selected from wells completed in Otter Park and Evie formations. The average mineral concentration of shale samples determined by x-ray diffraction (XRD) analysis is given in Table 5.2. The physical properties and average depth of intact shale samples used for imbibition tests are presented in Table 5.3.

Figure 5.1 shows the droplets of DI water and oil (kerosene) on the clean surfaces of the OP and EV samples. The pictures show that oil droplets completely spread on the rock surface. However, water droplets show a measurable contact angle. This

Table 5.2. Average mineral concentrations (wt.%) of the OP and EV shale samples determined by x-ray diffraction.

	Otter Park	Evie
Non-Clay Content		
Calcite	4.5	10
Quartz	55.5	31
Dolomite	1.5	4
Ankerite/Fe-Dolomite	4	5
Pyrite	2.5	5
K-Feldspar	0.5	6
Plagioclase	5	6
Clay Content		
Illite Mica	18.5	19
Illite Smectite	7	14
Chlorite	0.5	0

result indicates that samples are strongly oil wet and should spontaneously imbibe oil.

5.1.2 Test Procedure

A total of 22 imbibition/diffusion tests are conducted. The imbibition experiments are counter current as only one face of samples is open for imbibition and other faces are coated with epoxy. Figure 5.2 shows the experimental setup used for these experiments. During the tests, imbibition is monitored by measuring the weight change of samples as a function of imbibition time. Ion diffusion rates from shale samples into deionized water are monitored using an electrical conductivity meter.

The imbibition/diffusion experiments performed in this study can be categorized into three sets. The test procedures and objectives of each set are described below.

Set 1 (Imbibition/Diffusion Test for Dry and Wet Samples) The objective of this set is to investigate the effects of initial water saturation on liquid imbibition rates. Therefore, wet and dry samples are immersed into DI water and kerosene while only one face of samples is open for imbibition. Dry samples are prepared by heating samples at 200 $^{\circ}F$ for 24 hours. Wet samples are prepared by rehydrating shale samples. Rehydration process is carried out by equilibrating the samples in a controlled relative humidity condition. The method developed for this study (Chenevert, 1970b, Schmitt et al., 1994, Wayllace, 2008) consists of leaving shale samples in a vacuum desiccator. Figure 5.3 shows the pictures of desiccator used

Table 5.3. Mass, average depth, cross section area and thickness of shale samples used for this study

	Sample ID	Mass(g)	Area(cm^2)	Thickness (cm)	Depth (m)
Otter Park Samples	OP1	641.2	66.3	4.2	2454
	OP2	741.3	66.3	5.3	2454
	OP3	432.1	22.5	4.4	2454
	OP4	463.8	22.5	4.4	2454
	OP5	431.3	28.1	3.6	2516
	OP6	227.4	38	5.1	2516
	OP7	426.5	66.3	2.3	2486
	OP8	427.3	66.3	2.6	2486
	OP9	740.1	36	4.5	2465
	OP10	831.6	66.3	4.3	2465
	OP11	228.0	34.3	2.8	2486
	OP12	653.3	66.3	2.6	2486
Evie Samples	EV1	262.3	34.3	4.9	2671
	EV2	285.3	32.5	5.0	2671
	EV3	290.1	38.5	2.4	2671
	EV4	266.2	38.5	2.3	2671
	EV5	401.9	34.3	4.9	2671
	EV6	251.7	38.5	2.2	2671
	EV7	252.3	44.8	3.4	2671
	EV8	269.9	44.8	3.4	2671
	EV9	315.0	38.5	2.3	2671
	EV10	293.8	38.5	2.5	2671

for this study. The relative humidity inside the desiccator is controlled by a salt saturated solution (KCl solution with 25 wt.% is used for this study) and monitored by relative humidity meter. The vacuum condition inside the desiccator accelerates the rehydration process and more importantly avoid air entrapment inside the small pores.

The test procedures for Set 1 includes the following steps:

1. Measure the sample mass and bulk volume.
2. Coat all the faces of dry and wet shale samples with epoxy and leave one face open for imbibition tests.
3. Place the shale sample in the test cell and measure the weight change at the selected time intervals.

Set 2 (Imbibition/Diffusion Parallel and Perpendicular to the Bedding Plane) The objective of this set of experiments is to investigate the effects of

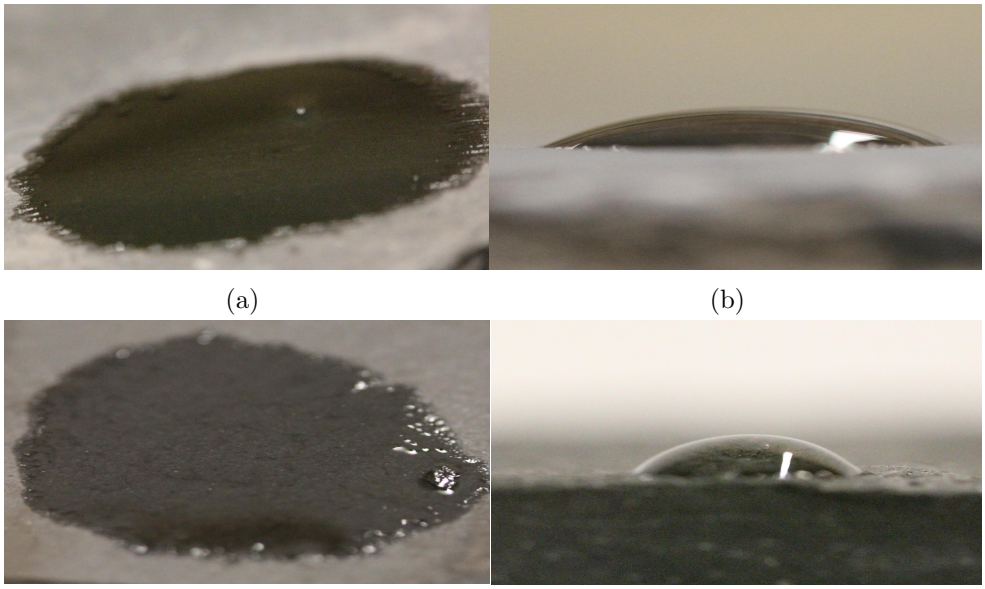

(a) (b)

(c) (d)

Figure 5.1. Equilibrated droplets of oil (left) and water (right) on the fresh surface of OP (a and b), and EV samples (c, and d). Oil completely spreads on the surfaces of all samples

anisotropy on liquid imbibition and ion diffusion rates. A total of 12 imbibition/diffusion experiments are conducted on OP and EV shale samples. These experiments are conducted parallel and perpendicular to the lamination of the shale samples. The boundary condition for this set of experiments is one face open. Therefore, impermeable epoxy polymer is used to coat the shale samples leaving one face open for imbibition. The open face is parallel or perpendicular to the lamination.

The sample preparation and test procedures for Set 2 includes the following steps:

1. Measure the sample mass and bulk volume.

2. Coat all the faces of shale samples with epoxy and leave one face open for imbibition/diffusion tests.

3. Rehydrate samples to their initial water saturation by placing them in vacuum desiccator with controlled humidity for 10 days.

4. Place the shale sample in the test cell and measure the weight change and electrical conductivity of the water at the selected time intervals.

To coat the shale samples, we used epoxy polymer. The rock face is exposed to the imbibition fluid while the other surfaces were covered by epoxy to make sure

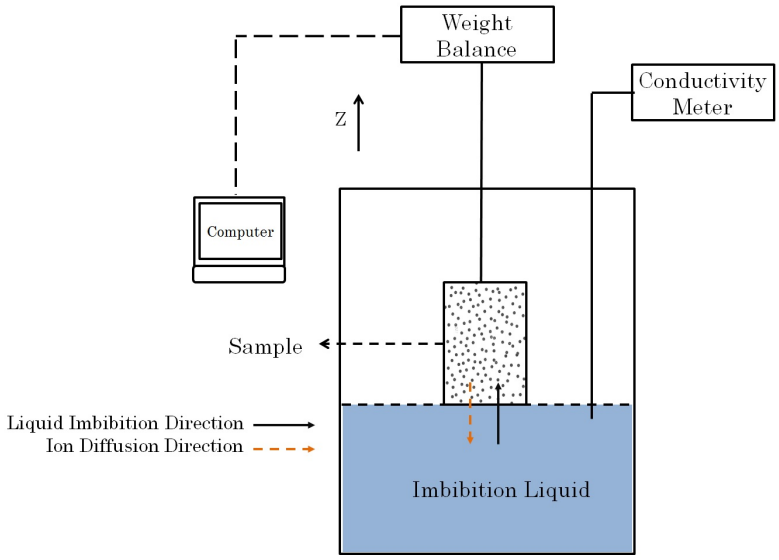

Figure 5.2. The cartoon of the experimental setup used for this study

that fluid could imbibe only through designated shale surface.

Set 3 (Imbibition/Diffusion Test for Confined and Unconfined Samples) The objective of this set is to investigate the impact of sample expansion and water-induced microfractures on water imbibition and ion diffusion rates. A total of 8 imbibition/diffusion experiments are conducted on unconfined and confined OP and EV shale samples. Samples were confined by aging in epoxy. Figures 5.4a and 5.4b show the cross section of confined shale samples prepared for imbibition/diffusion tests parallel and perpendicular to the lamination, respectively. The thick layer of epoxy firmly holds the samples and reduces the possibility of microfracture induction in confined samples. The unconfined samples are coated with epoxy. Therefore the boundary condition for confined and unconfined samples is one face open and this allow us to make a comparative study.

The sample preparation and test procedure for Set 3 include the following steps:

1. Measure the sample mass and bulk volume.
2. Put the sample in a closed-end PVC tube and fill it with epoxy.
3. Age the sample in epoxy for 48 hours and then cut it. Figure 5.5 shows the sample after taking out from PVC tube and before cutting. The sample is completely surrounded by epoxy.

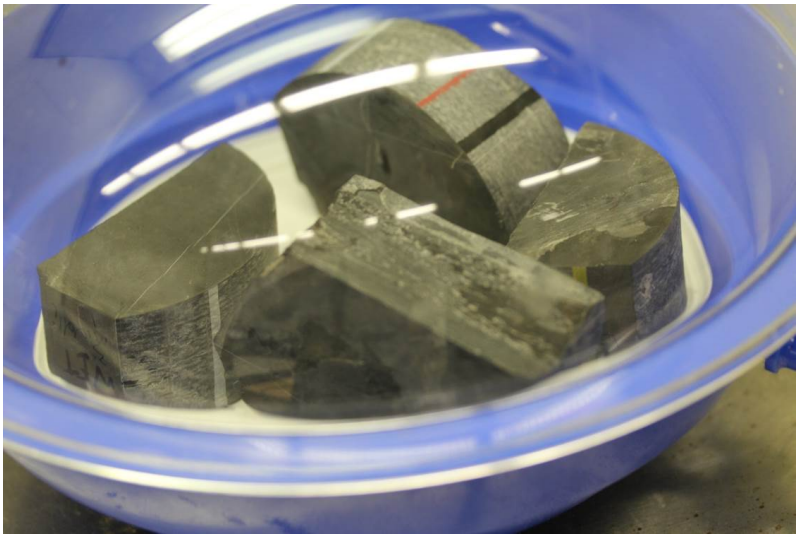

Figure 5.3. Picture of the desiccator and shale samples used for this study

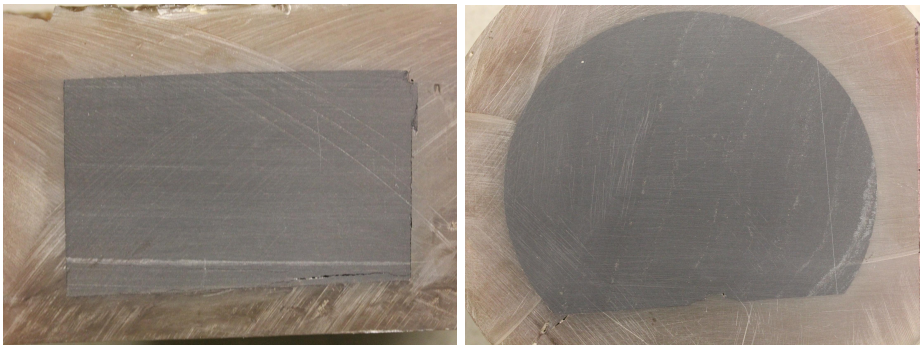

(a) (b)

Figure 5.4. The cross-section of confined samples used for imbibition/diffusion tests parallel (a) and perpendicular (b) to the lamination

4. Rehydrate samples to their initial water saturation by placing them in vacuum desiccator with controlled humidity for 10 days.

5. Place the shale sample in the test cell and measure the weight change and electrical conductivity of the water at the selected time intervals.

5.2 Results and Discussion

This section presents and discusses the results of the three sets of experiments in two subsections. In the first subsection, the imbibition profiles are compared to identify the key factors controlling spontaneous imbibition of liquid into shale samples. In the second subsection, the diffusion profiles are compared to understand the mechanisms

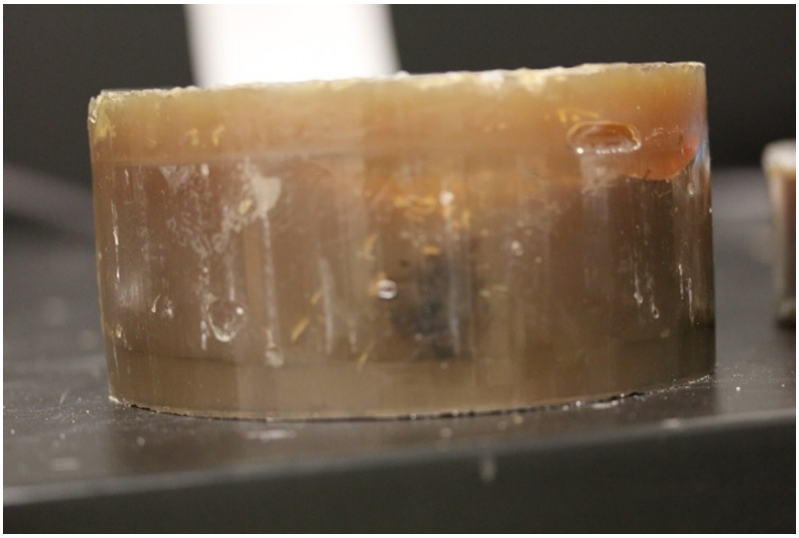

Figure 5.5. Picture of a sample after taking out from a closed-end PVC tube. The sample is completely surrounded by epoxy

controlling ion diffusion rates from shale samples into water.

5.2.1 Imbibition Results

Impact of Initial Water Saturation on Imbibition One of the concerns about previous imbibition experiments (Dehghanpour et al., 2013, 2012, Ghanbari et al., 2013, Roychaudhuri et al., 2011) was that shale samples used for imbibition experiments were dry. It can be argued that in situ shales may have some initial water saturation that has been shown to affect the spontaneous imbibition rates (Li et al., 2006). In this section, we investigate the effects of initial water saturation on water and oil imbibition rates.

Figure 5.6 compares the water and oil imbibition rates into EV shale samples with and without initial water saturation. The initial water content of wet samples used for water and oil imbibition tests is 0.0045 and 0.0032 wt %, respectively. The results suggest that water uptake of wet samples is lower than that of dry samples. However, initial water saturation has negligible effects on oil imbibition rates. This can be explained by the mixed wettability nature of the organic shale. Shale pores can be either in organic or inorganic materials (Lan et al., 2014a, Sondergeld et al., 2010). The organic part of the rock is hydrophobic (Mitchell, 1993), while the inorganic part can be hydrophilic, especially in the presence of clay minerals. When a shale sample contacts water vapor during rehydration stage, vapor initially condenses in the smallest and strongly water wet pores (Schmitt et al., 1994). Therefore,

before imbibition experiment, a portion of hydrophilic pore spaces of wet samples is initially occupied by water. This decreases the water imbibition rate into the wet shale samples. However, initial water saturation does not affect oil imbibition rate as oil mainly imbibes through hydrophobic pore network (Xu and Dehghanpour, 2014).

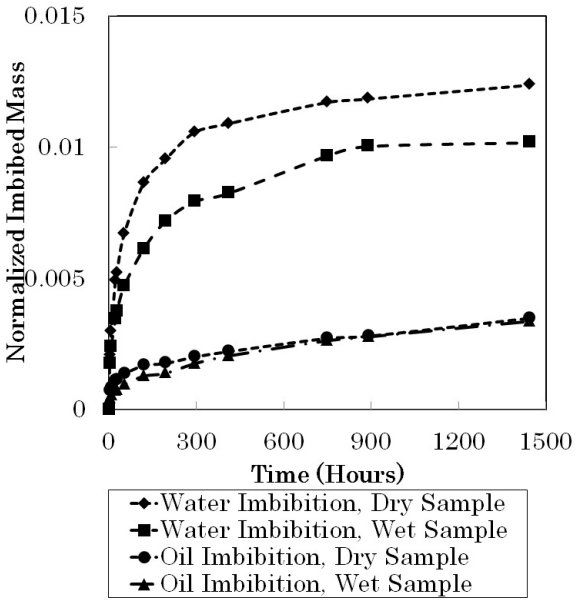

Figure 5.6. Comparison of water and oil imbibition profile for EV samples with initial water saturation (wet sample) and without initial water saturation (dry sample). The values are normalized by dividing to the mass of dry sample.

Impact of Anisotropy on Imbibition Figure 5.7 shows the normalized imbibition profiles of DI water and kerosene into OP and EV shale samples when the imbibition direction is parallel and perpendicular to the lamination. The comparison of the imbibition profiles reveals two key observations.

1. Both oil and water are spontaneously imbibed into shale samples. However, the imbibition rate and total imbibed volume of water for all shale samples are significantly higher than those of oil.

2. The imbibition rates of water and oil into the shale samples, parallel to the lamination, are significantly faster than those perpendicular to the lamination.

Observation 1 shows that both oleic and aqueous phases spontaneously imbibe into the Horn River shale samples. More surprisingly, the samples have more affinity

to water than to oil. However, based on the contact angle results, we expected that the samples would show strong affinity for oil. Significant water uptake of the Horn River shale samples may indicate that the hydrophilic pore network is relatively well-connected. On the other hand, insignificant oil uptake of these samples may indicate that the hydrophobic pore space, partly composed of organic carbon, is poorly connected (Xu and Dehghanpour, 2014). Furthermore, the significant water uptake of the Horn River samples can be explained by the presence of clay in the structure of shale samples. Recent studies, reveal that clay hydration can induce microfractures (Dehghanpour et al., 2013, 2012, Ghanbari et al., 2013). These microfractures increase the porosity and permeability of the shale samples. Therefore, they can be an additional cause of the excess water uptake of the shale samples. In the next section, we will analyze the imbibition results of crushed shale packs and BSE/EDX images to examine whether the excess water uptake is because of poor connectivity of hydrophobic pores. We will also present imbibition data for confined and unconfined shale samples to understand whether permeability/porosity enhancement due to sample expansion can increase the water uptake.

Observation 2 indicates that water and oil imbibition rates parallel to the lamination of the shale samples are higher than those perpendicular to the lamination. This result can be explained by two hypotheses. First, it can be suggested that the sensitivity of water imbibition rates to directional lamination are because of water induced microfractures. Recent studies (Dehghanpour et al., 2013, Ghanbari et al., 2013, Roychaudhuri et al., 2011) show that water uptake of shale samples induces microfractures and these microfractures are mainly oriented parallel to the lamination. As a result, the microfractures enhance the horizontal permeability of shale samples and consequently increase the water imbibition rate. As a second possibility, we hypothesize that clay layers and organic materials are oriented along the lamination. The existence of hydrophilic clay layers may hinder the oil flow perpendicular to lamination. In contrast, hydrophobic organic materials may restrict the water flow perpendicular to lamination. In the next section, we will compare the imbibition data for confined and unconfined samples and analyze the BSE/EDX images of shale samples to understand the reasons of higher liquid imbibition rates parallel to the lamination compared with those perpendicular to the lamination.

Impact of Sample Expansion and Water-Induced Microfracture on Imbibition In this section, we present the imbibition results for confined and unconfined samples to answer two questions: 1) Is the excess of water uptake of organic-shale compared with oil uptake is due to sample expansion and increased permeability/porosity? and, 2) are the water-induced microfractures responsible for the excess of water uptake along the lamination?

Figure 5.8 shows confined and unconfined OP and EV shale samples before and after exposure to DI water. The pictures show that water imbibition does not significantly alter shale samples, tested perpendicular to the lamination. However, water imbibition induces some microfractures in the shale samples, tested parallel to the lamination. The results also show that confining samples with epoxy reduces the number of water-induced microfractures for shale samples tested parallel to the lamination.

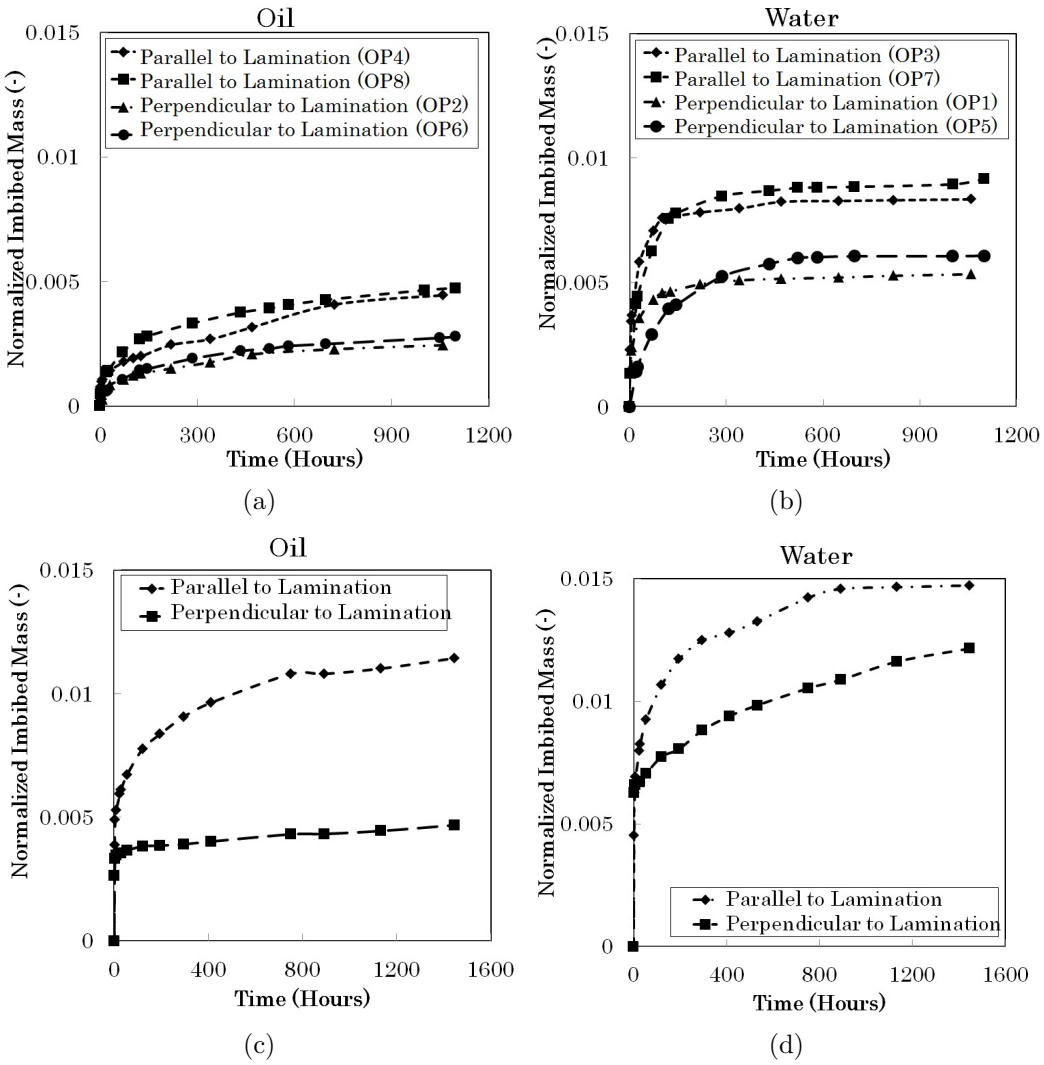

Figure 5.7. Normalized imbibed mass versus time for unconfined OP (a and b) and EV (c and d) shale samples tested parallel and perpendicular to the lamination. The values are normalized by dividing to the mass of dry sample.

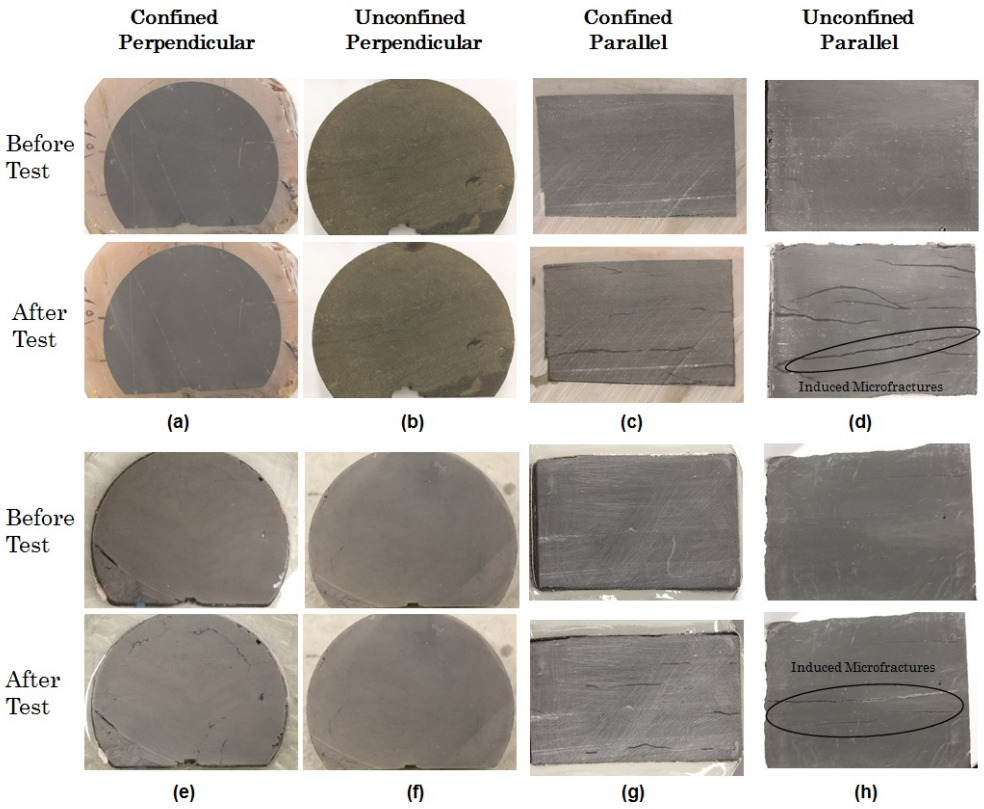

Figure 5.8. Pictures of OP (rows 1 and 2) and EV (rows 3 and 4) samples before and after exposure to DI water for 42 days. Before experiments, the sample were intact and there were no visible cracks on the shale samples. Water imbibition results in microfracture induction in samples tested parallel to the lamination. The number of water induced fractures is reduced in the confined samples

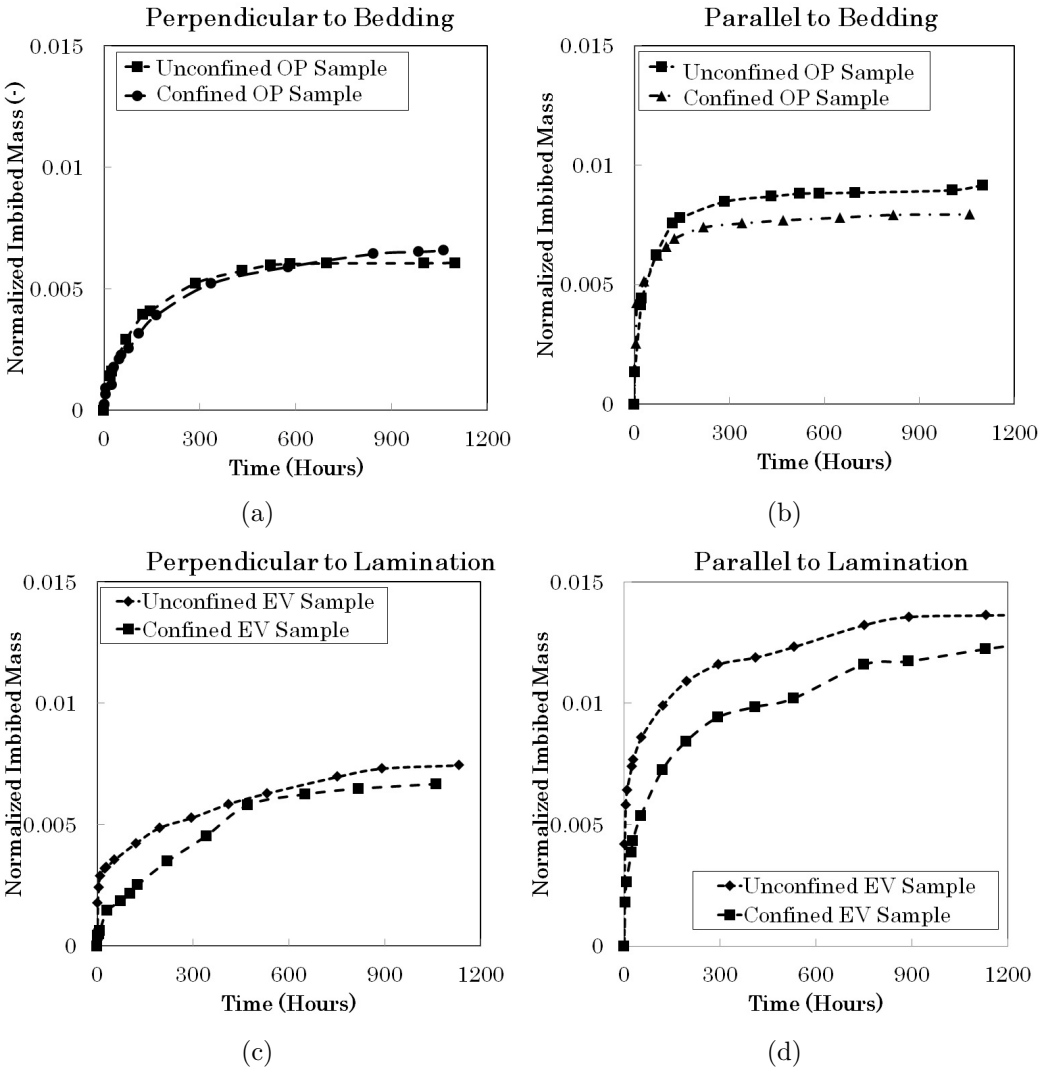

Figure 5.9. Normalized imbibed mass of water versus time for confined and unconfined OP (a and b) and EV (c and d) shale samples tested parallel and perpendicular to the lamination. The values are normalized by dividing to the mass of dry sample.

Figure 5.9 shows the profile of normalized water imbibition into confined and unconfined samples. The results suggest that confining has negligible effects on water uptake of the samples tested perpendicular to the lamination. However, the water uptake of unconfined samples, tested parallel to the lamination, is slightly higher than those of confined samples. Therefore, it can be interpreted that microfractures, induced along the lamination, can slightly increase the water imbibition rates through increasing porosity and permeability. However, the water-induced microfractures can not be the only reason, responsible for a higher liquid uptake parallel to the lamination compared with that perpendicular to the lamination. This

argument is evidenced by the fact that confined samples with reduced number of microfractures also show anisotropic behavior. More evidently, oil uptake of shale samples parallel to the lamination is higher than that perpendicular to the lamination, as shown in Figure 5.7. However, oil imbibition does not result in microfracture induction. Therefore, imbibition anisotropy is an intrinsic property of gas shales which can be enhanced by imbibition-induced microfractures.

Observations from BSE/EDX Images Here, we investigate the rock fabric to understand what causes imbibition anisotropy and the excess of water uptake over oil uptake. Figures 5.10 and 5.11 show the BSE and EDS images of the OP and EV samples, respectively. These pictures are taken from the thin section of shale samples. The images show that there is a trace of calcite and organic materials deposited parallel to the lamination. The frequency of these features, encountered in these samples, is large. The deposition of organic materials parallel to the lamination was also observed by Curtis et al. (2014). The EDS elemental map also confirms this statement, as shown in Figures 5.10 and 5.11. Therefore, the organic materials are surrounded by silica and calcite and thus organic pore network is poorly connected. This observation is in agreement with imbibition results of Horn River crushed-shale packs. Xu and Dehghanpour (2014) showed that the wetting affinity of crushed samples to oil is higher than that to water, in contrast to the behavior of the intact samples. Evidently, in a crushed sample, both hydrophilic and hydrophobic pores are artificially connected. Therefore, oil, which hardly flows through the intact samples, easily wets the artificially created hydrophobic surfaces and imbibes into the crushed pack. Furthermore, the existence of organic materials between shale layers can also explain the anisotropic behavior of shale samples. When water imbibes parallel to the lamination, hydrophobic organic materials, mainly distributed parallel to lamination, work as a nanofilter for hydrocarbon flow (Wang and Reed, 2009) and restrict the passage of water. In the same manner, water-wet clay layers, oriented along the lamination, hinder the passage of oil as oil imbibes perpendicular to the lamination.

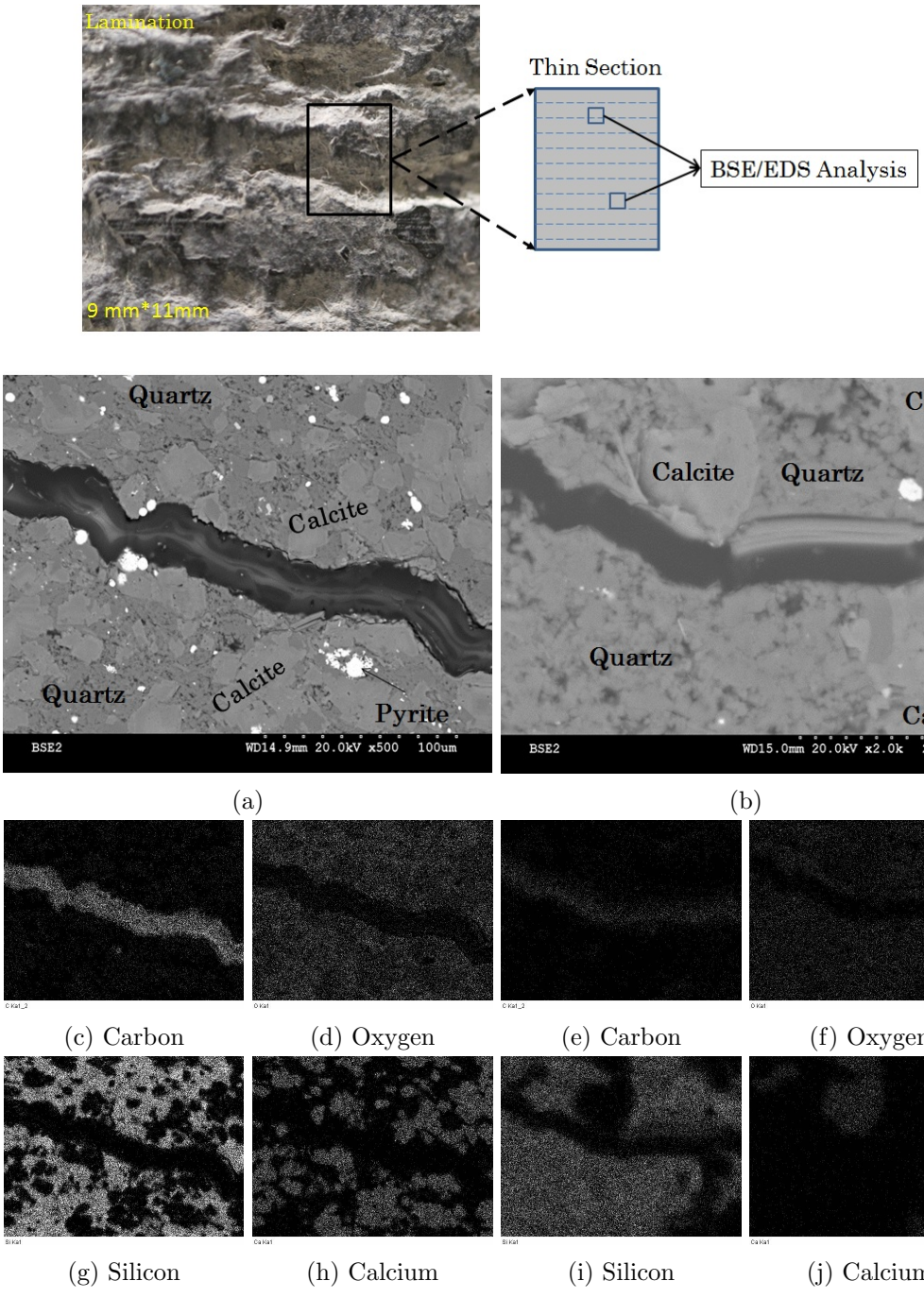

Figure 5.10. The BSE images (a and b) of OP thin section show that there are layers of organic materials surrounded by calcite and quartz. The EDS maps of carbon element which show the location of organic materials also confirm this statement.

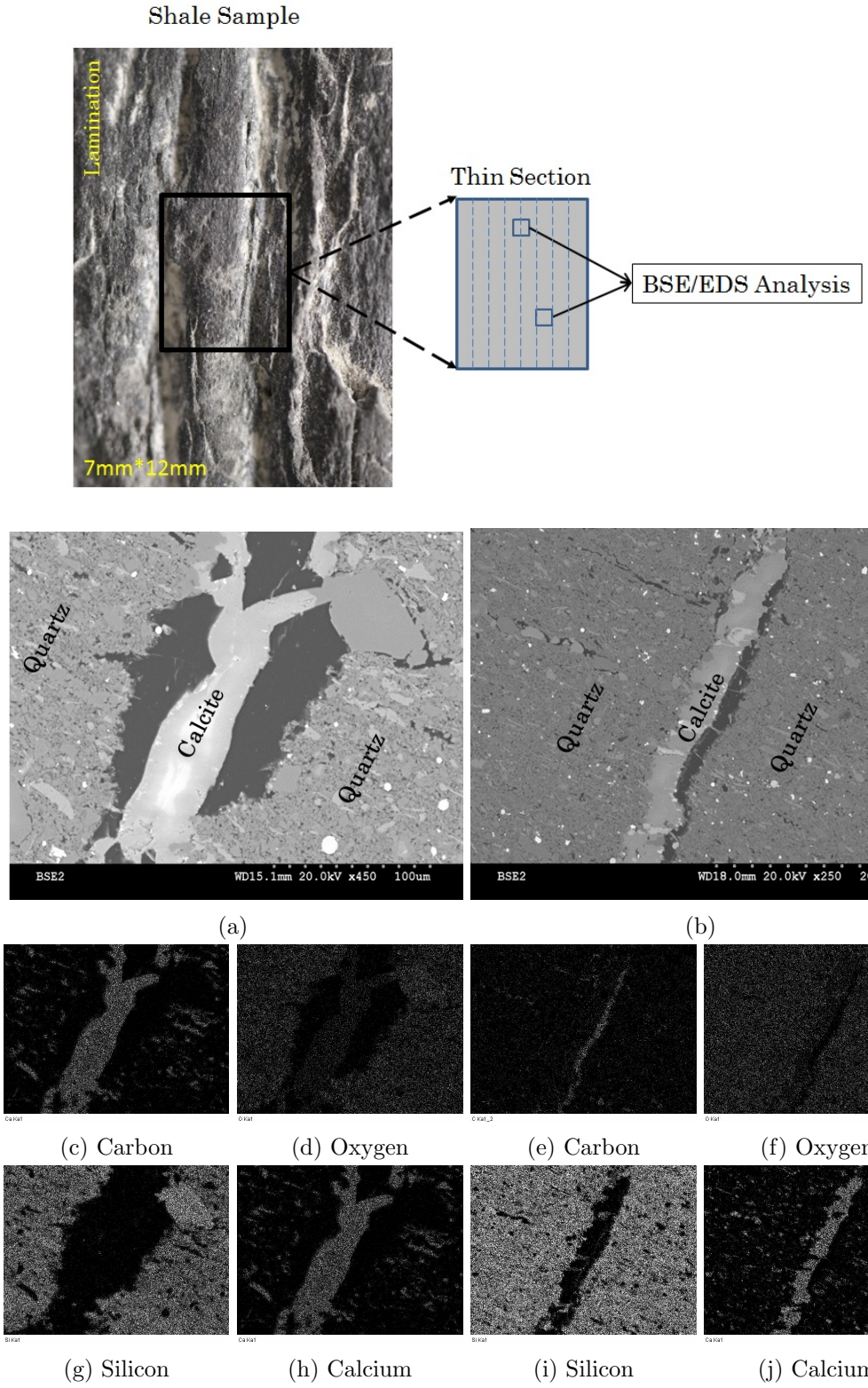

Figure 5.11. The BSE images (a and b) of EV thin section show that there are layers of organic materials surrounded by calcite and quartz. The EDS maps of carbon element which show the location of organic materials also confirm this statement.

5.2.2 Diffusion Results

Comparison of Ion Diffusion Parallel and Perpendicular to Bedding Figure 5.12 shows the increase in electrical conductivity profiles of OP and EV samples tested parallel and perpendicular to the lamination. The change in electrical conductivity indicates ion transport from rock into water. The salt precipitated from the pore-water can be one possible source of sodium and chloride. The water which is imbibed into the shale samples, dissolves the salt remained in the pore from formation water dehydration. Afterwards, the ions diffuse from rock into the water. Furthermore, illites existing in the shale samples can be another possible source of ions. Leaching of illitic shales yields relatively high concentrations of sodium and chloride (Keller and Liovando, 1989).

Advection and diffusion are the main transport mechanisms for ion transport in and out of a porous medium. Advection occurs when a sufficient pressure drop is applied to cause fluid flow. However, diffusion is independent of pressure gradient and results from concentration gradient (Ballard et al., 1994). In our experiments, the bulk motion of water is slow and is in the opposite direction of ion transport. Therefore, ion transport is mainly controlled by diffusion and the effects of advection are negligible. Furthermore, in the presence of clay layers, osmosis effect can play an important role on ion diffusion. The electrically charged clay layers existing in the shale samples can act as semi-permeable membrane that restrict the passage of solute without affecting the passage of solvent (Ballard et al., 1994, Mitchell, 1993, Steiger, 1982). Once low salinity water contacts with the clay particle existing in the shale samples, water molecules flow from low salinity side (imbibition fluid) of semi-permeable membrane to the high salinity side (pore water). This reduces the salinity in the pore and equalizes the concentration of dissolved salts in both sides (Fakcharoenphol et al., 2014). This phenomenon, known as osmosis water transport, increases the water uptake and physical alteration degree of the shale samples (Keijzer and Loch, 2001, Xu and Dehghanpour, 2014).

Figure 5.12 also shows that ion diffusion rate parallel to the lamination is higher than that perpendicular to the lamination. This result can be partially explained by the difference in permeability of shale samples, parallel and perpendicular to the lamination. The permeability of shale samples parallel to the lamination is known to be higher than that perpendicular to the lamination (Chalmers et al., 2012). As a

result, the diffusion rate parallel to the lamination is higher than that perpendicular to the lamination. Furthermore, osmosis effects can act as an additional cause that decreases the ion diffusion rate perpendicular to the lamination. When shale samples are in contact with water perpendicular to their lamination, semi-permeable clay layers restrict the flow of ions out of pore space. However, significant permeability parallel to the lamination can reduce the osmosis effect. This increases the ion diffusion rate parallel to the lamination.

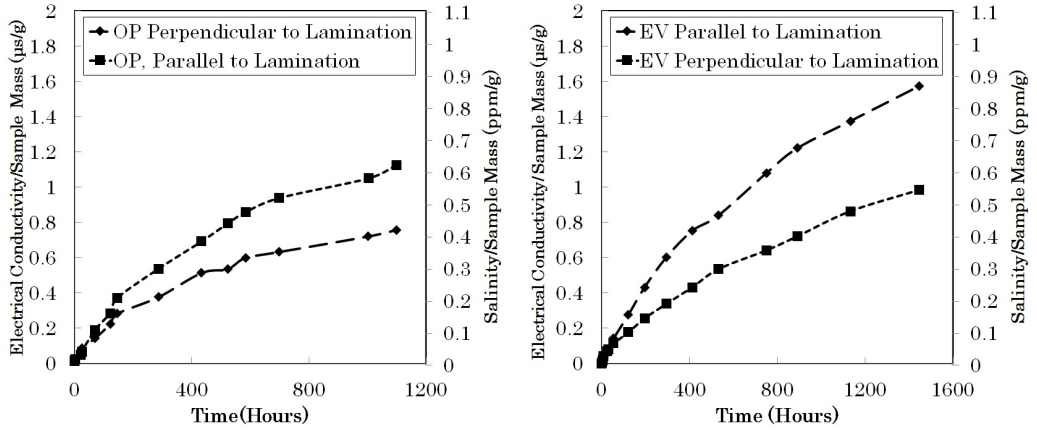

(a) (b)

Figure 5.12. Electrical conductivity profiles for (a) OP and (b) EV shale samples. Conductivity indicates the ion diffusion rates from sample into the water. The conversion factor from μS (micro Siemens) to ppm is 0.55.

Comparison of Ion Diffusion for Confined and Unconfined Samples In this section, we compare the ion diffusion rates from confined and unconfined shale samples into water, to investigate the effects of water induced microfractures on diffusion rate.

Figure 5.13 compares the electrical conductivity profiles for confined and unconfined shale samples. The results suggest that confining shale samples does not significantly affect the ion diffusion rate perpendicular to the lamination. However, the diffusion rate for confined samples tested parallel to the lamination are lower than those tested perpendicular to the lamination. This result shows that induced microfractures and sample expansion can increase the diffusion rate through increasing permeability and porosity.

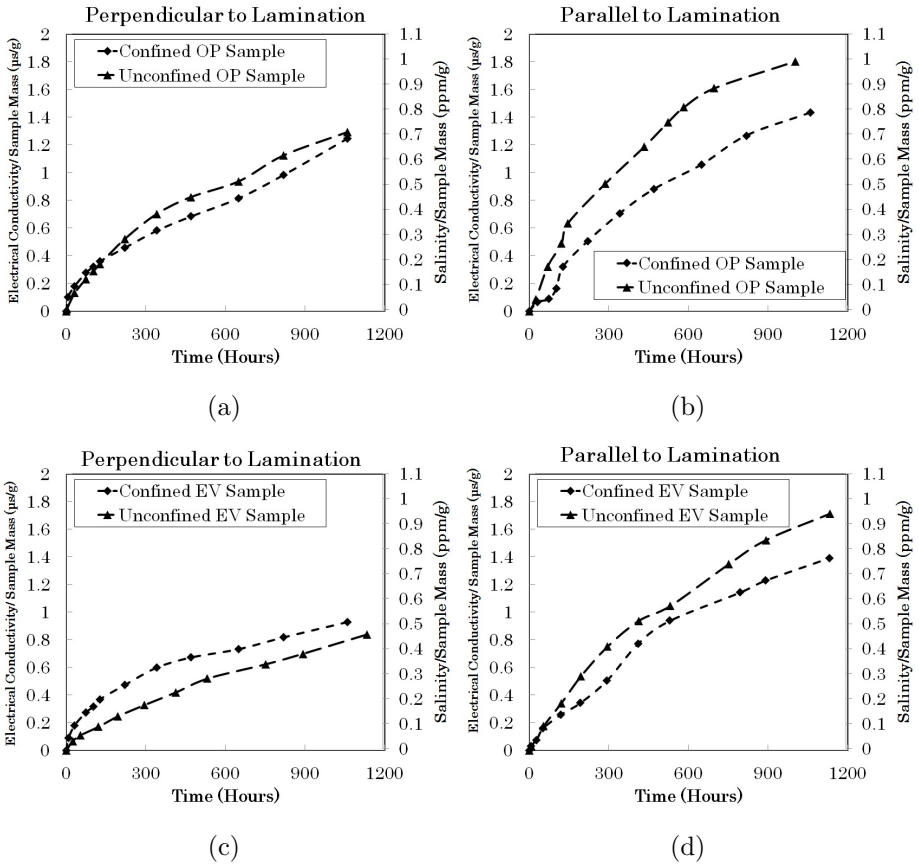

Figure 5.13. Electrical conductivity profiles for confined and unconfined OP (a and b) and EV (c and d) shale samples tested parallel and perpendicular to the lamination. The conversion factor from μS (micro Siemens) to ppm is 0.55.

5.3 Summary

We systematically measured and compared the imbibition rates of fresh water and oil into wet/dry and confined/unconfined rock samples from different shale members of the Horn River Basin. We also measured the ion diffusion rate from shale into water during imbibition experiments. The results show that initial water saturation decreases the water uptake of shale samples. However, it has no effect on oil imbibition rates. The results also suggest that confining the shale samples decreases the water imbibition rate, parallel to the lamination. Furthermore, confining does not significantly affect the ion diffusion rates. The comparative study suggests that, for both confined and unconfined samples, water uptake is higher than oil uptake. The liquid imbibition and ion diffusion rates along the lamination are higher than those against the lamination.

Chapter 6

Numerical Simulation of Flowback

In this chapter, we present numerical simulation of flowback process to investigate the effects of fracturing fluid imbibition into rock matrix on early time water and gas production. We also conduct a comprehensive sensitivity analysis to investigate the effects of reservoir and operational parameters such as shut-in time, capillary pressure and the complexity of created fracture network on early time water and gas production.

6.1 Model Description

This model considers the flow toward a fractured horizontal well in a reservoir. Basic reservoir, fracture and well properties used are listed in Table 6.1. A section of reservoir volume between two hydraulic fractures is modeled with the reservoir dimensions of 200 ft in x-direction, 357 ft in y-direction and 55 ft in z-direction, as shown in Figure 6.1. The fractures are created perpendicular to the horizontal wellbore with a fracture spacing of 100 ft and the fracture half-length of 357 ft. Logarithmic grid size distribution near the hydraulic fracture is used to capture flow behavior near the fracture. Figure 6.2 shows the relative permeability curves used to describe fluid flow through fractures and shale matrix. The numerical simulation also accounts for the effects of water imbibition and gravity segregation during the flowback process.

Water Imbibition When water injected during hydraulic fracturing treatment contacts the shale matrix through fracture surfaces, the water can imbibe into the rock matrix and affect the reservoir/well production performance (Bazin et al., 2010,

Table 6.1. Basic reservoir and well input parameters for base model

Parameters	Values
Matrix Permeability	0.001 md
Hydraulic Fracture Permeability	2000 md
Hydraulic Fracture Half-Length	357 ft
Hydraulic Fracture width	0.1 ft
Matrix Porosity	5 %
Primary Fracture Porosity	60 %
Flowing Wellbore Pressure	500 psi
Initial Reservoir Pressure	3000 psi

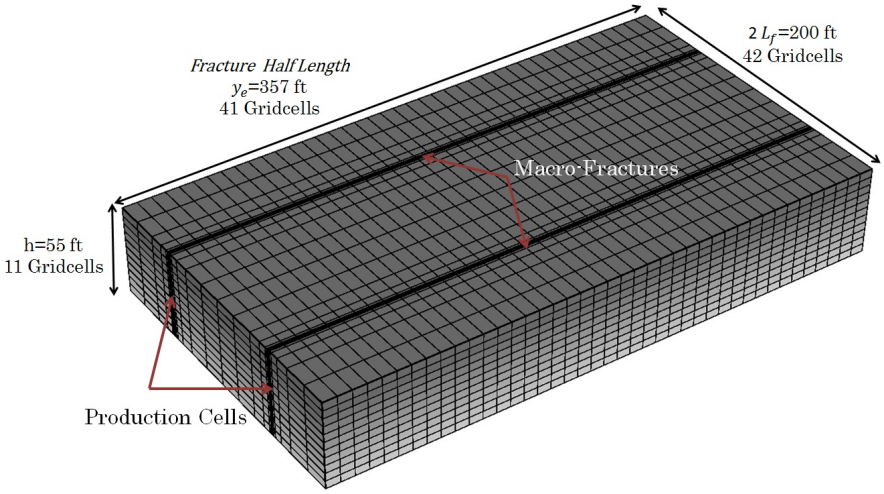

Figure 6.1. 3-D view of the simulation model used for simulating flowback

Dutta et al., 2014, Fan et al., 2010, Roychaudhuri et al., 2011). Capillary pressure, which is a function of rock wettability, pore radius and interfacial tension, controls spontaneous imbibition in both conventional (Babadagli, 2001, Cai et al., 2012, 2010, Ma et al., 1997, Zhang et al., 1996) and low-permeability reservoirs (Takahashi and Kovscek, 2010, Zhou et al., 2002) In low permeability reservoirs, the capillary pressure can be several hundred psi or even more (Holditch, 1979) and therefore the imbibition effects are considered to be significant. In this study, to simulate water-phase imbibition during fracturing operation and shut-in period, the fractures are initially saturated with water. Water is also injected into the fractures to increase the fracture pressure and to simulate the reservoir conditions just after hydraulic fracturing. This is followed with 150 days of shut-in time before the well is placed on production. During the shut-in time, water imbibes into the matrix through both forced and spontaneous imbibition and gas is expelled into the fractures. The

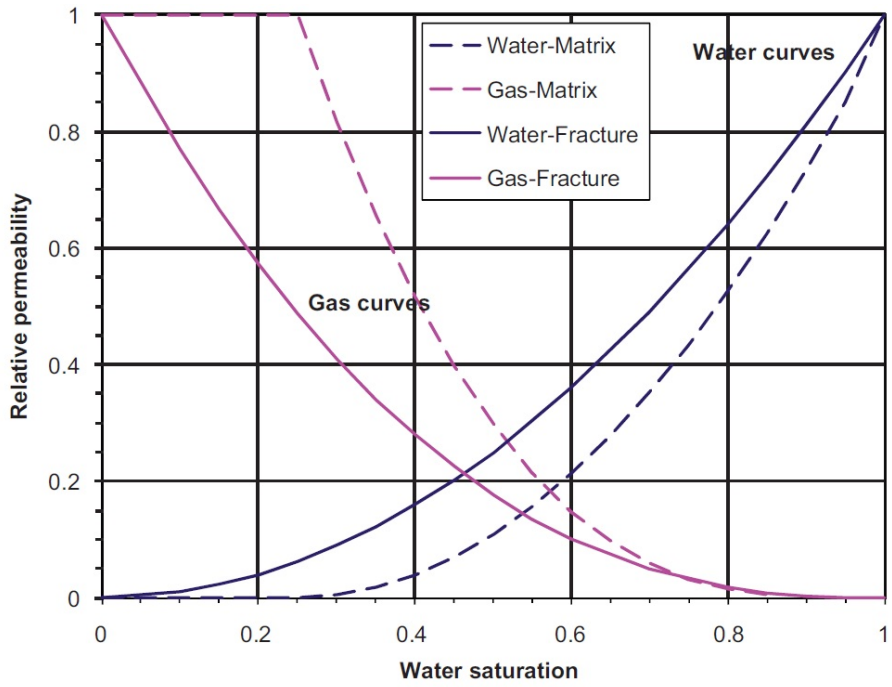

Figure 6.2. Relative permeability curves for matrix and fracture systems (Cheng, 2012)

capillary pressure curve used for shale matrix is generated based on the following empirical correlation presented by Gdanski and Fulton (2009).

$$P_c = \frac{\sigma}{a_2(S_w)^{a_1}}(\frac{\phi}{k})^{a_3} \tag{6.1}$$

Where P_c is capillary pressure, psi; σ is surface tension, dynes/cm; S_w is water saturation, fraction; ϕ is porosity, fraction; k is absolute permeability, md; and a_1, a_2 and a_3 are adjustable constants. The values of a_1, a_2 and a_3 for low permeability reservoirs are 1.86, 6.42 and 0.50, respectively. The capillary pressure curve for shale matrix used in this study are calculated from this correlation and is shown in Figure 6.3. For the fractures with large permeability, the capillary pressure is very small, considered as zero here.

Gravity Segregation In thick reservoirs with high permeability fractures, the gravity affects water and gas distribution in fractures. During shut-in period, when gas is expelled into fractures due to counter current imbibition, water is separated vertically from gas by gravity segregation (Agrawal and Sharma, 2013, Parmar et al., 2014, Taylor et al., 2011). In this study, eleven layers are used in Z-direction of reservoir model to account for the gravity effects.

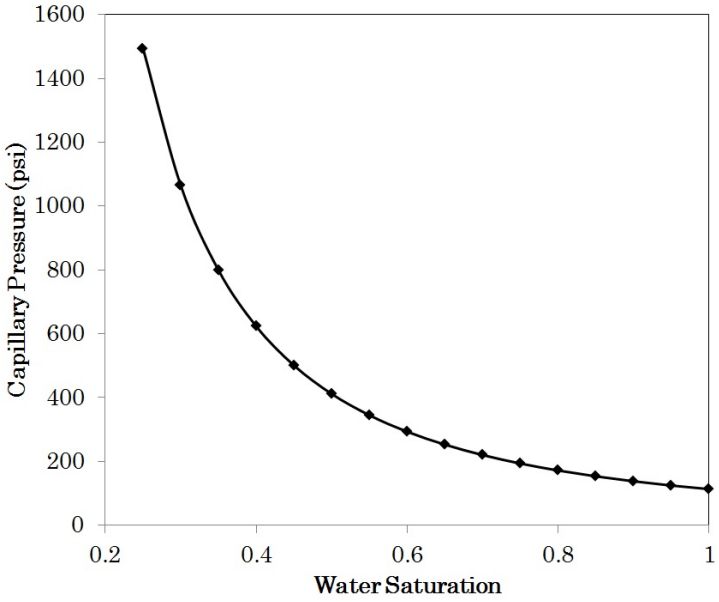

Figure 6.3. Capillary pressure curves used for shale matrix in simulation model

6.2 Initialization

The simulation was initialized by injecting 1900 bbl of water into fractures to increase fracture pressure to around 7000 psi which is close to the fracturing pressure. The injection phase was done to simulate reservoir condition after hydraulic fracturing operation. This process is followed by 150 days of shut-in period. Figure 6.4 show the water saturation profile in the hydraulic fracture plane at different times, during shut-in period. The extended shut-in period allows for imbibition, causing the buildup of the free gas saturation in the fracture network. The gas expelled from the matrix into the fractures gradually moves upward and accumulates at the top of fracture due to buoyancy effect. As a result, the upper part of fractures have significant gas saturation at the point when the well is opened for the flowback operation.

6.3 Flowback Simulation Results

Water and Gas Rate Profiles Figure 6.5a shows water and gas rates during flowback process. The simulation results clearly show the immediate gas production after placing the well on flowback. This is in agreement with actual field data obtained from the well pad in the Horn River Basin (see Chapter 3). As previously discussed, the immediate gas breakthrough is due to extended shut-in period and

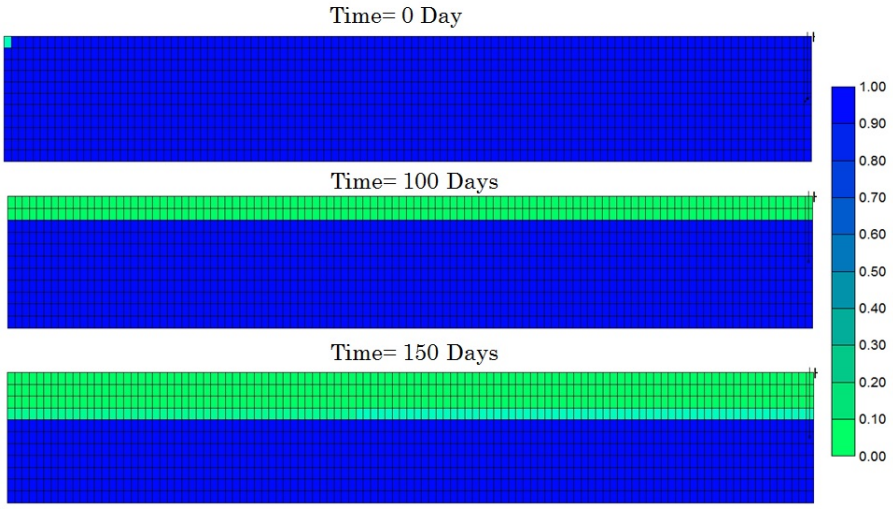

Figure 6.4. Water saturation of fracture plane at different times during shut in period. The dark blue color shows water saturation of 100 %.

strong counter current water imbibition into rock matrix. The counter current imbibition results in gas build-up in fractures and this free gas is immediately produced as the flowback process starts.

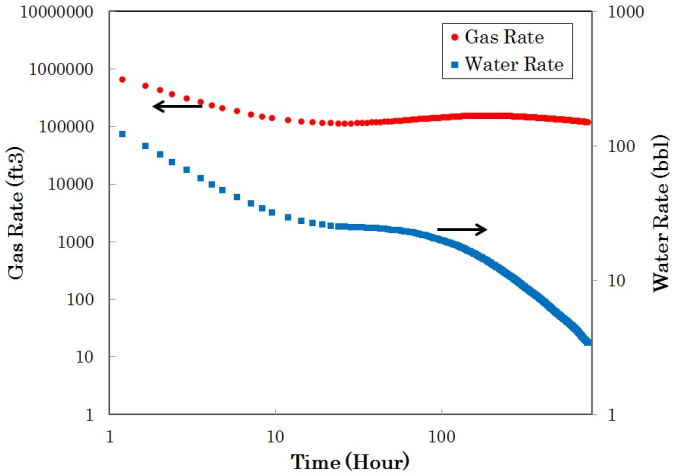

(a)

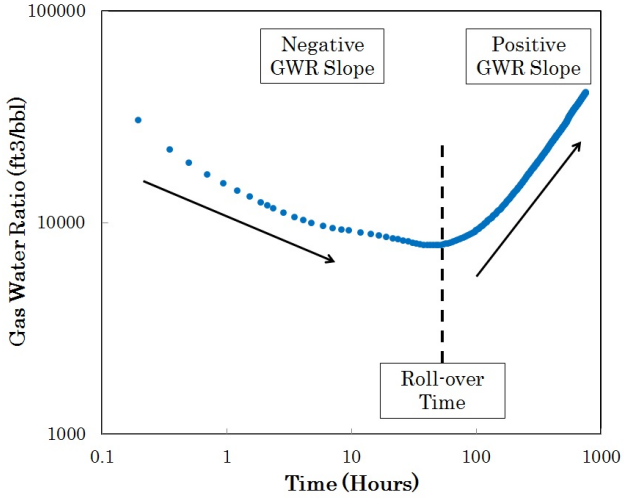

(b)

Figure 6.5. Water and gas flow rate profile (A) and gas water ratio profile for the simulated model

Gas Water Ratio Profile Figure 6.5b shows gas water ratio (GWR) profile of simulated model during flowback process. The V-shaped trend observed in the field data (see Chapter 3) is also observed in the simulated data. This confirms the fact that the observed V-shape production signatures in gas water ratio plots of Muskwa, Otter Park and Evie wells, are not an artifact of the poor data quality and variability of choke size. As we discussed in Chapter 3, the decreasing GWR trend (negative slope) during early time gas production indicates the depletion of free gas in the fracture network. This conclusion is backed by water saturation profile of fracture plane (Figure 6.4) after shut-in period. The decreasing trend of GWR profile is

followed by an increasing trend. This trend occurs at the later time scale (late time gas production) of flowback process. This trend indicates water displacement by the gas introduced from matrix. The depletion of water from fractures decreases the water saturation in the fractures and water production at the surface. The produced water from fractures is replaced by the gas introduced from matrix into fracture and stabilizes gas production rate (Figure 6.5a). This conclusion is backed by water saturation contour of fracture plane during late time gas production, as shown in Figure 6.6. The water saturation contour during late time gas production clearly shows water depletion from fracture plane and gas introduction from matrices into fractures. Interestingly, even after 800 hours of production, significant amount of water remains in the fracture due to poor sweep efficiency and gravity segregation (Agrawal and Sharma, 2013, Parmar et al., 2014, 2012, 2013).

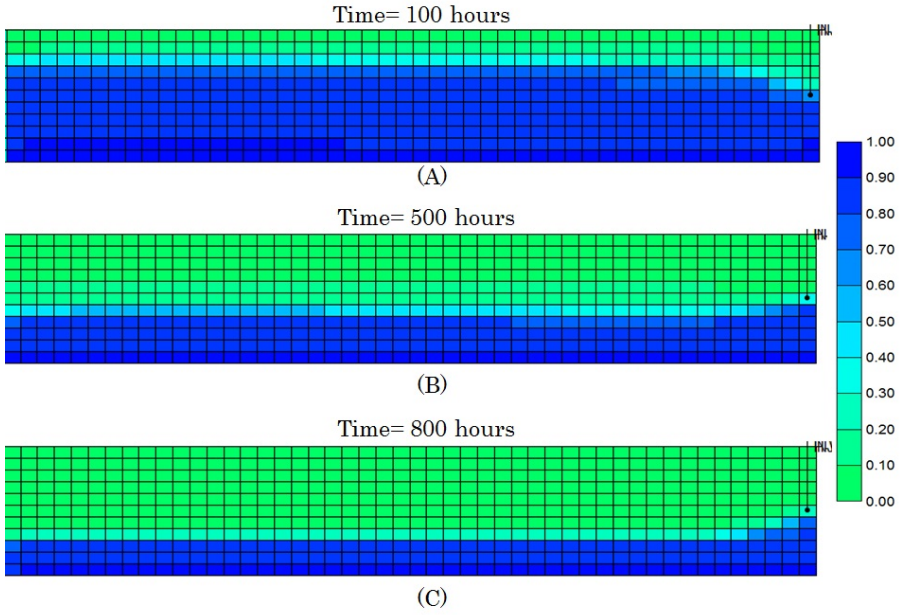

Figure 6.6. Water saturation contour of fracture plane at different times during late time gas production.

6.4 Sensitivity Analysis

The simulation cases were designed to evaluate the impact of various contributing mechanisms and operational parameters during shut-in and production periods on early time and late time gas production. These mechanisms and parameters include the effects of shut-in time, density of microfractures and capillary pressure.

6.4.1 Case 1: Impact of Shut-in Time

The duration of shut-in time after hydraulic fracturing is an ongoing debate within industry. Some researchers believe that that extended shut-in and water leak off into rock matrix due to capillary effect can cause reservoir damage (Bennion and Thomas, 2005, Holditch, 1979, Mahadevan et al., 2009, Shaoul et al., 2011). However, field data indicate that in some wells extended shut-in period surprisingly increases the early time gas flow rate (Cheng, 2012). In this section we investigate the effects of extended shut-in time on early and late time gas production of flowback process. Therefore, three different simulation cases with 50, 100 and 150 days of shut-in time are designed.

Figures 6.7a and 6.7b respectively show the cumulative water and gas production profiles. Extended shut-in reduces the cumulative water and gas production rate at the end of flowback process, however it has negligible effects on cumulative gas production. The low water recovery can be explained by the significant counter-current water imbibition from fracture into the shale matrix during extended shut-in period. However, the volume of free gas in the fractures at the end of shut-in period is negligible compared to the volume of gas produced from matrix and therefore, the cumulative gas production for all cases remains relatively constant. Furthermore, extended shut-in time also affects the V-shape of GWR profile, as shown in Figure 6.8. The volume of free gas in the fracture prior to the flowback is higher for simulation case with 150 days of shut-in period. Therefore, the gas flow rate during early time production of flowback process is higher for the case with 150 days of shut-in time. Furthermore, longer shut-in results in more water imbibition and reduces the early time water flow rate. As a results, the V-shape trend in GWR plots is more pronounced for cases with longer shut-in time.

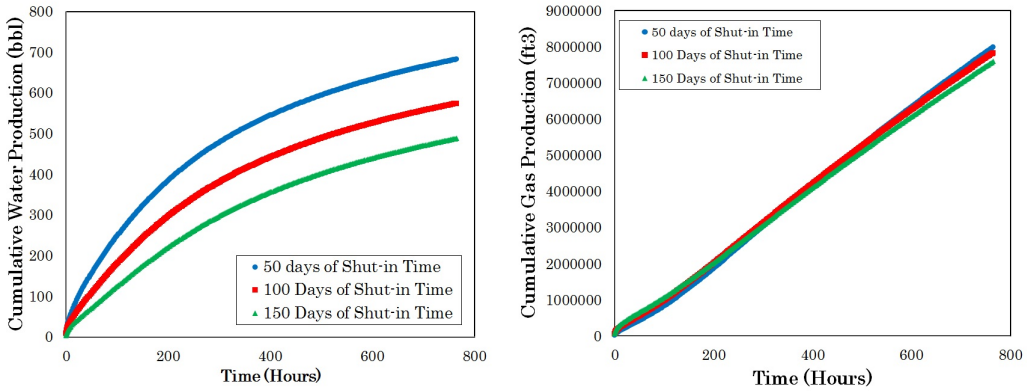

(a) (b)

Figure 6.7. Impact of shut-in time on cumulative water production (A) and cumulative gas production (B) during flowback period. Extended shut-in time decreases water production and ultimate gas production. However, it increases the gas production before the roll over time

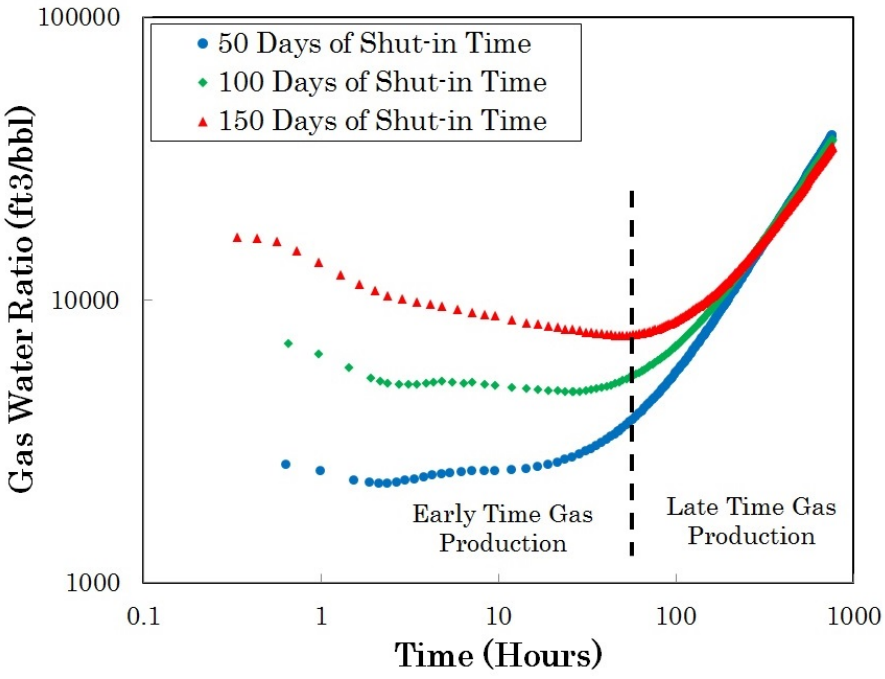

Figure 6.8. Impact of shut-in time on gas water ratio. Longer shut-in time results in higher early time gas production and gas water ratio has a sharper V-shape

6.4.2 Case 2: Impact of Secondary Fracture Density

Hydraulic fracturing in gas shale reservoirs has often resulted in complex fracture network, as evidenced by microseismic monitoring (Fisher et al., 2002). Furthermore, fracture distribution studies of outcrop show a wide range fracture width

and length (Kazemi et al., 2005). An induced dendritic fracture network combined with pre-existing and re-activated natural fractures can significantly influence the fluid flow during the shut-in and flowback processes. Thus, to have a more realistic reservoir model, we include secondary fractures in the numerical model and analyze sensitivity of the early time water and gas flow rates and the V-shape behavior on the density of secondary fractures. Therefore, three simulation models with secondary fracture spacing of 51 ft (low density), 34 ft (medium density) and 26 ft (high density) are created to investigate the effects of secondary fracture density on V-shape in gas water ratio plots. To uniquely characterize fracture density, we define a approximation of fracture complexity as

$$FCI = \frac{V_{sf}}{V_{pf} + V_{sf}} \tag{6.2}$$

Where, FCI is fracture complexity index, V_{sf} is volume of secondary fractures and V_{pf} is volume of primary fractures. Based on this definition, the properties of the simulation cases designed for this study are summarized in Table 6.2. Figure 6.9 shows the 3-D view of simulation cases created for investigating the effects of fracture complexity.

Table 6.2. Simulation cases created for investigating the effects of fracture complexity on early time gas production

Cases	Secondary Fracture Spacing	FCI
No Secondary Fractures	-	0
Low density	51 ft	0.13
Medium Density	34 ft	0.18
High Density	26 ft	0.22

Figure 6.10 shows the water saturation contour of primary fracture plane for cases with different FCI before opening the wells for flowback (after 150 days shut in). The gas saturation in the fracture is the highest in the model with the highest FCI. Increasing fracture complexity results in a higher contact surface area for the imbibition process to take place. This increases the counter current water imbibition from fracture into matrix during shut-in time that increase early time gas production and decreases the water production.

Figures 6.11a and 6.11b respectively show the load recovery and cumulative gas production for simulation cases with different FCI values. As we expected, the load recovery of cases with the highest FCI is lowest and it is due to extensive water

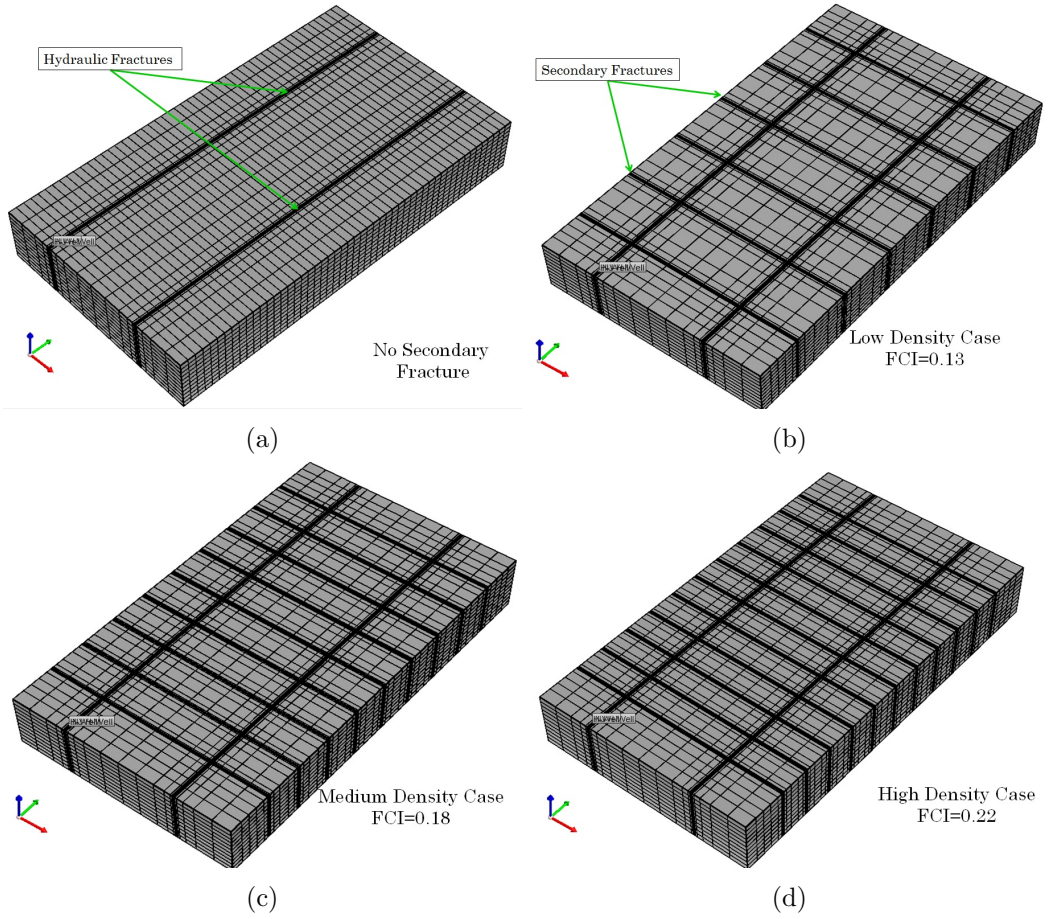

Figure 6.9. 3D view of the simulation models used for investigating the effects of fracture complexity on early time water and gas production

imbibition from fracture into rock matrix. Furthermore, increasing FCI results in more gas production which is due to 1) more contact surface and 2) extensive counter current water imbibition.

Figure 6.12 compares the various GWR plots for cases with different FCI. The addition of secondary fractures significantly increases the slope of GWR curves before roll-over time. Another major observation from the analysis is that all 4 curves converge to the same point after production rolls over to the gas dominant phase. Therefore, gas build-up in fractures mainly affects the early time of GWR plot. A similar trend is also reflected in the quantity of gas produced during the early time gas production phase of the flowback operation as shown in Table 6.3. Cumulative gas produced during the early time also increases with increasing the density of secondary fractures. Before roll-over time, the cumulative gas production for case with high density secondary fractures is almost two times higher than that of

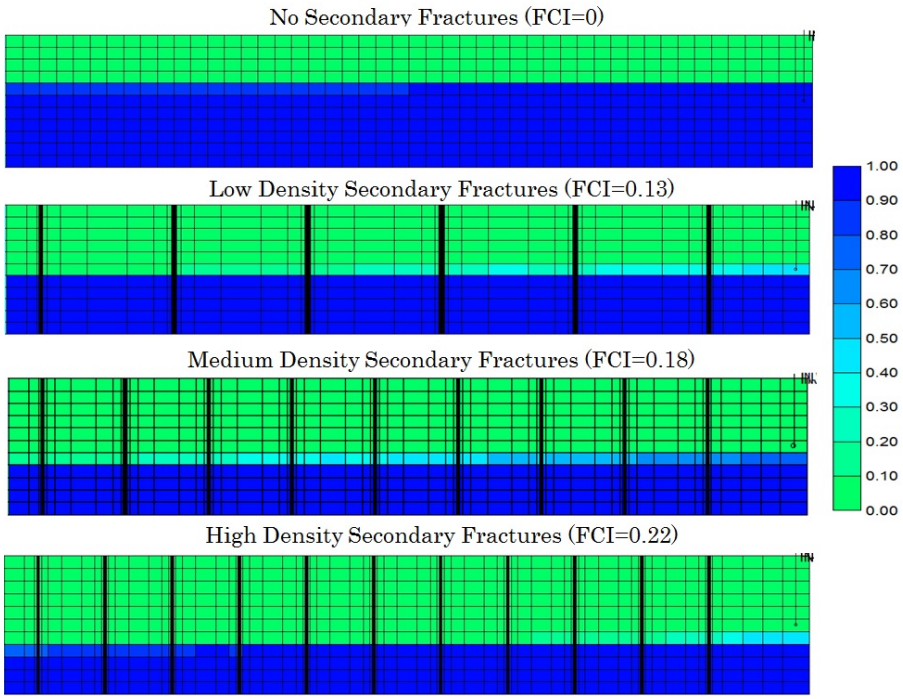

Figure 6.10. Comparison of water saturation contour of primary fracture plane for cases with different FCI at the end of shut-in period. The shut-in time for all cases is 150 days. Increasing the FCI, water imbibition from fracture into matrix increases due to higher contact surface between fracture and matrix.

case with no secondary fractures. Furthermore, the addition of secondary fractures also decreases the load recovery Increasing secondary fracture density provides more interface for water imbibition into and counter-current gas expelling shale.

Table 6.3. Effect of secondary fractures density on early time cumulative gas production and load recovery

Cases	Cumulative Gas Production (ft^3)	Load Recovery
FCI=0	812,032	4.1 %
FCI=0.13	1,232,759	3.4 %
FCI=0.18	1,527,728	3.1 %
FCI=0.22	1,769,432	3.0 %

6.4.3 Case 3: Impact of Capillary Pressure

Spontaneous imbibition in conventional and unconventional reservoir is mainly controlled by capillary pressure (Takahashi and Kovscek, 2010, Zhou et al., 2002). Therefore, the several numerical experiments are conducted to investigate the contribution of the matrix capillary pressure on early time water and gas production.

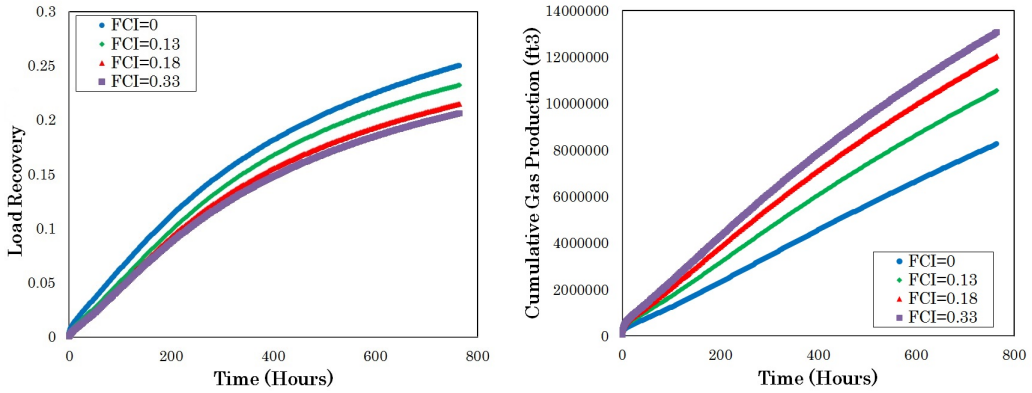

(a) (b)

Figure 6.11. Impact of fracture complexity index on load recovery (A) and cumulative gas production (B) during flowback period. Increasing the fracture complexity index, increases the counter current water imbibition into matrix and therefore reduces load recovery and increases the cumulative gas production

Three simulation models with different capillary pressure curves are created. Figure 6.13 shows the capillary pressure curves used for this study.

Figure 6.14 compares the water saturation contour of fracture plane for models with different capillary pressure curves at the end of shut-in period. Decreasing the matrix capillary pressure decreases the imbibition potential of the reservoir. Therefore, the gas build-up in fractures for model with higher capillary pressure (Case PC1) is higher than that for other cases.

Figures 6.15a and 6.15b show the cumulative gas and water production during flowback phase. Interestingly, the capillary pressure affects the early time and late time gas production during flowback phase. Before roll-over time, the cumulative gas production for case PC1 is higher than that of other cases. However, the ultimate gas production for case PC3 is higher than that of other cases. Before roll-over time, gas production is mainly from the build-up gas in the fractures due to counter current water imbibition during shut-in time. The counter current water imbibition rate for case PC1 is higher than that for cases PC2 and PC3. Therefore, this case produces more gas at the early time stage of flowback process. On the other hand, water imbibtion into shale matrix decreases the gas relative permeability at the fracture faces and results in reservoir damage. This reduces the gas production rate at the late time stage of flowback process. Furthermore, higher water imbibition rate of case PC1 results in lower water production as water can not effectively be

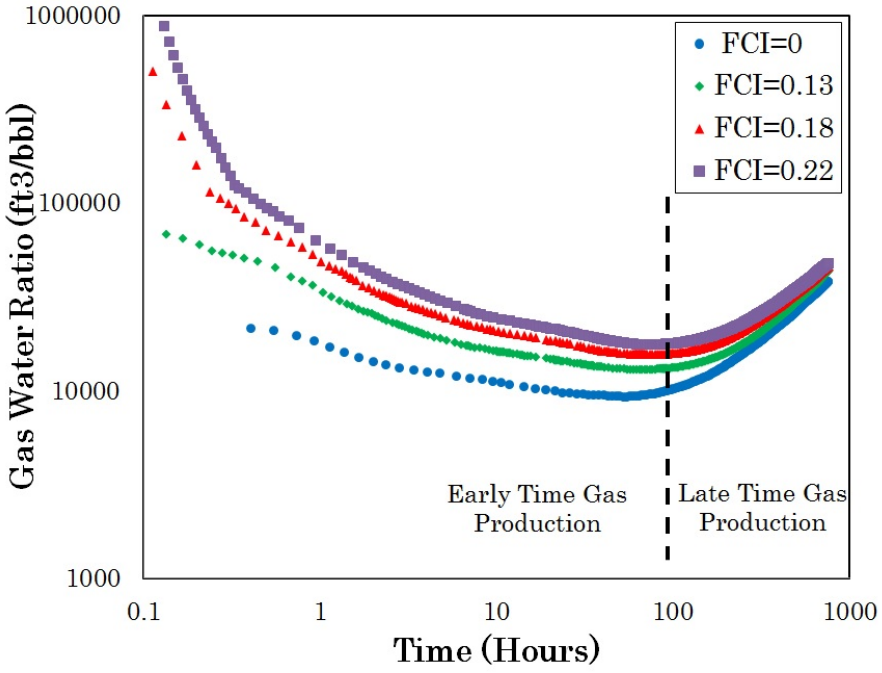

Figure 6.12. Comparison of Gas water ratio for cases with different fracture complexity index. Increasing FCI results in sharper V-shape in gas water ratio plot. This is due to increased (1) contact surface and (2) counter current water imbibition into rock matrix.

produced from matrix due to high capillary pressure (Figure 6.15b).

Figure 6.16 compares the GWR of simulation cases with different capillary pressure. The high gas volume in the fractures for case PC1 results in a clear V-shape trend in GWR plot. However, we can not identify the V-shape trend for case PC3 which has the lowest capillary pressure. Again, all curves converge to one point at the end of flowback phase. Therefore, it can be interpreted that the slope of gas water ratio curve during early time flowback phase is an indication of the amount of free gas in the fracture prior to placing the well on flowback.

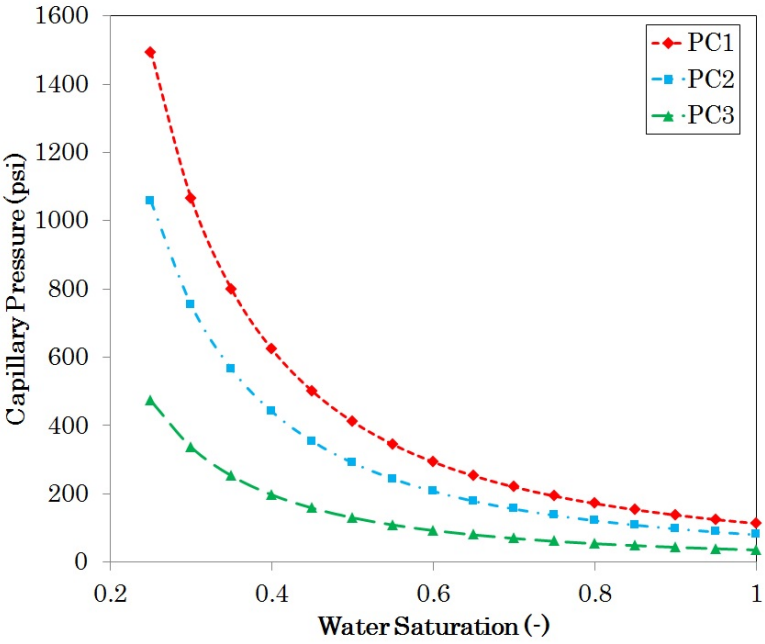

Figure 6.13. Capillary pressure curves used for simulation model

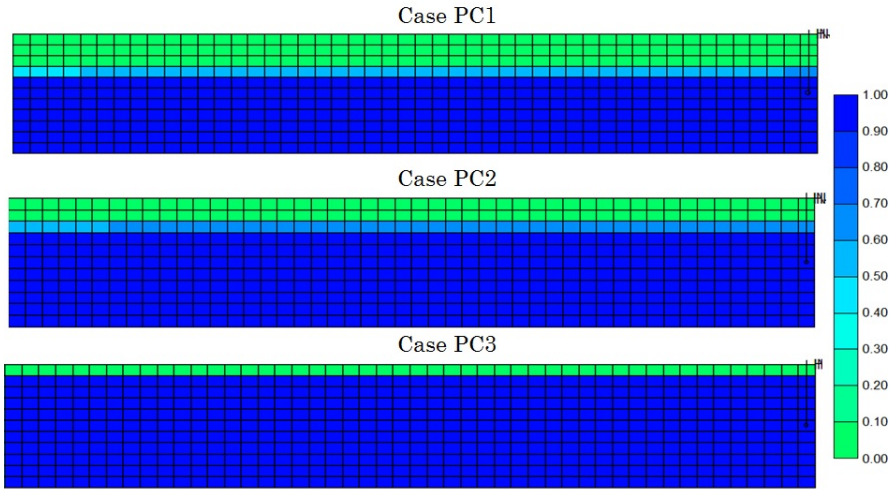

Figure 6.14. Comparison of water saturation contour of fracture plane for cases with different capillary pressure at the end of shut-in period. Decreasing the capillary decrease water imbibition from fracture into matrix

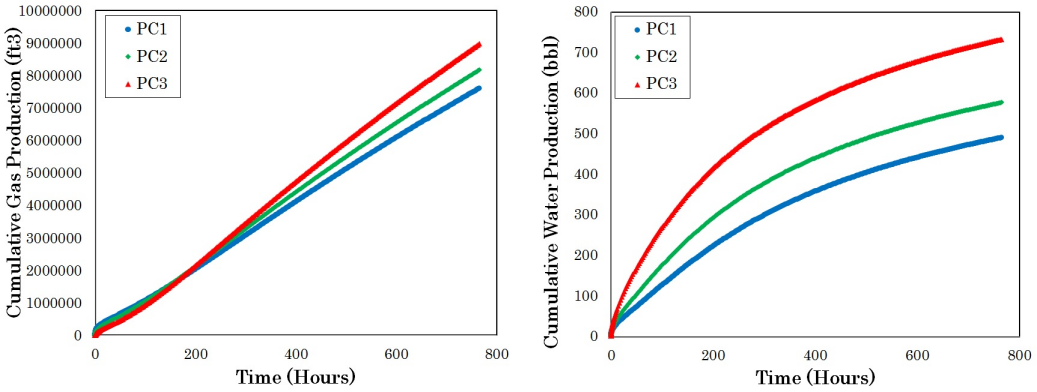

(a) (b)

Figure 6.15. Impact of capillary pressure on cumulative gas production (A) and cumulative water production (B) during flowback period. Increasing the capillary pressure decreases ultimate water and gas production

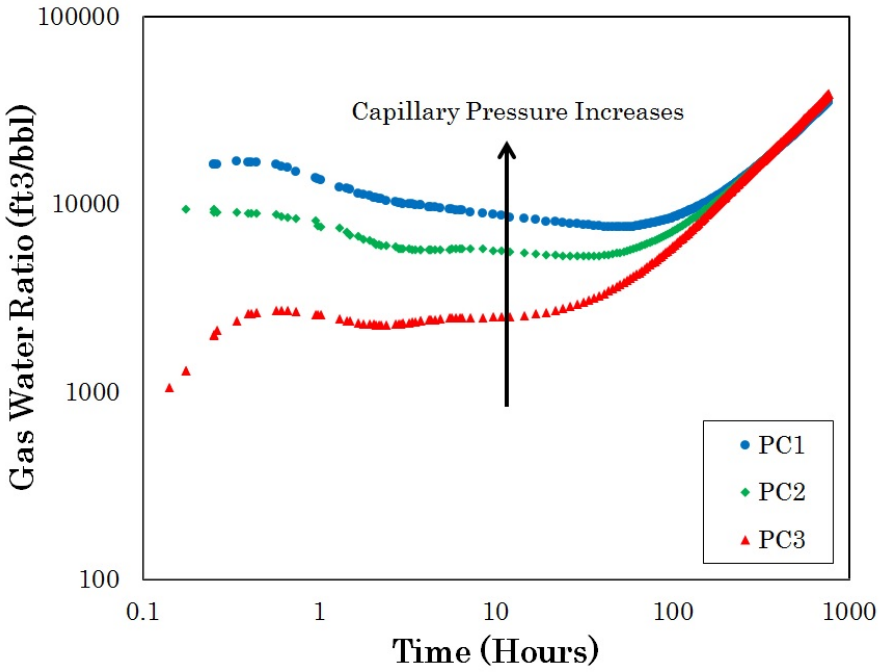

Figure 6.16. Comparison of gas water ratio for cases with different capillary pressure curves. Increasing the capillary pressure results in sharper V-shape in gas water ratio plot. This is due to increased counter current water imbibition into rock matrix.

Chapter 7

Conclusions and Recommendations

7.1 Conclusions

In this study, we investigate investigate the dominant mechanisms that could explain (1) the observed behavior of early time water and gas production and (2) the increase in salt concentration of flowback water. The following conclusions can be drawn based on this study:

7.1.1 Chemical and Volumetric Analysis of Flowback Data

- Analyses of early time water and gas production data of multi-fractured horizontal wells completed in the Horn River Basin show that wells with low flowback efficiency generally have higher early time gas production. On the other hand, wells with high flowback efficiency have low gas production.

- A diagnostic plot of the gas water ratio versus time shows two different regions. The first region is the initial drop of gas water ratio which shows the free gas depletion. The second region is the increase in gas water ratio and can be an evidence of water depletion in fractures.

- Flowback water from wells completed in Horn River Basin contains high concentration of salt and the salinity of water increases with time. The salt concentration profile of flowback water can be used to improve our understanding of the producing fracture network.

7.1.2 Liquid Imbibition and Salt Diffusion

- Contact angle measurement is not an efficient method for determining the wettability for organic gas shales. The Horn River samples show more affinity to oil based on contact angle measurements while the samples show more affinity to water based on imbibition experiments.

- The liquid flow in the organic shale greatly depends on the bedding structure of the samples. The directional imbibition experiments and BSE/ EDX images suggest that the presence of hydrophobic organic materials between shale layers can decrease the water imbibition rates perpendicular to the lamination.

- Rock fabrics of shale samples also has a significant effect on ion diffusion rates from shale samples into water. Ion diffusion rate parallel to the lamination is higher than that perpendicular to the lamination.

- The crushed shale packs imbibe more oil than water while the intact samples imbibe more water than oil. This contrary results can be explained by poor connectivity of organic materials and hydrophobic pore network. This argument is backed by complete spreading of oil droplets, strong oil imbibition into shale packs and BSE/EDX images.

- Water uptake of unconfined organic-shale samples results in microfracture induction and sample disintegration. The degree of physical alteration is correlated to the clay content of the samples. The imbibition-induced microfractures are mainly along the lamination. These microfractures increase the liquid imbibition and ion diffusion rates through increasing porosity and permeability.

- Sodium and chloride are the dominant ions that diffuses from rock into the water. These ions possibly originate from (1) the remained salt in the pores after shale sample dehydration and (2) leaching of clay minerals such as illite.

- Electric double layer properties of clays may restrict the diffusion of chloride into the water however fractured shales may act as a leaky membrane favoring the transport of anions.

- Initial water saturation state of shale samples decreases the water imbibition rate. However, it has negligible effects on oil imbibition rate.

7.1.3 Simulation Study of Flowback

- The V-shape trend observed in gas water ratio diagnostic plots for shale gas reservoir is an artifact of counter current water imbibition during shut-in period. The negative slope of this V-shape trend is correlated to the volume of gas in the fracture prior to the flowback operation.
- The early time gas production is really sensitive to shut-in time, matrix capillary pressure and fracture complexity density.
- The gas production rates from reservoir with higher capillary pressure may look promising at the beginning of flowback process but the production rates falls later due to reservoir damage.
- The created fracture network during hydraulic fracturing process has a great effect on load recovery and gas production. As the complexity increases the gas production rate increases and load recovery decreases. This is mainly due to (1) higher contact surface created between fractures and shale matrices and (2) better counter current water imbibition.

7.2 Recommendations

To further investigate the interactions of fracturing fluid and reservoir system and their effects on early- and late-time production, the following experimental and numerical studies are recommended:

- To better simulate reservoir condition during and after hydraulic fracturing, the spontaneous imbibition experiments can be followed by a series of forced imbibition experiments. It is also recommended to measure the ion diffusion rate during the forced imbibition experiments. Performing forced imbibition can help us for choosing appropriate fracturing fluid.
- More study is needed to understand the contributions of mineral dissolution, ion diffusion and water mixing to flowback water chemistry. Reservoir simulations that include these chemical processes can then be used to examine various fracture network geometries to describe the reservoir architectures that are capable of matching the measured flowback water chemistry in the field. Upscaling the salinity data obtained from diffusion experiments to field scale can give us valuable information about the created fracture volume.

- The simulation study presented in this study can be extended by considering different types of pores (hydrophilic and hydrophobic), capillary end effect, gas desorption and stress-dependant fracture permeability. It is also recommended to conduct a comprehensive simulation study on the effects of fracture complexity density on the V-shape in GWR plot. This can be done by creating several simulation models with different secondary fracture parameters such as width and length. The simulation results can be then history matched with field data to define the complexity of fracture network created by hydraulic fracturing treatment.

Bibliography

Abbasi, M. A., Dehghanpour, H., and Hawkes, R. V. (2012). Flowback Analysis for Fracture Characterization. *Paper SPE-162661-MS presented at SPE Canadian Unconventional Resources Conference, Calgary, Alberta, Canada.* http://dx.doi.org/10.2118/162661-MS.

Abbasi, M. A., Ezulike, D. O., Dehghanpour, H., and Hawkes, R. V. (2014). A Comparative Study of Flowback Rate and Pressure Transient Behavior in Multifractured Horizontal Wells Completed in Tight Gas and Oil Reservoirs. *J. of Natural Gas Sci. Eng.*, 17:82–93. http://dx.doi.org/10.1016/j.jngse.2013.12.007.

Adefidipe, O. A., Dehghanpour, H., and Virues, C. J. J. (2014). Immediate Gas Production from Shale Gas Wells: A Two-Phase Flowback Model. *Paper SPE-168982-MS presented at SPE Unconventional Resources Conference, The Woodlands, Texas, USA.* http://dx.doi.org/10.2118/168982-MS.

Agrawal, S. and Sharma, M. M. (2013). Impact of Liquid Loading in Hydraulic Fractures on Well Productivity. *Paper SPE-1638837-MS presented at SPE Hydraulic Fracturing Technology Conference, The Woodlands, Texas, USA.* http://dx.doi.org/10.2118/163837-MS.

Ali, A. J., Siddiqui, S., and H., D. (2013). Analyzing the production data of fractured horizontal wells by a linear triple porosity model: Development of analysis equations. *Journal of Petroleum Science and Engineering*, 17:117–128. http://dx.doi.org/10.1016/j.petrol.2013.10.016.

Aloisi, G., Drews, M., Wallmann, K., and Bohrmann, G. (2004). Fluid expulsion from the Dvurechenskii mud volcano (Black Sea): Part I. Fluid sources and relevance to Li, B, Sr, I and dissolved inorganic nitrogen cycles. *Earth and Planetary Science Letters*, 225:347–363. http://dx.doi.org/10.1016/j.epsl.2004.07.006.

Asadi, M., Woodroof, R. A., and Himes, R. E. (2008). Comparative Study of Flowback Analysis Using Polymer Concentrations and Fracturing-Fluid Tracer Methods: A Field Study. *SPE Prod. & Oper. J.*, 23(2):147–157. SPE–101614–PA. http://dx.doi.org/10.2118/101614-PA.

Babadagli, T. (2001). Scaling of Cocurrent and Countercurrent Capillary Imbibition for Surfactant and Polymer Injection in Naturally Fractured . *SPE J.*, 6(4):465–478. http://dx.doi.org/doi:10.2118/74702-PA.

Bai, M. and Elsworth, D. (1993). Dual-porosity poroelastic approach to behaviour of porous media over a mining panel. *Transactions of the Institution of Mining and Metallurgy, Section A*, 102:114–124.

Ballard, T. J., Beare, S. P., and Lawless, T. A. (1994). Fundamentals of Shale Stabilization: Water Transport through Shales. *SPE Formation Eval. J.*, 9(2):129–134. SPE 24974–PA. http://dx.doi.org/10.2118/24974-PA.

Barenblatt, G., Zheltov, I., and Kochina, I. (1960). Basic concepts in the theory of seepage of homogeneous liquids in fissured rocks [strata]. *Journal of Applied Mathematics and Mechanics*, 24(5):1286–1303.

Bassiouni, Z. (1994). Theory, Measurement and Interpretation of Well Logs. *SPE Textbook Series VOL. 4*.

Bazin, B., Peysson, Y., Lamy, F., Martin, F., Aubry, E., and Chapuis, C. (2010). In-situ water-blocking measurements and interpretation related to fracturing operations in tight gas reservoirs. *SPE Prod. & Oper.*, 25(4):431–437. http://dx.doi.org/10.2118/121812-PA.

BC Minstry of Energy and Mines (2011). Ultimate Potentioal for Unconventional Natural Gas in Northeastern British Columbia's Horn River Basin. *Oil and Gas Report*.

Bearinger, D. (2013). Message in a Bottle. *Paper URTeC-1618676 presented at at the Unconventional Resources Technology Conference held in Denver, Colorado, USA*.

Beaudoin, B. and Shaw, J. (2009). Characterization of the Horn River Basin Thermogenic Shale Gas Play in Northeastern BC: Frontiers and Innovation. *CSPG CSEG CWLS Convention*.

Behmanesh, H., Hamdi, H., and Clarkson, C. R. (2013). Production Data Analysis of Liquid Rich Shale Gas Condensate Reservoirs. *Paper SPE-167160-MS presented at the SPE Unconventional Resources Conference-Canada held in Calgary, Alberta, Canada*. http://dx.doi.org/10.2118/167160-MS.

Bello, R. (2009). *Rate Transient Analysis in Shale Gas Reservoirs with Transient Linear Behavior*. PhD thesis, Texas A&M U., College Station, Texas.

Bennion, D. B. and Thomas, F. B. (2005). Formation Damage Issues Impacting the Productivity of Low Permeability, Low initial Water Saturation Gas Producing Formations. *Energy Resour. Technol. J*, 127:240–247. http://dx.doi.org/10.1115/1.1937420.

Blaunch, M. E., Myers, R. R., Moore, T. R., Lipiniski, B. A., and Houston, N. A. (2009). Marcellus Shale Post-Frac Flowback Waters - Where is All the Salt Coming from and What are the Implications? *Paper SPE-125740-MS presented at SPE Eastern Regional Meeting, Charleston, West Virginia, USA*. http://dx.doi.org/10.2118/125740-MS.

Bustin, R. M., Bustin, A., Ross, D., Chalmers, G., Murthy, V., Laxmi, C., and Cui, X. (2009). Shale Gas Opportunities and Challenges. *Search and Discovery Articles*, pages 20–23.

Bustin, R. M. and Clarkson, C. R. (1998). Geological controls on coalbed methane reservoir capacity and gas content. *International Journal of Coal Geology*, 38(1):3–26. http://dx.doi.org/10.1016/S0166-5162(98)00030-5.

Cai, J., Hu, X., Standnesc, D. C., and You, L. (2012). An Analytical Model for Spontaneous Imbibition in Fractal Porous Media Including Gravity. *Colloids and Surfac.*, 414(20):228–233. http://dx.doi.org/10.1016/j.colsurfa.2012.08.047.

Cai, J., Yu, B., Zou, M., and Luo, L. (2010). Fractal Characterization of Spontaneous Co-current Imbibition in Porous Media. *Energy & Fuels*, 24(3):1860–1867. http://dx.doi.org/10.1021/ef901413p.

Chalmers, G. R., Ross, D. J., and Bustin, R. M. (2012). Geological controls on matrix permeability of Devonian Gas Shales in the Horn River and Liard basins, northeastern British Columbia, Canada. *International Journal of Coal Geology*, 103:120–131. http://dx.doi.org/10.1016/j.coal.2012.05.006.

Chenevert, M. E. (1970a). Shale alteration by water adsorption. *J. of Pet. Technol.*, 22(9):240–247, SPE–2401–PA. http://dx.doi.org/10.2118/2401-PA.

Chenevert, M. E. (1970b). Shale control with balanced-activity oil-continuous muds. *Journal of Petroleum Technology*, 22(10):1309–1316. http://dx.doi.org/10.2118/2559-PA.

Cheng, Y. (2012). mpact of Water Dynamics in Fractures on the Performance of Hydraulically Fractured Wells in Gas-Shale Reservoirs. *J. of Can. Pet. Technol.*, 51(2):143–151. SPE–127863–PA. http://dx.doi.org/10.2118/127863-PA.

Cheng, Y., Lee, W., and MacVay, D. (2009). A New Approach for Reliable Estimation of Hydraulic Fracture Properties Using Elliptical Flow Data in Tight Wells. *SPE Res. Eva. & Eng. J.*, 20:254 – 262, SPE–105767–PA. http://dx.doi.org/10.2118/105767-PA.

Cipolla, C. L., Lolon, E., Erdle, J., and Tathed, V. S. (2009). Modeling Well Performance in Shale-Gas Reservoirs. *Paper SPE-125532-MS presented at SPE/EAGE Reservoir Characterization and Simulation Conference, Abu Dhabi, UAE*. http://dx.doi.org/10.2118/125532-MS.

Clarkson, C. R., Solano, N., Bustin, R. M., Bustin, A. M. M., Chalmers, G. R. L., He, L., Melnichenko, Y. B., Radliski, A. P., and Blach, T. (2013). Pore Structure Characterization of North American Shale Gas Reservoirs Using USANS/SANS, Gas Adsorption, and Mercury Intrusion. *Fuel*, 103:606–616. http://dx.doi.org/10.1016/j.fuel.2012.06.119.

Crafton, J. W. (1998). Well Evaluation Using Early Time Post-Stimulation Flowback Data. *Paper SPE-49223-MS presented at SPE Annual Technical Conference and Exhibition, 27-30 September, New Orleans, Louisiana*. http://dx.doi.org/10.2118/49223-MS.

Crafton, J. W. (2008). Modeling Flowback Behavior or Flowback Equals Slowback.. *Paper SPE-119894-MS presented at SPE Shale Gas Production Conference, 16-18 November, Fort Worth, Texas, USA*. http://dx.doi.org/10.2118/119894-MS.

Crafton, J. W. (2010). Flowback Performance in Intensely Naturally Fractured Shale Gas Reservoirs. *Paper SPE-131785-MS presented at SPE Unconventional Gas Conference, 23-25 February, Pittsburgh, Pennsylvania, USA*. http://dx.doi.org/10.2118/131785-MS.

Crafton, J. W. and Gunderson, D. W. (2006). Use of Extremely High Time-Resolution Production Data to Characterize Hydraulic Fracture Properties. *Paper SPE 103591-MS presented at the SPE Annual Technical Conference and Exhibition held in San Antonio, Texas*. http://dx.doi.org/10.2118/103591-MS.

Crafton, J. W., Penny, G. S., and Borowski, D. M. (2009). Micro-Emulsion Effectiveness for Twenty Four Wells, Eastern Green River, Wyoming. *Paper SPE-123280-MS presented at SPE Rocky Mountain Petroleum Technology Conference, 14-16 April, Denver, Colorado*. http://dx.doi.org/10.2118/123280-MS.

CSUG (2010). Candian society for unconventional gas (csug). ucg facts. retrieved august 10, 2010, from canadian society for unconventional gas.

Curtis, M. E., Goergen, E. T., Jernigen, J. D., Sondergeld, C. H., and Rai, C. S. (2014). Mapping of Organic Matter Distribution on the Centimeter Scale with Nanometer Resolution. *Report by Gas Technology Institute, Des*

Plaines, IL, for the Marcellus Shale Coalition. http://dx.doi.org/10.15530/urtec-2014-1922757.

Dawson, M. (2005). Unconventional Gas in Canada: The Foundation for Future Energy Supplies. *Seventh Unconventional Gas Conference. Calgary, AB: Canadian Society for Unconventional Gas*.

Dehghanpour, H., Lan, Q., Saeed, Y., Fei, H., and Qi, Z. (2013). Spontaneous Imbibition of Brine and Oil in Gas Shales: Effect of Water Adsorption and Resulting Microfractures. *Energy & Fuels*, 27(6):3039–3049. http://dx.doi.org/10.1021/ef4002814.

Dehghanpour, H., Zubair, H. A., Chhabra, A., and Ullah, A. (2012). Liquid intake of organic shales. *Energy & Fuels*, 26(9):5750–5758. http://dx.doi.org/10.1021/ef3009794.

Drake, S. (2007). Unconventional Gas Plays. Southwest Land Institute Presentation. *American Association of Professional Landmen*.

Dresel, P. and Rose, A. (2010). Chemistry and Origin of Oil and Gas Well Brine in Western Pennsylvania. *Open file report*.

Dutta, R., Lee, C., Odumabo, S., Ye, P., Walker, S. C., Karpyn, Z. T., and Ayala, L. F. (2014). Experimental Investigation of Fracturing-Fluid Migration Caused by Spontaneous Imbibition in Fractured Low-Permeability Sands. *SPE Res. Eval. & Eng.*, 17(1):74–81. http://dx.doi.org/10.2118/154939-PA.

Economides, M. and Martin, M. T. (2007). Modern Fracturing: Enhancing Natural Gas Production. *Houston, Texas: Energy Tribune Publishing, Inc.*

Energy Minerals Division (2010). Gas shales. *American Association of Petroleum Geologists*.

Ezulike, D. O. and Dehghanpour, H. (2014a). A model for simultaneous matrix depletion into natural and hydraulic fracture networks. *Journal of Natural Gas Science and Engineering*, 16:57–69. http://dx.doi.org/10.1016/j.jngse.2013.11.004.

Ezulike, D. O. and Dehghanpour, H. (2014b). A Workflow for Flowback Data Analysis Creating Value out of Chaos. *Paper SPE-1922047-MS presented at the SPE/AAPG/SEG Unconventional Resources Technology Conference, Denver, Colorado, USA*. http://dx.doi.org/10.15530/urtec-2014-1922047.

Ezulike, D. O. and Dehghanpour, H. (2014c). Development of Specialized Plots for Production Data Analysis of Tight Reservoirs with Secondary Fractures. *Paper SPE-171589-MS presented at the SPE/CSUR Unconventional Resources Conference, Calgary, Alberta, Canada*. http://dx.doi.org/10.2118/171589-MS.

Ezulike, D. O. and Dehghanpour, H. (2014d). Modelling flowback as a transient two-phase depletion process. *Journal of Natural Gas Science and Engineering*, 19: 258–278. http://dx.doi.org/10.1016/j.jngse.2014.05.004.

Fakcharoenphol, P. (2013). *A Coupled Flow and Geomechanics Model for Enhanced Oil and Gas Recovery in Shale Formations*. PhD thesis, Colorado School of Mines.

Fakcharoenphol, P., Kazemi, H., Wu, Y.-S., Kurtoglu, B., and Charoenwongsa, S. (2014). The Effect of Osmotic Pressure on Improve Oil Recovery from Fractured Shale Formations. *Paper SPE-168998-MS presented at SPE Unconventional Resources Conference, The Woodlands, Texas, USA*. http://dx.doi.org/10.2118/168998-MS.

Fan, L., Thompson, J. W., and Robinson, J. R. (2010). Understanding Gas Production Mechanism and Effectiveness of Well Stimulation in the Haynesville Shale Through Reservoir Simulation. *Paper SPE 136696 presented at Canadian Unconventional Resources and International Petroleum Conference, Calgary, Alberta, Canada*. http://dx.doi.org/10.2118/136696-MS.

Faraj, B., Williams, H., Addison, G., and McKinstry, B. (2004). Gas potential of selected shale formations in the Western Canadian Sedimentary Basin. *Canadian Resources*, 10(1):21–25.

Fisher, M. K., Wright, C. A., Davidson, B. M., Goodwin, A. K., Fielder, E. O., Buckler, W. S., and Steinsberger, N. P. (2002). Integrating Fracture Mapping Technologies to Optimize Stimulations in the Barnett Shale. *Paper SPE-77441-MS presented at SPE Annual Technical Conference and Exhibition, 29 September-2 October, San Antonio, Texas*. http://dx.doi.org/10.2118/77441-MS.

Fisher, M. K., Wright, C. A., Davidson, B. M., Goodwin, A. K. Fielder, E. O., Buckler, W. S., and Steinsberger, N. P. (2005). Integrating Fracture-Mapping Technologies To Improve Stimulations in the Barnett Shale. *SPE Production & Facilities J.*, 20:85 – 93, SPE–77441–PA. http://dx.doi.org/10.2118/77441-PA.

Frantz, J. H., Jr., and Jochen, J. V. (2005). Shale Gas. *Schlumberger White Paper*.

Fredd, C. N., McConnell, S. B., Boney, C. L., and England, K. W. (2001). Experimental study of fracture conductivity for water-fracturing and conventional fracturing applications. *SPE Journal*, 6(3):288–298. http://dx.doi.org/10.2118/74138-PA.

Gale, J. F. W., Reed, R. M., and Holder, J. (2007). Natural fractures in the Barnett Shale and their importance for hydraulic fracture treatments. *AAPG Bulletin*, 91(4):603–622. http://dx.doi.org/10.1306/11010606061.

Gdanski, R. D. and Fulton, D. D. andd Shen, C. (2009). Fracture-Face-Skin Evolution During Cleanup. *J. of SPE Prod. & Oper.*, 24(1):22–34. http://dx.doi.org/doi:10.2118/101083-PA.

Gdanski, R. D., Fulton, D. D., and Johnson, B. J. (2010). Returns Matching Reveals New Tools for Fracture/Reservoir Evaluation. *Paper SPE-133806-MS presented at Tight Gas Completions Conference, San Antonio, Texas, USA*. http://dx.doi.org/10.2118/133806-MS.

Gdanski, R. D., Weaver, J. D., and Slabaugh, B. F. (2007). A New Model for Matching Fracturing Fluid Flowback Composition. *Paper SPE-106040-MS presented at SPE Hydraulic Fracturing Technology Conference, 29-31 January, College Station, Texas, U.S.A.* http://dx.doi.org/10.2118/106040-MS.

Ghanbari, E., Abbasi, M. A., Dehghanpour, H., and Bearinger, D. (2013). Flowback Volumetric and Chemical Analysis for Evaluating Load Recovery and Its Impact on Early-Time Production. *Paper SPE-167165-MS presented at SPE Unconventional Resources Conference Canada, Calgary, Alberta, Canada*. http://dx.doi:10.2118/167165-MS.

Graham, M. (2009). Encana estimates up to 900 trillion cubic feet in horn river basin.

Hale, A. H., Mody, F. K., and Salisbury, D. P. (1993). The Influence of Chemical Potential on Wellbore Stability. *SPE Drilling & Completion J.*, 8(3):207–216, SPE–23885–PA. http://dx.doi.org/10.2118/23885-PA.

Haluszczak, L. O., Rose, A. W., and Kump, L. R. (2013). Geochemical evaluation of flowback brine from Marcellus gas wells in Pennsylvania, USA. *Applied Geochemistry J.*, 28:55–61. http://dx.doi.org/10.1016/j.apgeochem.2012.10.002.

Hamblin, A. P. (2006). The "Shale Gas" Concept in Canada: A Preliminary Inventory of Possibilities. *Ottawa, ON: Geological Survey of Canada, Open File*, (5384).

Harper, J. (2008). The marcellus shalean old new gas reservoir in pennsylvania. *Pennsylvania Geology*, 38(1):2–13.

Hayes, T. (2009). Sampling and analysis of water streams associated with the development of Marcellus shale gas. *Report by Gas Technology Institute, Des Plaines, IL, for the Marcellus Shale Coalition.* http://www.bucknell.edu/MarcellusShaleDatabase.

Heffernan, K. and Dawson, F. M. (2010). An Overview of Canada's Natural Gas Resources. *Canadian Society for Unconventional Gas.*

Holditch, S. A. (1979). Factors Affecting water Blocking and Gas Flow From Hydraulically Fractured Gas Wells. *J. of Pet. Tecnol.*, 31(12):1515–1524. SPE–7561–PA. http://dx.doi.org/10.2118/7561-PA.

Holditch, S. A. and Tschirhart, N. (2005). Optimal Stimulation Treatments in Tight Gas Sands. *Paper SPE-96104-MS presented at SPE Annual Technical Conference and Exhibition, Dallas, Texas.* http://dx.doi:10.2118/96104-MS.

Howard, G. and Fast, C. (1970). Hydraulic fracturing. *Monograph Series, SPE, Richardson, Texas* **2**.

Hutcheon, I. (1998). The Potential Role of Pyrite Oxidation In Corrosion And Reservoir Souring. *J. of Canadian Petroleum Technology*, 37:PETSOC–98–01–05. http://dx.doi.org/10.2118/98-01-05.

Ilk, D., Currie, S. M., Symmons, D., Broussard, N. J., and Blasingame, T. A. (2010). A Comprehensive Workflow for Early Analysis and Interpretation of Flowback Data from wells in Tight Gas/Shale Reservoir Systems. *Paper SPE-135607-MS presented at the SPE Annual Technical Conference and Exhibition, Florence, Italy.* http://dx.doi.org/10.2118/135607-MS.

Jenkins, C. D. and Boyer II, C. M. (2008). Coalbed- and shale-gas reservoirs. *Journal of Petroleum Technology*, 60(2):92–99. http://dx.doi.org/10.2118/103514-JPT.

Kazemi, H., Atan, S., Al-Matrook, M., Dreier, J., and Ozkan, E. (2005). Multilevel Fracture Network Modeling of Naturally Fractured Reservoirs. *Paper SPE-93053-MS presented at the SPE Reservoir Simulation Symposium, The Woodlands, Texas.* http://dx.doi.org/10.2118/93053-MS.

Kazemi, H., Merrill, L., Porterfield, K., and Zeman, P. (1976). Numerical simulation of water-oil flow in naturally fractured reservoirs. *Society of Petroleum Engineers Journal*, 16(6):317–326. http://dx.doi.org/10.2118/5719-PA.

Keijzer, T. J. and Loch, J. P. G. (2001). Chemical osmosis in compacted dredging sludge. *Soil Science Society of America Journal*, 65(4):1045–1055. http://dx.doi.org/10.2136/sssaj2001.6541045x.

Keller, W. D. and Liovando, M. d. C. (1989). Comparative Chemical Compositions of Aqueous Extracts from Representative Clays. *American Mineralogis*, 74:1142–1146.

King, G. (2010). Thirty Years of Gas Shale Fracturing: What Have We Learned? *Paper SPE-133456-MS presented at SPE Annual Technical Conference and Exhibition, 19-22 September, Florence, Italy.* http://dx.doi.org/10.2118/133456-MS.

King, G. (2012). Hydraulic Fracturing 101: What Every Representative, Environmentalist, Regulator, Reporter, Investor, University Researcher, Neighbor and Engineer Should Know About Estimating Frac Risk and Improving Frac Performance in Unconventional Gas and Oil Wells. *Paper SPE 152596-MS presented at SPE Hydraulic Fracturing Technology Conference, The Woodlands, Texas, USA*. http://dx.doi.org/10.2118/152596-MS.

Kuila, U., McCarty, D. K., Derkowski, A., Fischer, T. B., and Prasad, M. (2014). Total Porosity Measurement in Gas Shales by the Water Immersion Porosimetry (WIP) Method. *Fuel*, 117:1115–1129. http://dx.doi.org/10.1016/j.fuel.2013.09.073.

Lan, Q., Dehghanpour, H., Wood, J., and Sanei, H. (2014a). Wettability of the Montney Tight Gas Formation. *Paper SPE 171620-MS presented at the SPE/CSUR Unconventional Resources Conference Canada*. http://dx.doi.org/10.2118/171620-MS.

Lan, Q., Ghanbari, E., Dehghanpour, H., and Hawkes, R. (2014b). Water Loss versus Soaking Time: Spontaneous Imbibition in Tight Rocks. *Energy Technology,*. http://dx.doi.org/10.1002/ente.201402039R2.

Lenar, J. (2000). Laboratory Evaluations in Anode Manufacturing. *Paper SPE-00679 presented at Corrosion, Orlando*.

Li, K., Chow, K., and Horne, R. N. (2006). Influence of Initial Water Saturation on Recovery by Spontaneous Imbibition in Gas/Water/Rock Systems and the Calculation of Relative Permeability. *SPE Reservoir Evaluation & Engineering*, 9(4):295–301. http://dx.doi.org/10.2118/99329-PA.

Ma, S., Morrow, N. R., and Zhang, X. J. (1997). Generalized Scaling of Spontaneous Imbibition Data for Strongly Water-wet Systems. *J. of Pet. Sci. and Eng.*, 18:165–178. http://dx.doi.org/10.1016/S0920-4105(97)00020-X.

Mackay, E. J., Jordan, M. M., and Torabi, F. (2003). Predicting brine mixing deep within the reservoir, and the impact on scale control in marginal and deepwater developments. *J. of SPE Production & Facilities*, 18:210–220, SPE–85104–PA. http://dx.doi.org/10.2118/85104-PA.

Mahadevan, J., Le, D., and Hoang, H. (2009). Impact of Capillary Suction on Fracture Face Skin Evolution in Water Blocked Wells. *Paper SPE-119585-MS presented at SPE Hydraulic Fracturing Technology Conference, The Woodlands, Texas*. http://dx.doi.org/10.2118/119585-MS.

Makhanov, K. (2013). An experimental study of spontaneous imbibition in horn river shales. Master's thesis, University of Alberta, Edmonton, Alberta. (Summer 2013).

Makhanov, K., Habibi, A., Dehghanpour, H., and Kuru, E. (2014). Liquid Uptake of Gas Shales: A Workflow to Estimate Water Loss During Shut-in Periods after Fracturing Operations. *J. of Unconventional Oil and Gas Resources*, 7:22–32. http://dx.doi.org/10.1016/j.juogr.2014.04.001.

Mayerhofer, M. J., Richardson, M. F., Walker, R. N., Meehan, D. N., Oehler, M. W., and Browning, R. R. (1997). Proppants? We Don't Need No Proppants. *Paper SPE-38611-MS presented at SPE Annual Technical Conference and Exhibition, San Antonio, Texas*. http://dx.doi.org/10.2118/38611-MS.

Medeiros, F., Ozkan, E., and Kazemi, H. (2008). Productivity and Drainage Area of Fractured Horizontal Wells in Tight Gas Reservoirs. *SPE Res Eval & Eng*, 11(5):902 – 911, SPE–108110–PA. http://dx.doi.org/10.2118/108110-PA.

Mitchell, J. K. (1993). Fundamentals of Soil Behavior. *Wiley, New York NY, USA*.

Moench, A. (1983). Well test analysis in naturally fissured, geothermal reservoirs with fracture skin. *In: the 9th Stanford Geothermal Workshop.*

National Energy Board (2006). Northeast British Columbias Ultimate Potential for Conventional Natural Gas. http://www.neb-one.gc.ca.

Ning, X., Fan, J., Holditch, S. A., , and Lee, W. J. (1993). The Measurement of Matrix and Fracture Properties in Naturally Fractured Cores. *Paper SPE-25898 presented at Low Permeability Reservoirs Symposium, Denver, Colorado.* http://dx.doi.org/10.2118/25898-MS.

Novlesky, A., Kumar, A., and Merkle, S. (2010). Shale Gas Modeling Workflow: From Microseismic to Simulation - A Horn River Case Study. *Paper SPE-14810-MS presented at the Canadian Unconventional Resources Conference held in Calgary, Alberta, Canada.* http://dx.doi.org/10.2118/148710-MS.

Olphen, V. H. (1953). Interlayer Forces in Bentonite. *Second National Conference on Clays and Clay Minerals, Publication 327, National Academy of Sciences - National Research Council, Washington, D. C.*, pages 418–438.

Overbey, W. K., Yost, A. B., and Wilkins, D. A. (1988). Inducing Multiple Hydraulic Fractures From a Horizontal Wellbore. *Paper SPE-18249-MS presented at SPE Annual Technical Conference and Exhibition, 2-5 October, Houston, Texas.* http://dx.doi.org/10.2118/18249-MS.

Palisch, T. T., Vincent, M., and Handren, P. J. (2010). Slickwater Fracturing: Food for Thought. *SPE Prod. & Oper. J.*, 25(3):327–344. SPE–115766–PA. http://dx.doi:10.2118/115766-PA.

Palisch, T. T., Vincent, M. C., and Handren, P. J. (2005). Slickwater Fracturing: Food for Thought. *Paper SPE-115766-MS presented at SPE Annual Technical Conference and Exhibition, Denver, Colorado, USA.* http://dx.doi.org/10.2118/115766-MS.

Parmar, J., Dehghanpour, H., and Kuru, E. (2014). Displacement of Water by Gas in Propped Fractures: Combined Effects of Gravity, Surface Tension, and Wettability. *J. of Unconventional Oil and Gas Resources*, 17:10–21. http://dx.doi.org/10.1016/j.juogr.2013.11.005.

Parmar, J. S., Dehghanpour, H., and Kuru, E. (2012). Unstable Displacement: A Missing Factor in Fracturing Fluid Recovery. *Paper SPE 162649 presented at SPE Canadian Unconventional Resources Conference, Calgary, Alberta, Canada.* http://dx.doi.org/10.2118/162649-MS.

Parmar, J. S., Dehghanpour, H., and Kuru, E. (2013). Drainage Against Gravity: Factors Impacting the Load Recovery In Fractures. *Paper SPE-164530-MS presented at SPE Unconventional Resources Conference - USA, Woodlands, TX, USA.* http://dx.doi.org/10.2118/164530-MS.

Pearson, C. M., Lynch, K. W., Schmidt, J. H., and McCaslin, N. F. (1988). Improvement of Massive Hydraulic Fracture Treatments in the Cotton Valley Formation of East Texas. *Paper SPE-17714-MS presented at SPE Gas Technology Symposium, Dallas, Texas.* http://dx.doi.org/10.2118/17714-MS.

Penny, G. S., Conway, M. W., and Lee, W. (1985). Control and modeling of fluid leakoff during hydraulic fracturing. *Journal of Petroleum Technology*, 37(6):1071–1081. http://dx.doi.org/10.2118/12486-PA.

Penny, G. S., Dobkins, T. A., and Pursley, J. T. (2006). Field Study of Completion Fluids To Enhance Gas Production in the Barnett Shale. *Paper SPE-100434-MS presented at the SPE Gas Technology Symposium, Calgary, Alberta, Canada.* http://dx.doi.org/10.2118/100434-MS.

Pritz, M. E. and Kirby, C. S. (2010). Geochemical investigation of Marcellus Shale natural gas hydro fracturing waters. *Geological Society of America Annual Meeting*, 42(1):121.

Pruess, K. (1985). A practical method for modeling fluid and heat flow in fractured porous media. *Society of Petroleum Engineers Journal*, 25(1):14–26. http://dx.doi.org/10.2118/10509-PA.

Rice, D. D. (1993). Composition and origins of coalbed gas. *Hydrocarbons from coal: AAPG Studies in Geology*, 38:159–184.

Rogers, S., Elmo, D., Dunphy, R., and Bearinger, D. (2010). Understanding Hydraulic Fracture Geometry and Interactions in the Horn River Basin Through DFN and Numerical Modeling. *Paper SPE 137488-MS presented at Canadian Unconventional Resources and International Petroleum Conference, Calgary, Alberta, Canada*. http://dx.doi.org/10.2118/137488-MS.

Rokosh, C. D., Pawlowicz, J. G., Berhane, H., Anderson, S. D., and Beaton, A. P. (2009). What is Shale Gas? An Introduction to Shale-Gas Geology in Alberta. *Energy Resource Conservation Board and Alberta Geological Survey*.

Ross, D. J. K. and Bustin, R. M. (2008). Characterizing the shale gas resource potential of Devonian-Mississippian strata in the Western Canada sedimentary basin: Application of an integrated formation evaluation. *AAPG Bull.*, 92(1):87–125. http://dx.doi.org/10.1306/09040707048.

Rowan, E. L., Engle, M. A., Kirby, C. S., and Kraemer, T. F. (2011). Radium Content of Oil- and Gas-field Produced Waters in the Northern Appalachian Basin (USA): Summary and Discussion of Data. *Geological Survey Scientific Investigations Report*, page 5135.

Roychaudhuri, B., Tsotsis, T., and Jessen, K. (2011). An Experimental and Numerical Investigation of Spontaneous Imbibition in Gas Shales. *Paper SPE-147652-MS presented at SPE Annual Technical Conference and Exhibition, Denver, Colorado, USA*. http://dx.doi.org/10.2118/147652-MS.

Russum, D. (2005). Status of Unconventional Gas in North America. *Seventh Unconventional Gas Conference. Calgary, AB: Canadian Society for Unconventional Gas*.

Samandarli, O., Valbuena, E., and Ehlig-Economides, C. (2012). Production Data Analysis in Unconventional Reservoirs with Rate-Normalized Pressure (RNP): Theory, Methodology, and Applications. *Paper SPE-155614-MS presented at SPE Americas Unconventional Resources Conference, Pittsburgh, Pennsylvania, USA*. http://dx.doi.org/10.2118/155614-MS.

Schein, G. (2005). The Application and Technology of Slickwater Fracturing. *Society of Petroleum Engineers*.

Schmitt, L., Forsans, T., and Santarelli, F. J. (1994). Shale Testing and Capillary Phenomena. *Int. J. Rock Mech. Min. Sci. & Geomech. Abstr.*, 31(5):411–427. http://dx.doi.org/10.1016/0148-9062(94)90145-7.

Scott, H., Patey, I. T. M., and Byrne, M. T. (2007). Return Permeability Measurements - Proceed With Caution. *Paper SPE-107812-MS presented at European Formation Damage Conference, Scheveningen, The Netherlands*. http://dx.doi.org/10.2118/107812-MS.

Settari, A., Sullivan, R. B., and Bachman, R. C. (2002). The Modeling of the Effect of Water Blockage and Geomechanics in Waterfrac. *Paper SPE-77600 presented at the SPE Annual Technical Conference and Exhibition, San Antonio, Texas, USA*. http://dx.doi.org/10.2118/77600-MS.

Shaoul, J., Zelm, L. V., and Pater, C. J. D. (2011). Damage Mechanisms in Unconventional-Gas-Well StimulationA New Look at an Old Problem. *SPE Prod. & Oper*, 26(4):388–400. SPE–142479–PA. http://dx.doi.org/10.2118/142479-PA.

Siddiqui, K., Ali, A., and Dehghanpour, H. (2012). New Advances in production data analysis of hydraulically fractured tight reservoirs. *Paper SPE-162830-MS presented at the SPE Canadian Unconventional Resources Conference, Calgary, Canada*. http://dx.doi.org/10.2118/162830-MS.

Sondergeld, C. H., Ambrose, R. J., Rai, C. S., and Moncrieff, J. (2010). Micro-Structural Studies of Gas Shales. *Paper SPE-131771-MS presented at SPE Unconventional Gas Conference, Pittsburgh, Pennsylvania, USA*. http://dx.doi.org/10.2118/131771-MS.

Song, B. and Ehlig-Economides, C. (2011). Rate-normalized pressure analysis for determination of shale gas performance. *Paper SPE-144031-MS Presented at the North American Unconventional Gas Conference, The Woodlands, Texas*. http://dx.doi.org/10.2118/144031-MS.

Steiger, R. P. (1982). Fundamentals and Use of Potassium/Polymer Drilling Fluids to Minimize Drilling and Completion Problems Associated With Hydratable Clays. *J. Pet. Technol.*, 34(8):1661–1670. SPE–10100–PA. http://dx.doi.org/10.2118/10100-PA.

Takahashi, S. and Kovscek, A. R. (2010). Spontaneous Countercurrent Imbibition and Forced Displacement Characteristics of Low-permeability, Siliceous Shale Rocks. *J. of Pet. Sci. and Eng.*, 70(1):47–55. http://dx.doi.org/10.1016/j.petrol.2010.01.003.

Taylor, R. S., Barree, R. D., Aguilera, R., Hotch, O., and Storozhenko, K. K. (2011). Why Not to Base Economic Evaluations on Initial Production Alone. *Paper SPE-148680-MS presented at Canadian Unconventional Resources Conference, Alberta, Canada*. http://dx.doi.org/10.2118/148680-MS.

Todd, A. C. and Yuan, M. D. (1992). Barium and Strontium Sulfate Solid-Solution Scale Formation at Elevated Temperatures. *J. of SPE Production Engineering*, 7:85–92, SPE–19762–PA. http://dx.doi.org/10.2118/19762-PA.

Veatch, R. W. J., Moschovidis, Z. A., and Fast, C. R. (1989). An overview of hydraulic fracturing. in recent advances in hydraulic fracturing,. *ed. J.L. Gidley, S.A. Holditch, D.E. Nierode, and R.W. Veatch Jr., Vol.12, Chap. 1, 138. Richardson, Texas: Henry L. Doherty Monograph Series, SPE.*

Wang, F. P. and Reed, R. M. (2009). Pore Networks and Fluid Flow in Gas Shales. *Paper SPE-124253-MS presented at SPE Annual Technical Conference and Exhibition, New Orleans, Louisiana*. http://dx.doi.org/10.2118/124253-MS.

Wang, Q., Guo, B., and Gao, D. (2012). Is Formation Damage an Issue in Shale Gas Development? *Paper SPE 149623-MS presented at SPE International Symposium and Exhibition on Formation Damage Control, Lafayette, Louisiana, USA*. http://dx.doi.org/10.2118/149623-MS.

Warpinski, N., Kramm, R. C., Heinze, J. R., and Waltman, C. K. (2005). Comparison of Single-and Dual-Array Microseismic Mapping Techniques in the Barnett Shale. *Paper SPE-95568-MS presented at SPE Annual Technical Conference and Exhibition, Dallas, Texas*. http://dx.doi.org/10.2118/95568-MS.

Warren, J. and Root, P. (1963). The behavior of naturally fractured reservoirs. *Society of Petroleum Engineers Journal*, 3(3):245–255. http://dx.doi.org/10.2118/426-PA.

Wayllace, A. (2008). *Volume Change and Swelling Pressure of Expansive Clay In the Crystalline Swelling Regime*. PhD thesis, University of Missouri.

Williams-kovacs, J. (2012). New methods for shale gas prospect analysis. Master's thesis, University of Calgary, Calgary, Alberta.

Williams-kovacs, J. and Clarkson, C. R. (2011). Using Stochastic Simulation To Quantify Risk and Uncertainty in Shale Gas Prospecting and Development. *Paper SPE-148867-MS presented at Canadian Unconventional Resources Conference, Alberta, Canada*. http://dx.doi.org/10.2118/148867-MS.

Woo, I., Kim, J. G., Lee, G. H., Park, H. J., and Um, J. G. (2007). Evaluation of the Mechanical And Physical Properties of Rock Containing Pyrite By Leaching Tests. *Paper ARMA-07-105 presented at 1st Canada - U.S. Rock Mechanics Symposium, Vancouver, Canada*.

Woodroof, R. A. J., Asadi, M., and Warren, M. N. (2003). Monitoring Fracturing Fluid Flowback and Optimizing Fracturing Fluid Cleanup Using Chemical Frac Tracers. *Paper SPE-82221-MS presented at the SPE European Formation Damage Conference*. http://dx.doi.org/10.2118/82221-MS.

Wu, Y. S., Liu, H. H., and Bodvarsson, G. S. (2004). A triple-continuum approach for modeling flow and transport processes in fractured rock. *Journal of Contaminant Hydrology*, 73(1-4):145–179.

Xu, M. and Dehghanpour, H. (2014). Advances in Understanding Wettability of Gas Shales. *Energy & Fuels*, 28(7):4362–4375. http://dx.doi.org/10.1021/ef500428y.

Yeung, A. T. and Mitchell, J. K. (1993). Coupled Fluid, Electrical and Chemical Flows in Soil. *Geotechnique*, 43(1):121–134. http://dx.doi.org/10.1680/geot.1993.43.1.121.

Yost, A. B. and Overbey, W. K. (1989). Production and Stimulation Analysis of Multiple Hydraulic Fracturing of a 2,000-ft Horizontal Well. *Paper SPE-19090-MS presented at SPE Gas Technology Symposium, 7-9 June, Dallas, Texas*. http://dx.doi.org/doi:10.2118/19090-MS.

Zhang, X., Morrow, N. R., and Ma, S. (1996). Experimental Verification of a Modified Scaling Group for Spontaneous Imbibition. *SPE Res. Eng. J.*, 11(4):280–285. http://dx.doi.org/doi:10.2118/30762-PA.

Zhou, D., Jia, L., Kamath, J., and Kovscek, A. R. (2002). Scaling of Counter-current Imbibition Processes in Low-permeability Porous Media. *J. of Pet. Sci. and Eng.*, 33(1):61–74. http://dx.doi.org/10.1016/S0920-4105(01)00176-0.

Zolfaghari, A., Ghanbari, E., Dehghanpour, H., and Bearinger, D. (2014a). Fracture Architecture from Flowback Signature: A Model for Salt Concentration Transient. *Paper SPE-168598-MS presented at the SPE Hydraulic Fracturing Technology Conference, The Woodlands, Texas, USA*. http://dx.doi.org/10.2118/168598-MS.

Zolfaghari, A., Noel, M., Dehghanpour, H., and Bearinger, D. (2014b). Understanding the Origin of Flowback Salts: A Laboratory and Field Study. *Paper SPE-171647-MS presented at SPE/CSUR Unconventional Resources Conference-Canada*. http://dx.doi.org/10.2118/171647-MS.

Appendix A

Salinity Profile

Here, we present the salinity profiles for 18 wells completed in Muskwa, Otter Park and Evie formations.

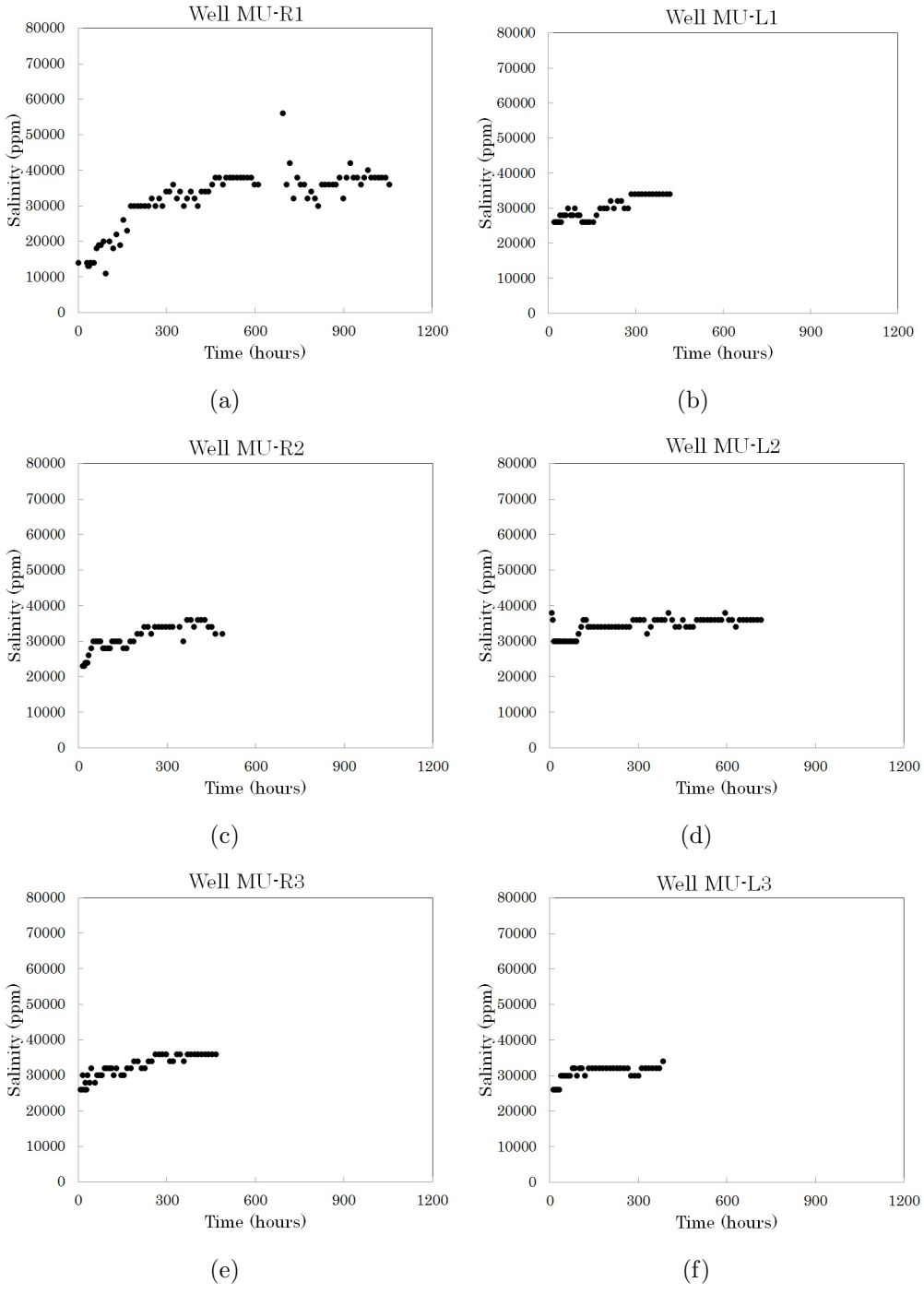

Figure A.1. The change of salinity of flowback water versus production time for wells completed in Muskwa formation

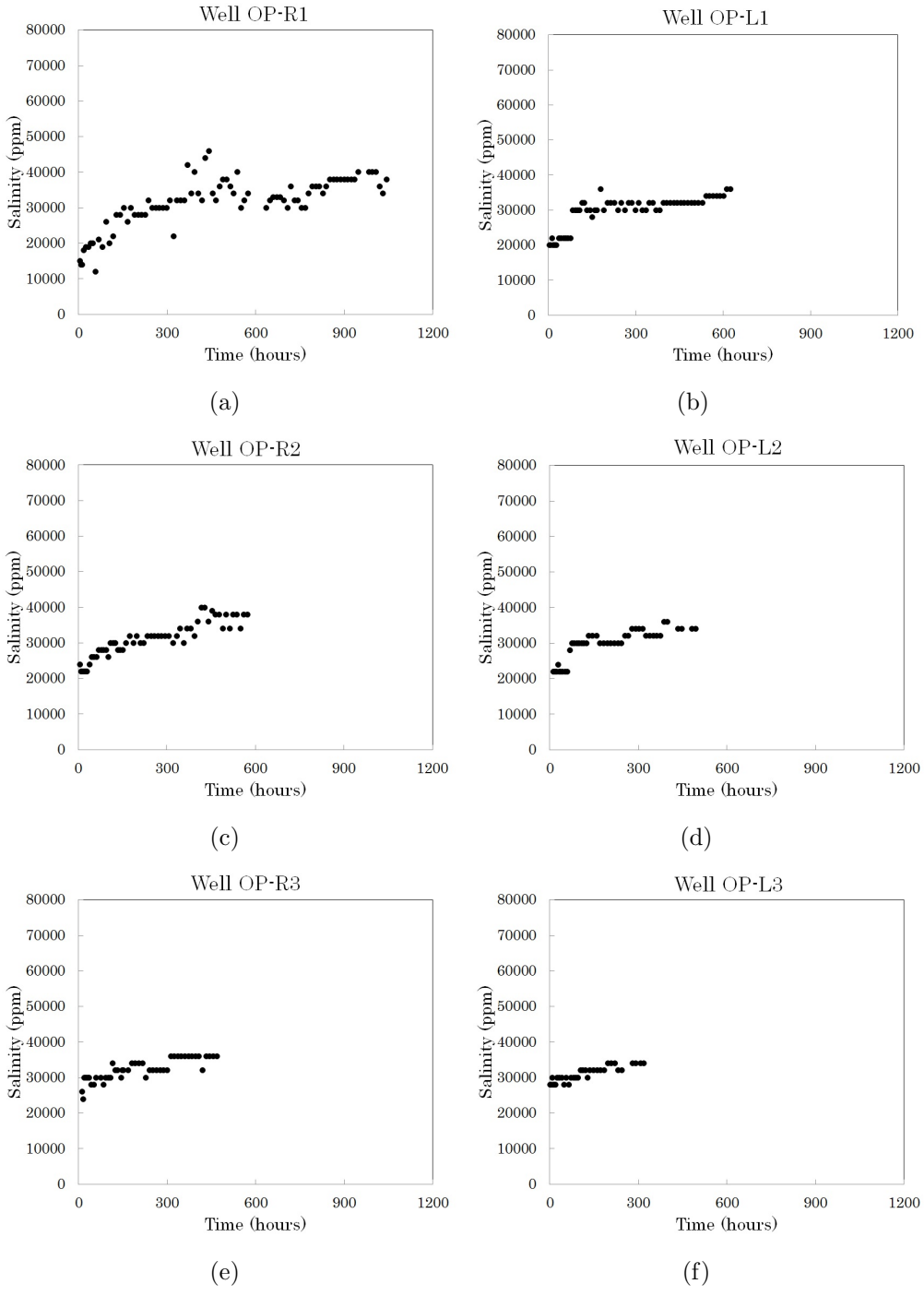

Figure A.2. The change of salinity of flowback water versus production time for wells completed in Otter Park formation

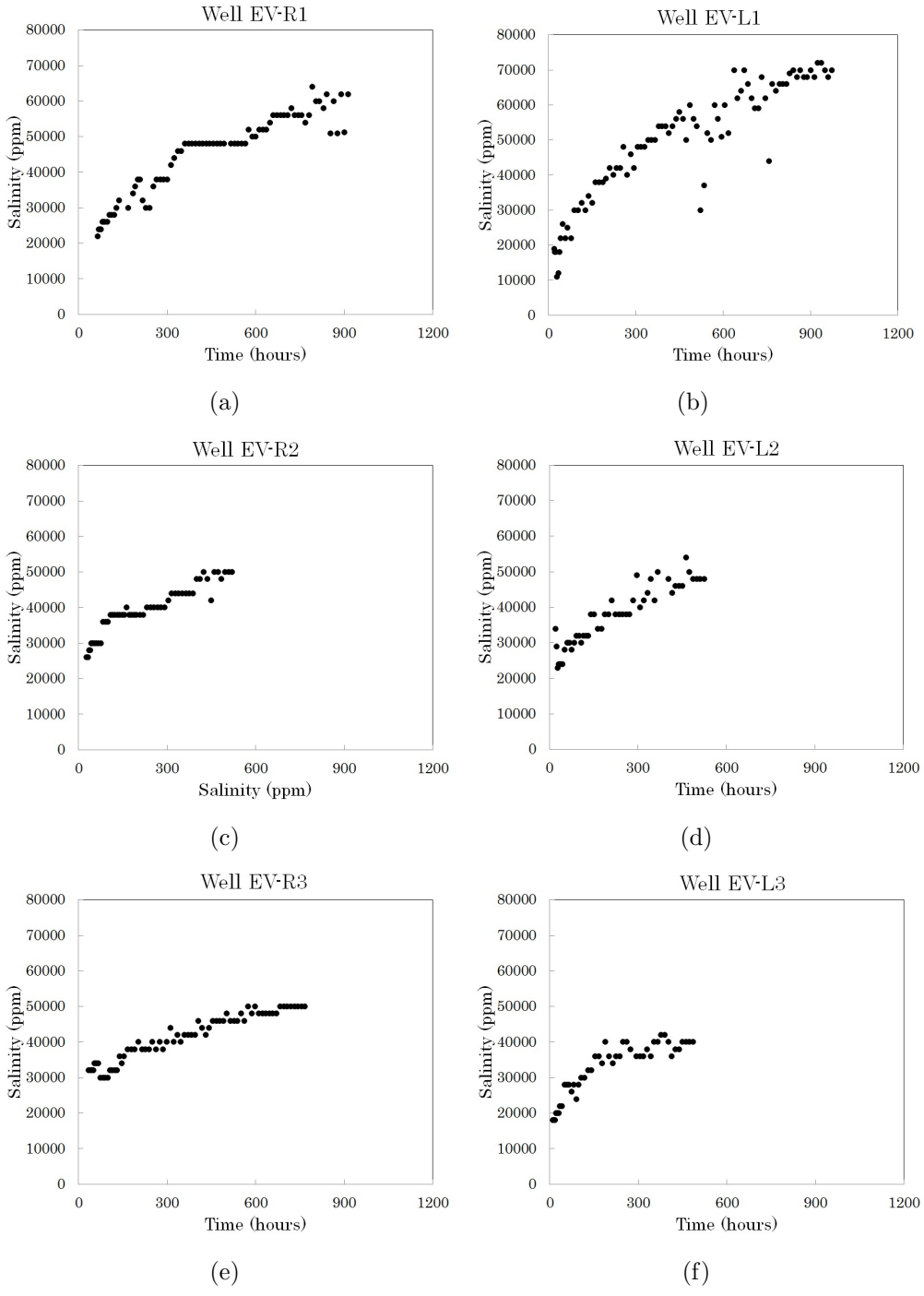

Figure A.3. The change of salinity of flowback water versus production time for wells completed in Evie formation

Appendix B

Barium Concentration Profile

Here, we present the barium concentration profiles for 18 wells completed in Muskwa, Otter Park and Evie formations.

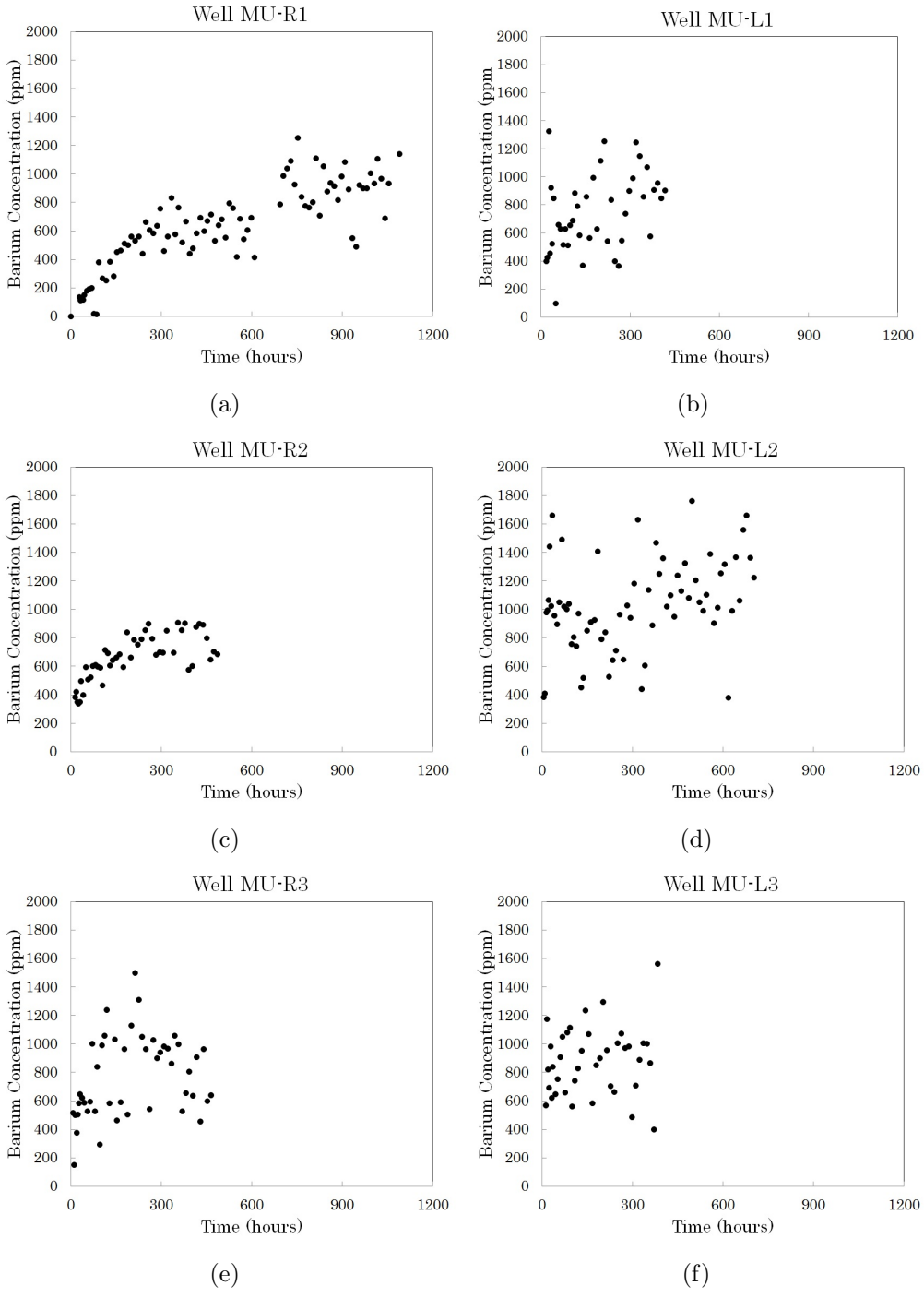

Figure B.1. The change of barium concentration in flowback water for wells completed in Muskwa formation

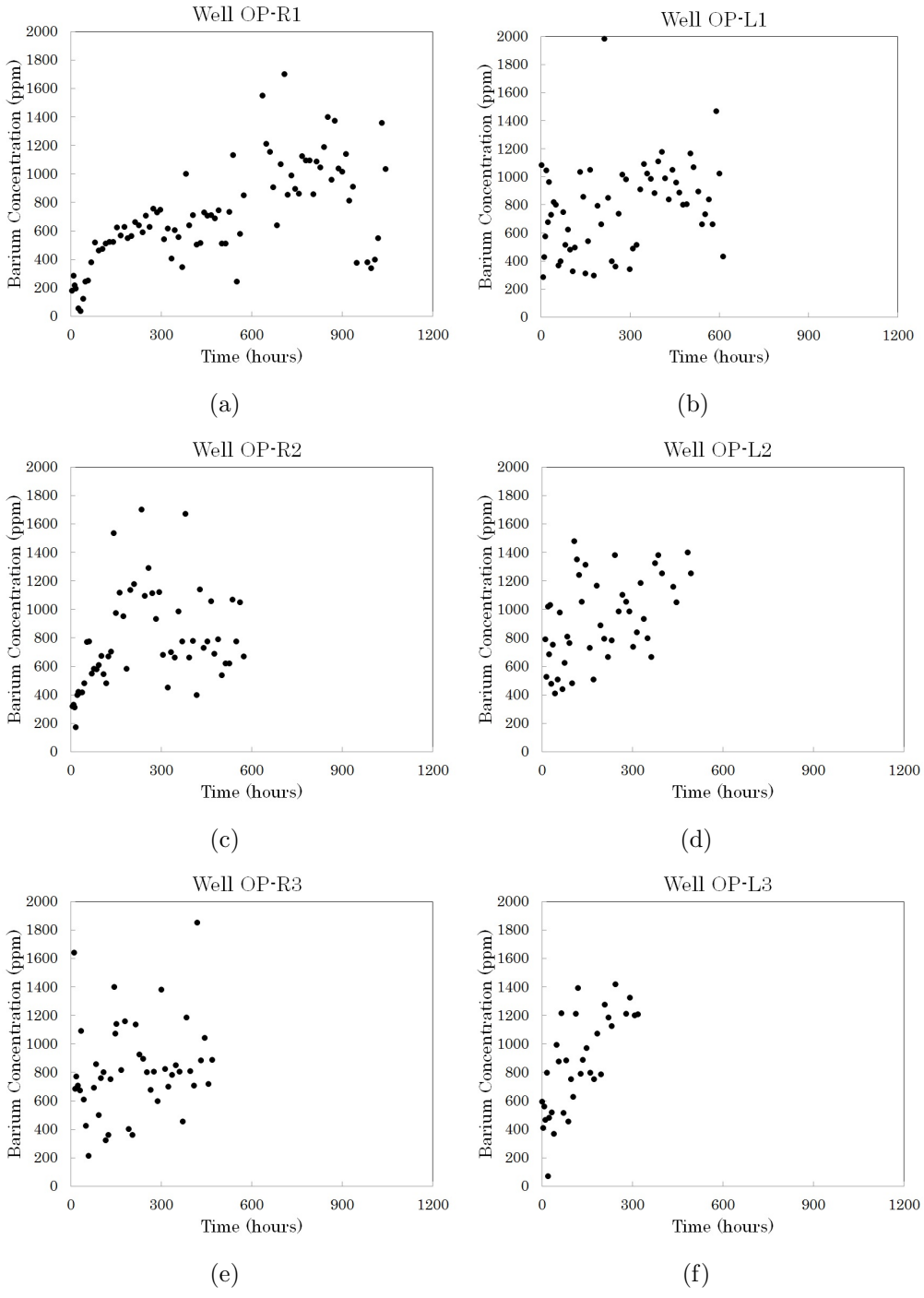

Figure B.2. The change of barium concentration in flowback water for wells completed in Otter Park formation

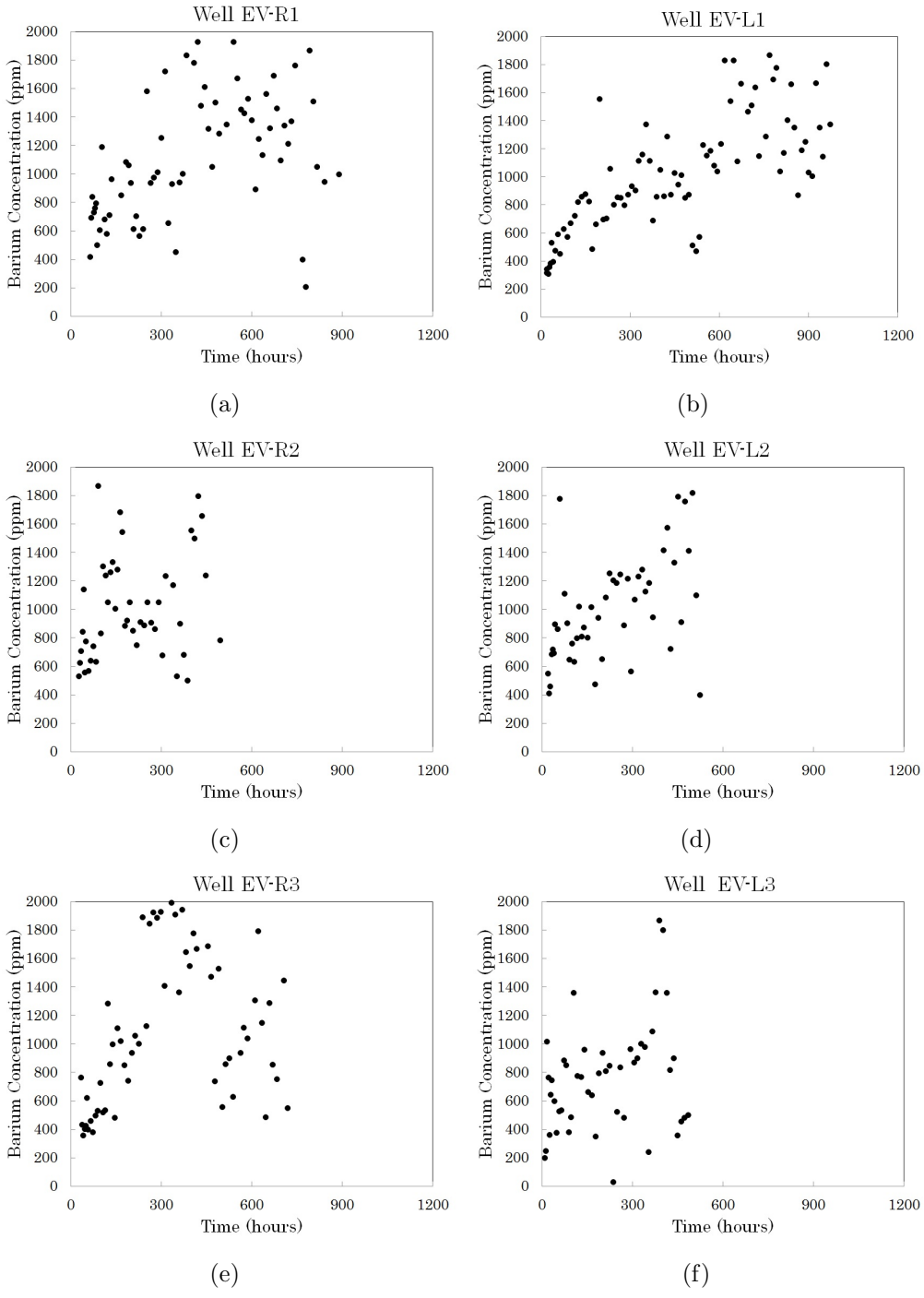

Figure B.3. The change of barium concentration in flowback water for wells completed in Evie formation